

AD 718140

①

UNDERWATER SOUND IN THE ARCTIC OCEAN

by

R. H. Mellen

and

H. W. Marsh

AVCO Marine Electronics Office

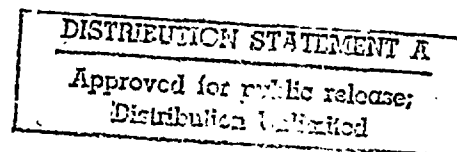
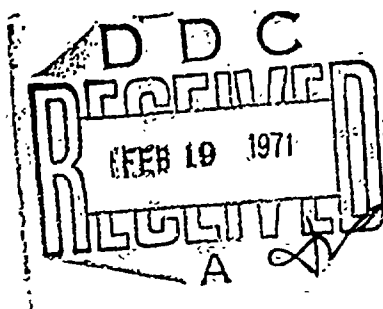
New London, Connecticut

Submitted to:

U. S. Navy Underwater Sound Laboratory

New London, Connecticut

August 16, 1965



The work summarized in this report was supported by the

U. S. Navy Underwater Sound Laboratory

and the

Acoustics Programs, Office of Naval Research

under contract number Nonr 3353 (00)

**BEST
AVAILABLE COPY**

MED-65-1002

①

UNDERWATER SOUND IN THE ARCTIC OCEAN

by

R. H. Mellen

and

H. W. Marsh

AVCO Marine Electronics Office

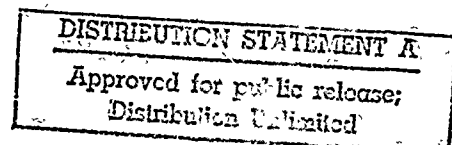
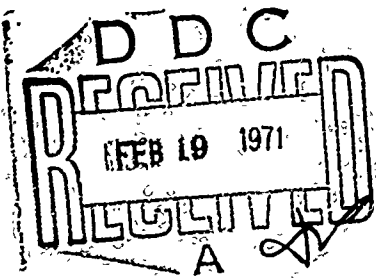
New London, Connecticut

Submitted to:

U. S. Navy Underwater Sound Laboratory

New London, Connecticut

August 16, 1965



The work summarized in this report was supported by the

U. S. Navy Underwater Sound Laboratory

and the

Acoustics Programs, Office of Naval Research

under contract number Nonr 3353 (00)

MED-65-1002

ABSTRACT

Summary results of U. S. Navy Underwater Sound Laboratory experimental program to investigate acoustic phenomena in the Arctic Ocean are presented.

Since the sound velocity is an increasing function of depth, propagation is characterized by upward refraction and surface reflection (RSR). A rough-surface model of the ice cover accounts for both forward and back-scatter. The roughness-wavelength spectrum calculated from reverberation measurements is similar to that for the sea surface, although the level is much higher. Forward scatter loss depends on total roughness and is responsible for severe attenuation of high frequencies. Propagation and reverberation data both imply an R. M. S. roughness of from two to three meters, which is consistent with under-ice profile measurements. Propagation of explosive waves is described by normal mode and ray theories. At short ranges convergence zones are observed. Because the ice cover shows a "critical angle" dependence, the time dispersion of the wave train at long range in deep water is quite well defined ($\cong 1\%$). In shallow water, the bottom may produce bottom reflection modes, reduced dispersion of the refracted mode.

Unusually low ambient noise levels are observed during undisturbed periods. Spectra indicate that the noise background arises mainly via long range propagation at these times. In periods of high wind and particularly rapid temperature change, characteristic ice noises are predominantly of local origin. Occasionally during the summer biological sounds of various forms of marine life are heard.

TABLE OF CONTENTS

	Page
ABSTRACT	ii
1. INTRODUCTION	1
1.1 Brief History.	1
1.2 Propagation	2
1.3 Reverberation	3
1.4 Noise.	4
2. ARCTIC PROPATATION	5
2.1 Experimental Procedure.	5
2.2 Data Analysis	7
2.3 Experimental Results	8
2.4 Transmission Loss (Experimental).	10
2.5 Normal Mode and Ray Theories.	12
2.6 Transmission Loss Theory	16
3. REVERBERATION	19
3.1 Experimental Results	19
3.2 Reverberation Theory and Interpretation.	21
4. AMBIENT NOISE	25
4.1 Experimental Procedures	25
4.2 Experimental Results	26
5. ACKNOWLEDGMENT.	29
6. BIBLIOGRAPHY.	30

LIST OF ILLUSTRATIONS

Figure	Page
1. Drift Station Locations and Aircraft Tracks	33
2. Local Shot Pressure Signature	34
3. Local Shot Missilyzer Spectra	35
4. Narrow Band Analysis Spectrum	36
5. Long Range Graphic Recordings	37
6. Long Range Missilyzer Recordings	38
7. Dispersion Time vs Travel Time	39
8. Sound Velocity Profile	40
9. Bottom Profiles	41
10. Bottom Profiles	42
11. Bottom Profiles	43
12. Missilyzer Spectra	44
13. Missilyzer Spectra	45
14. Energy Flux Spectrum	46
15.	47
to Transmission Loss vs Frequency	to
27.	59
28. Weston's Source Level Spectrum	60
29. Short Range Shot Spectra	61
30. Long Range 1 lb. Shot Signatures	62
31. Hankel Function	63
32. Eigen Value Nomograph for Bilinear Gradient	64
33. Group Velocity Nomograph for Bilinear Gradient	65
34. Frequency Dispersion vs Group Velocity for Bilinear Gradient	66
35. Transmission Loss vs Frequency at 800 Km.	67
36. Reverberation Level vs Time for 100 lb. Charge	68
37. Reverberation Level vs Time for 1.8 lb. Charge	69
38. Reverberation Grazing Angle vs Time	70

LIST OF ILLUSTRATIONS (cont'd)

Figure		Page
39.	Roughness Spectrum.	71
40.	Geophysical Elevation Spectra.	72
41.	Scattering Strength vs Grazing Angle.	73
42.	Reflectivity vs Grazing Angle	74
43.	Roughness Spectra.	75
44.	Scattering Strength vs Grazing Angle	76
45.	Vertical Reflection Coefficient vs Frequency.	77
46.	System Noise Spectra	78
47.	Ambient Noise Spectra.	79
48.	Seismic/Acoustic Ice Surface Velocity Spectrum.	80
49.	Biological Noise Missilyzer Spectra	81

LIST OF TABLES

TABLE		Page
I	Propagation Study Shot Data.	82
II	Ray Calculations.	89
III	Reverberation Study Shot Data.	90
IV	Experimental Values of Scattering Strength (dB).	91
V	Ice Thickness Distribution.	92

This Document Contains
Missing Page/s That Are
Unavailable In The
Original Document

OR are
Blank pgs.
that have
Been Removed

**BEST
AVAILABLE COPY**

1. INTRODUCTION

1.1 Brief History

In the summer of 1958, the Underwater Sound Laboratory (USL) began an experimental study of underwater sound propagation in the Arctic Ocean.¹ Signals from underwater explosives were exchanged between two drift stations, Fletcher's Ice Island (T 3) and Station Alpha, which at that time were some 800 km apart. These early experiments revealed some of the unique features of long range propagation under the ice cover. Notably, the arrivals were found to consist of a dispersive quasi-sinusoidal wave train of 10-100 Hz, frequency range. The dispersion and transmission loss were qualitatively explained by a half space sound channel model in which the attenuation of high frequencies was ascribed to scattering by the rough undersurface of the ice.

During the summer of 1959, the experimental program was continued between T 3 and Station Charlie at a range of about 1200 km.² In order to study propagation as a function of range, a series of aircraft flights were made in which practice depth charges (PDC) were dropped at intervals. The locations of the stations and aircraft drops are shown in Figure 1. Signals were recorded at both stations to provide data for a variety of propagation paths of varying length, involving both deep and shallow water. In September, the visit of the icebreaker Staten Island provided the opportunity to obtain data at intermediate ranges which was difficult to obtain with fast moving aircraft. Other local measurements were made in the vicinity of T 3 out to a range of 10 km.

During April and May of 1962, a cooperative experiment by USL, Lamont Geophysical Laboratory and the Pacific Naval Laboratory was

carried out between three drift stations: T 3, Arlis II and Polar Pack I at locations shown in Figure 1. The main purpose of this series was to obtain supplementary cold weather data prior to the summer warmup.

Some aspects of the program have been previously reported in two papers, one on propagation³ and another on reverberation.⁴ This report is a summary of the USL experimental and theoretical results pertaining to propagation, reverberation and ambient noise. Published results of other investigators are also included for comparison.

1.2 Propagation

In the Arctic Ocean, the speed of sound is usually an increasing function of depth. The propagation of a transient signal can be described by rays which are refracted upward and suffer repeated reflection at the surface (RSR). At long range the deepest rays arrive first. This earliest arrival may be limited by the bottom, or by a "critical angle" of reflection at the ice surface. As time progresses, rays arrive with decreasing vertex depth and with increasing rate until the train terminates with rays traveling near the surface.

If the first rays are bottom limited, the signal onset is governed by the bottom grazing ray. For greater grazing angles, the rays are reflected at the bottom and the group velocity is less. Thus bottom reflection modes appear as a sequence of discrete arrivals, with the spacing governed by grazing angle and water depth. These overlap the refracted modes, and often persist for a longer time. When the surface grazing angle is greater than the "critical angle" however, the bottom modes are rapidly attenuated.

At long range, the normal mode theory also provides a simple description of the refracted wave dispersion (Sec. 2. 5). Because of the losses produced by repeated scattering at the surface, ordinarily no more than two or three modal harmonics are observed.

At short range, however, the normal mode calculations are more complex because the arrivals are less uniformly dispersed. Since the scattering loss is also much less, a greater number of harmonics and a wider range of frequencies are received. Convergence phenomena may also occur which produce concentrations of energy periodic in range. Thus we may have one or more group velocity minima in normal mode theory corresponding in ray theory to inflections at particular surface grazing angles.

In the simplified theoretical method for estimating transmission loss, we consider only the effects of refraction and scattering (Sec. 2. 6). Since the predominant energy at moderately long ranges arrives near termination of the signal, spreading loss is approximated for the prevailing half-channel conditions, while the scattering loss is taken as the loss per reflection (Marsh) times the number of reflections. For the scattering model, we use the wind-driven sea surface model, with the R. M. S. roughness adjusted to fit the experimental data.

1. 3 Reverberation

The validity of the scattering model is confirmed by the roughness-wave number spectrum calculated from measurements of backscatter (reverberation) from an explosive source (Sec. 3. 2). The scattering strength depends on wavelength and angle of incidence, so that the roughness-wave-length spectrum levels are calculated from the reverberation frequency

spectrum. The procedure is to determine the scattering strength as a function of time and frequency. The surface grazing angle (for single incidence) is then calculated, considering shot depth and refraction effects. The incident sound wavelength and grazing angle then determine the corresponding wavelength of the surface roughness spectrum. The roughness amplitude is finally calculated from the scattering strength for the appropriate wavelength.

1.4 Noise

A summary of ambient noise measurements is presented in Sec. 4.2. In undisturbed periods, the noise background in the Arctic Ocean is often below sea state zero equivalent. Under these conditions, measurements with the DT 99 were system-noise limited. For this reason a special low noise system was developed for ambient observation, which permitted measurement to some 40 dB below the Knudsen sea state zero spectrum. For slightly disturbed conditions, the spectra are similar to Knudsen's. During prolonged quiet periods, however, the high frequencies drop off markedly, leaving a noticeable peak in the "pass band" of the sound channel. This is interpreted as noise propagated from distant sources. Comparison is also made between acoustic and seismic ambient noise measurements.

Other interesting features of ambient noise unique to the Arctic include thermal "popping" and explosive cracking after a rapid drop in air temperature. Blowing snow noise during winter storms may also reach very high levels (sea state 3 or more). Generally, however, the summer calms are characterized by very quiet conditions. At these times, sounds of a great variety of marine life are occasionally heard. The sources of these whistles, glides, chirps, grunts, etc., have not been identified, but probably include cetaceans, seals, walrus, etc.

2. ARCTIC PROPAGATION

2.1 Experimental Procedure

In the propagation experiments between the drift stations, shooting schedules were prearranged or coordinated directly by radio communication. Electrical detonation was used, and both firing and arrival times were measured by chronometer to an accuracy of ± 0.5 sec. Since the stations were continuously drifting in an unpredictable manner, it was impossible to determine the range between stations to equal accuracy. Sun positions were taken by theodolite whenever sky conditions permitted, but the average error was no less than a few kilometers. Daily drifts on the order of a magnitude greater complicated the navigation problem.

In the aircraft runs, practice depth charges (PDC) were dropped at intervals along a predetermined track whenever suitable openings in the ice cover could be sighted. The PDC's were set to explode at a depth of 15 or 60 meters* and the detonation time was taken as the time of impact plus the estimated sinking time. Aircraft drop positions were determined by sun shots and dead reckoning, and are considerably less accurate than the positions of the islands.

At the drift stations, the shot signals were detected by means of hydrophones lowered through holes drilled in the sea ice. Since the ice islands are as much as 30-40 meters thick, a minimum depth for the hydrophones of 60 meters was chosen to prevent possible shadowing. Some

* The depth settings of the PDC pressure actuators are actually 50 and 200 feet. For consistency, all length measurements will be expressed in the metric system.

measurements were made with the phones as deep as 180 meters. However, the greater depths were found to be of marginal interest since the simpler procedure of varying shot depth showed most of the essential features.

In all the earlier experiments, a standard PQM (DT 99) hydrophone was used. The disadvantages of this hydrophone were that the multi-conductor cable was somewhat unwieldy and the associated preamplifier was subject to saturation by strong signals. The overall frequency response was 10-10,000 Hz. For later tests, a new system was developed using a bilaminar-disc hydrophone. Because of their high capacitance ($0.1 \mu F$), these units could efficiently drive several hundred feet of lightweight shielded cable directly without a preamplifier. The system noise was much lower than it was using the DT 99; however, high frequency response was sacrificed since resonance occurred at 2 kHz. Another disadvantage was that the hydrophone could not withstand more than 100 meters submergence without mechanical failure.

The signals from the hydrophone were recorded by means of a graphic recorder with frequency response to 100 Hz. Magnetic tape recordings (FM and/or direct) were also made with full system frequency response for later analysis. Calibration of the system was accomplished by injecting sinusoidal signals of known voltage at selected frequencies. A single master gain control provided adjustment of the system gain for calibration, signal and ambient noise recording.

During the earlier tests, it was found that the explosions often delivered varying yields, as result of incomplete detonation. To circumvent this difficulty, a procedure was established to record the shot at the transmitting site when possible. The effective yield was determined from the

bubble pulse period and depth. The record in Figure 2 is a pressure vs time signature for a typical shot at 1 km showing the shockwave and bubble pulses (positive pressure), and surface reflections (negative pressure). If the system were overloaded or cluttered with interfering arrivals, the bubble pulse period could be obtained from the periodic envelope modulation of the spectrum. The two spectra shown in Figures 3a, b, which are shot signatures at 1 km and 50 km range respectively, show this clearly.

2.2 Data Analysis

Analysis of the data is of three general types. First, graphic recordings made on the spot furnished direct pressure amplitude vs time traces. These show qualitatively the effects of shot size and depth, as well as the quasi-sinusoidal and interference features of the propagation. The times of onset and termination also provide measures of time-dispersion and travel time.

Secondly, the magnetic tape recordings were analyzed by means of a Kay Missilyzer Spectrum Analyzer to provide the frequency spectrum vs time. These graphs are useful in analyzing the frequency-time dependence of the normal modes and harmonic relations between them as well as the interference effect of the bubble pulse.

Finally, the magnetic tapes were used to make continuous loop recordings of the shot signals, which were scanned by means of a variable frequency, narrow band filter. A typical result of this technique is shown in Figure 4. Together with the calibration tapes, this permits calculation of the received energy flux spectrum as a function of range, shot size, depth, etc. Knowing the source energy flux spectrum at 1 m range (Weston)⁵, the transmission loss is calculated. Since the received signal varies in

time and frequency in a complex fashion because of source and modal interference effects, the peak envelope method of analysis was used in much of this work. A smooth curve was fitted to the "average" spectral peaks so as to eliminate mode and bubble pulse modulation. This is the solid curve seen in Figure 4. In another technique, logit filters were used and the total (integrated) energy flux spectrum levels calculated. The two methods were found to be in quite reasonable agreement.

2.3 Experimental Results (General)

The pertinent data for the analyzed shots are contained in Table I. Each record is identified both serially and with the notation of the original experiment log.

Figure 5 shows typical graphic recordings made at ARLIS II from shots of several sizes detonated at T-3. All were at 120 meters depth except the 375 lb. shot, which was fired at 100 meters. The travel time corresponding to termination of the water wave is 563 sec. For a sound speed of 1438 m/sec, the calculated range is 810 km, agreeing with the navigational value within a few km. It should be noted that the receiving system gain was adjusted to compensate for source level changes. The time dispersion varies between 6.6 and 7.1 seconds, increasing with shot size. For the smaller shots, the complexity of the beginning of the water wave is particularly noticeable. This is due to contributions from several modes as well as from interference of the bubble pulse. For the larger shots, the spectral energy is concentrated at lower frequencies, the relative excitation of higher frequencies is less and the bubble pulse frequency is lower. Source interference effects persisting throughout the entire train are clearly evident.

Figure 6 shows Missilyzer recordings of two typical shots. Note that the lowest (zero) mode begins near 10 Hz and increases with time to about 70 Hz at termination. The first modal harmonic is visible throughout the trace, while the second and higher modes vanish soon after the beginning of the wave. Bubble pulse interference effects are evident from the amplitude modulation of the mode lines at multiples of the bubble pulse frequency. Normal mode theory is discussed in Section 2.5.

The received signals characteristically have an abrupt beginning and end with a duration proportional to travel time. Figure 7 contains a plot of time duration (dispersion) vs. travel time for some fifty shots, detonated under various conditions and times during the experimental program. The data show a mean time dispersion ratio of slightly more than 1%. The factors governing onset and termination of the water wave are discussed elsewhere.

Figure 8 gives a typical sound velocity profile for summer conditions. The two major zones of interest are the deep water isothermal gradient beginning near 300 meters and the overlying layer of some 3 or 4 times greater average gradient. In the upper zone, there is some detailed structure which depends on season.

Table II contains ray calculations for the velocity profile of Figure 8 (see Section 2.5). It is notable that the time dispersion corresponds to ray depths less than 1500 meters and surface grazing angles less than 13° . Since the minimum water depths for some of the experimental paths were in excess of 2000 meters (Figures 9-11), it is clear that the onset of the wave train is not always governed by the bottom. If this is true, the onset must be limited by the surface reflection coefficient of the ice cover, which apparently diminishes rapidly for grazing angles greater than 13° .

Figures 12a, b show Missilyzer traces for the propagation path profiles of Figures 11a, c. In 11c, an underwater obstacle (the Chukchi Rise) shadows all rays deeper than 200 meters, leaving only one second of the dispersion pattern remaining. The deep-water duration is in excess of ten seconds.

Under some circumstances, the bottom reflection mode is received along with the RSR mode. In this case the onset corresponds to a group velocity maximum. This effect is seen in Figure 13a which is a recording of a shot dropped from an aircraft and received 572 seconds later. The first hundred kilometers of the propagation path were in shoaling water (10a) and gave rise to more than twenty identifiable bottom arrivals which obscure the RSR mode. Figure 13b is another shot at almost the same range but received some 20 minutes later. The bottom topography (10b) has changed, so that an obstacle intervenes and cuts out the bottom mode completely.

2.4 Transmission Loss (Experimental)

Figure 14 shows a typical energy flux vs frequency spectrum (L_r) measured as described in Section 2.2. Transmission loss vs. range data for all shots (computed from the relation $N_{v/r} = L_s - L_r$) are shown in Figures 15 through 27. The source level spectrum at 1 meter, L_r , was taken from Weston for the appropriate yield, corrected (where possible) by the bubble-pulse-period-vs-depth method mentioned earlier. It should be noted that Weston's shot spectra account for bubble pulse interference only at the fundamental frequency, while the true spectra shows maxima and minima over many harmonics. Thus, the Weston spectrum represents a quasi-envelope of the actual one (Figure 28). The narrow band analysis method used here clearly shows these and other interferences and an envelope was drawn similar to Weston's to average them out.

The transmission loss data show considerable scatter which is taken to represent the combined effects of variations in the transmission path and ice cover, as well as experimental error. Some of the short range levels are considerably higher than predicted for the half channel and are interpreted as possible results of convergence. This effect is illustrated in Figure 29 a, b where arrivals from #8 caps at two different ranges are shown. The first at 1 km shows only a discrete arrival followed by a bottom reflection. The second at 5 km also apparently shows a delayed convergence arrival for which the level is about 20 dB higher than the direct arrival. Buck⁶ has also observed high signal levels at short range which may be ascribed to convergence.

Milne's⁷ transmission losses out to 90 km have been included in the figures for comparison. These measurements were made in the spring and may represent differences in the ice condition or a change in the refraction.

The theoretical transmission loss curves are discussed in Section 2.6. The curve 'S' is the surface scattering model representing the "average" loss for a long transmission path. The curve 'A' is absorption loss only and represents a lower limit for short range where no surface reflections are involved.

Various factors may be responsible for the transmission loss "anomalies". For example, in deep water the early arrivals may dominate and the high frequency loss may be low because the number of reflections is less. Thus the transmission loss depends on the bottom topography as well as the condition of the surface and the sound velocity profile.

However, the scatter of the transmission loss data is evidently not due to short term changes in the medium, which, in fact, is remarkably stable. Figure 30 shows a series of 1 lb. shots at 80 meters depth received over

an 800 kilometer path. The two hydrophones (a, b) were 1 km apart and the time between shots was 2 hours. The similarities indicate both space and time stability of the acoustic path.

2.5 Normal Mode and Ray Theories⁸

To illustrate the connection between normal mode and ray theories, we consider first a single positive gradient defined by $c_z = c_0 (1 + gz)$, where c_z is the depth dependent sound velocity, g is the velocity gradient (m^{-1}), c is the sound velocity, (ms^{-1}) at the pressure release surface and z is the depth (m). The resulting separated equation for the depth dependent portion of the velocity potential is then approximately given by:

$$\phi_{\zeta\zeta} + \zeta\phi = 0 \quad (1)$$

$$\text{where } \zeta = \left(-\frac{2\omega^2 g}{c_0^2} \right)^{-2/3} \left[\frac{\omega^2}{c_0^2} - k^2 - \frac{2g\omega^2 z}{c_0^2} \right] \quad (2)$$

Here, ω is the angular frequency (s^{-1}), and K is the wavenumber (m^{-1}). The eigenfunctions of Equation (1) are modified Hankel functions of order $1/3$. $h_1(\zeta)$ and $h_2(\zeta)$ represent "downward" and "upward" going waves. For our purposes we consider only $h_1(\zeta)$. The eigenvalues are obtained from the zeroes which have the argument $\pi/3$ (Figure 31).

Thus, for the pressure release surface, the first mode $\phi = 0$, $z = 0$, $n = 1$ is identified as point (a), while the curve to the right represents the depth/frequency dependence which increases to its maximum and then decays exponentially. Similarly, the curve to the right of point (b) represents the second mode $n = 2$.

Good approximation of the zeroes of h_1 are given by

$$x^{3/2} = \frac{3\pi}{2} \left(n - \frac{1}{4}\right) \quad n = 1, 2, 3 \quad (3)$$

where $x = \xi(z=0)$. From this, the phase velocity of the n^{th} mode becomes

$$c_n = \frac{\omega}{k} \cong c_0 \left(1 + \frac{1}{3} \left[\frac{3\pi c_0 g}{\omega} \left(n - \frac{1}{4}\right) \right]^{2/3} \right) \quad (4)$$

and the group velocity, u_n , is obtained from the relation

$$u_n = c_n + \omega \frac{dc_n}{d\omega} \quad (5)$$

Substituting $f = \frac{\omega}{2\pi}$, the final result is:

$$u_n \cong c_0 \left(1 + \frac{1}{6} \left[\frac{3 c_0 g}{2f} \left(n - \frac{1}{4}\right) \right]^{2/3} \right) \quad (6)$$

The frequency-time behavior of a wave received at a distant surface point from a surface impulsive source is simply the frequency-mode number components delayed according to the appropriate value of the group velocity.

To compare ray theory, the familiar equations for the positive gradient g is:

$$r_0 = \frac{2 \sin \theta_0}{g \cos \theta_0} \quad (7)$$

where r_0 is the horizontal distance between surface reflections and θ is the grazing angle. Also,

$$t_0 = \frac{2}{c_0 g} \int_0^{\theta_0} \frac{d\theta}{\cos \theta} \cong \frac{2}{c_0 g} \left(\theta_0 + \frac{\theta_0^3}{3} \dots \right) \quad (8)$$

where t_0 is the travel time for the distance r_0 . From this, the group velocity u is obtained:

$$u = c_0 \left(1 + \frac{\theta_0^2}{6} \dots \right) \quad (9)$$

To determine the frequency f , the reciprocal of the time T between the N th and $(N+1)$ th arrivals at a distance R is taken. That is:

$$f = \frac{1}{T_N - T_{N+1}} = \frac{dN}{dT} \quad (10)$$

Since the range $R = Nr_0$ and the travel time $T = Nt_0$, then

$$f^{-1} \cong t_0^2 \frac{du}{dr_0} \quad (11)$$

From the above,

$$u \cong c_0 \left(1 + \frac{\theta^2}{6} \right) \text{ and } \theta^3 = \frac{3 c_0 g}{2 f} \quad (12)$$

Combining the previous results yields

$$u \cong c_0 \left(1 + \frac{1}{6} \left[\frac{3 c_0 g}{2 f} \right]^{2/3} \right) \quad (13)$$

Comparing Equations (6) and (13), we find the only difference between the two lies in the mode number term. In fact, the ray frequency is $3/4$ the lowest mode frequency.

For the bilinear case,

$$\begin{aligned} c_z &= c_0 (1 + g_0 z) & 0 < z < z_1 \\ c_z &= c_1 (1 + g_1 z) & z_1 < z < \infty \end{aligned} \quad (14)$$

The approximate equation analogous to Equation 3 is:

$$x^{3/2} + a(x-1)^{3/2} = b \quad (15)$$

where

$$a = (g_0 c_1^2 / g_1 c_0^2 - 1)$$

$$b = \frac{3\pi}{2} \left(n - \frac{1}{4}\right) \frac{1}{(2g_0 z_1)^{1/2}} \frac{1}{kz_1}$$

The resulting group velocity is:

$$\begin{aligned} u &\approx c_0 \left[1 + g_0 z_1 \left(x + \omega \frac{dx}{d\omega} \right) \right] \\ &\approx c_0 \left[1 + g_0 z_1 \frac{b/3 + a(x-1)^{1/2}}{x^{1/2} + a(x-1)^{1/2}} \right] \end{aligned} \quad (16)$$

In the above, $x - 1$ is replaced by zero when $x < 1$, and in this case

$$u_n \approx c_0 \left(1 + \frac{f}{6} \left[\frac{3c_0 g}{2f} \left(n - \frac{1}{4} \right) \right]^{2/3} \right) \quad (17)$$

which is the same as Equation (6).

A graphical solution of Equation 15 is readily obtained with the aid of the nomographs (Figures 32, 33). To obtain x , use the auxiliary equation $b = \sigma/f$, locate f on the abscissa of Figure 32, proceed vertically to the appropriate b curve (marked with the value σ), proceed horizontally to the appropriate a curve, and thence downward to read x on the abscissa. Given x , locate the abscissa in Figure 33, obtain $a(x-1)^{1/2}$ as the corresponding ordinate, locate $b/3$ as the ordinate corresponding to the chosen f (abscissa); obtain $x^{1/2} + a(x-1)^{1/2}$ as ordinate corresponding to abscissa x , and complete the calculation. Figure 34 shows the resulting frequency dispersion vs. group velocity for this bilinear

gradient model with appropriate values calculated from Equation 16.

The corresponding ray equations are:

$$r_0 = \frac{2}{g_0 \cos \theta_0} \left[\left(\frac{g_0}{g_1} \right) \sin \theta_1 + \sin \theta_0 - \sin \theta_1 \right] \quad (18)$$

$$t_0 = \frac{1}{g_0 c_0} \left[\frac{g_0 - g_1}{g_1} \left(\ln(1 + \sin \theta_1) - \ln(1 - \sin \theta_1) \right) + \ln(1 + \sin \theta_0) - \ln(1 - \sin \theta_0) \right] \quad (19)$$

The calculations for the multilinear gradient (Table II) were obtained by a ray computer program for ten gradients fitted to the depth profile of Figure 8. The frequencies were calculated from Equation (11).

2.6 Transmission Loss Theory

Earlier, the bottom grazing ray for the bilinear gradient was identified with a group velocity maximum. This determines the time of onset of the wave train, provided the surface grazing angle is less than 13° . For the bilinear gradient (large - small) model, this is the only group velocity extremum, except for the trivial minimum at termination of the wave where the ray vertex depth goes to zero and the frequency increases without limit. In the multilinear gradient case, the situation is quite different since there is a group velocity minimum for a surface grazing angle of 7.7° . Since the vertex depth for this ray is only about 240 meters, no significant convergence is expected if source or receiver are deeper than this. If they are less deep the main effect at long range will be a sudden and apparently premature termination of the wave train. At short ranges, however, convergence focusing is important. Thus, as the range increases, we expect concentration of energy at multiples of the skip distance. After a few surface

bounces, zones should tend to spread and overlap because of scattering, so that the decay eventually becomes a monotonic function of range. At long range, therefore, near the termination of the wave train, the total transmission loss may be estimated from the combined effects of refraction and scattering as nearly:

$$N_w = 10 \log r_0 + 10 \log R + N a_s \quad (20)$$

where r_0 is the ray skip distance, R is the range in meters, N is the number of surface incidences and a_s is the loss per reflection. As a scattering model, the wind generated ocean spectrum is taken to approximate the ice roughness. According to Marsh,⁹

$$a_s = -10 \log (1 - 2.57 \times 10^{-4} f^{3/2} h^{8/5} \sin \theta) \quad (21)$$

where f is the frequency (Hz) and h is the R.M.S. roughness in meters. For a small loss per bounce, (20) becomes approximately:

$$N_w \cong 20 \log r_0 + 10 \log N + N (1.10 \times 10^{-3} f^{3/2} h^{8/5} \sin \theta) \quad (22)$$

where $R = N r_0$

To give specific results, take $\theta = 7.7^\circ$, $r_0 = 6021$ meters, $h = 2.4$ meters, and $N = 134$. Then

$$N_w \cong 97 + R \times 10^{-7} f^{3/2} \quad (23)$$

For these conditions, which correspond to shot 31B at 810 kilometers, the following is calculated:

f (Hz)	10	20	30	40	50	60	70	80
a_s (dB)	3	7.1	13	20	27	37	48	57
N_w (dB)	10	104	110	117	124	134	145	154

Figure 35 shows a plot of Equation (23) (solid line), together with the experimental transmission loss values (circles) computed by $N_w = L_s - L_r$ (Section 2-4). In the frequency range shown, the fit is quite good; however, above 100 Hz, the theoretical scattering loss apparently becomes excessive.

Figures 15 through 27 show the compiled transmission loss data. In Figures 15-24, the curve S is Equation (22). The straight lines are the first two terms of Equation 20, giving the spreading loss only. The usual absorption loss is the curve A in Figures 24-27 (which includes scattering loss). For the water temperature of 0° C, absorption loss is taken as $0.12f^2$ dB/km, where f is the frequency in kHz. The curve A is included to show the lower limit of transmission loss in the absence of scattering (high frequency - short range). Both the S and A curves are shown in Figure 24 to illustrate the transition region.

Equation 22 appears to give a fairly pessimistic approximation and is probably applicable when the water is less than 500 meters deep over a portion of the transmission path. For deeper water, the high frequencies tend to be dominated by the deeper rays (earlier arrivals) which perhaps accounts for the low loss anomalies. It is doubtful, however, that more detailed consideration of ray paths and bottom topography would significantly improve the picture at this point, since the grazing angle dependence of the surface is not known.

3. REVERBERATION

3.1 Experimental Results

The results reported here concern the local scattering or reverberation produced by the rough underside of the ice in the vicinity of explosive sources. The explosives were monitored and recorded through hydrophones some hundreds of meters away. Table III gives the pertinent data identifying the shots and recordings. The magnetic tape records were subsequently played back through a Bruel-Kjaer analyzer, using 1/3-octave (10% bandwidth) filters centered at frequencies between 40 and 8000 Hz.

The filtered waveforms of shot 8 and a composite of shots 10-12 are shown in Figures 36 and 37, respectively. It should be noted that the time scales of the two differ by a factor of 10. In the figures, time is marked from the shot instant. Figure 37 shows an early arrival, particularly at the lower frequencies, which is probably an ice wave. Shortly after that comes the direct and surface scattered wave, which decays for a second or so before the first bottom arrival is seen. Additional orders of bottom reflections may be seen a bit later in the figure. In Figure 36, these arrivals are compressed within the first few seconds of the record, and the main curve, lasting up to nearly two minutes, consists of reverberations returning from the ice and the bottom.

Quantitative results are conveniently presented in terms of the scattering strength, N_S .

$$N_S = L_R - L_S + 2N_{WR} - 10 \log A \quad (24)$$

In Equation (24), L_R is the level of reverberation at time t (dB// μ bar), L_S is the level of the source (dB// μ bar), $2N_{WR}$ is the propagation loss from source to reverberating area plus loss from reverberating area to receiver, and A is the effective reverberating area at time t . The reverberating area is the elliptical annulus on the surface of width determined by the duration of the incident wave and generally located by the travel time from source to surface to receiver. Table IV presents selected values of N_S tabulated from the shots of Table III. Marsh has shown how the scattering strength may be expected to depend upon the properties of the scattering surface, and upon the geometry of the situation. With the bistatic setup prevailing in the present experiments, it is quite difficult to interpret directly the scattering strength for comparison with other geometry or other surfaces. For this reason, the ice roughness spectra is derived from the observed scattering strengths, and then the scattering calculated for other geometries. This is done below.

For L_S the values of Weston are used of the spectrum level for the appropriate yield, to which $20 \log(\text{bandwidth})$ is added. The yields were determined experimentally from missilyzer recordings, in which the bubble periods were evident. These yields in several cases differ markedly from the design yield based on weight of explosive. $2N_{WR}$ is taken to be simply $40 \log ct$, c being the mean velocity in meters per second. Finally, the reverberating area is approximately $\pi c^2 t \tau / 2$, τ being the effective pulse length, twice the reciprocal bandwidth. These approximations are adequate to rectify the experimental values of N_S , producing a quantity which is a function only of frequency at a given time, and whose variation with time can be interpreted in terms of the prevailing propagation conditions.

3.2 Reverberation Theory and Interpretation

Marsh⁹ gives the scattered intensity I_s in terms of the intensity I of waves incident upon a rough surface and the wave number spectrum of surface roughness $A^2(k)$ in the form

$$I_s = \iint I \Gamma d\lambda d\mu \quad (25)$$

$$\Gamma = \gamma^2 k^3 A^2(k\alpha) \quad (26)$$

The direction cosines of the incident wave are α , β , γ , and those of the scattered wave are λ , μ , ν . So, for instance, the sine of the grazing angle of incidence is $\gamma = \sin \theta$. The quantity α is $[(\lambda - \alpha)^2 + (\mu - \beta)^2]^{\frac{1}{2}}$

The reverberation returning at times greater than about 10 seconds comes from an approximately circular annulus. The separation of source and receiver may be ignored. Under these conditions, the integral may be carried out explicitly. In so doing, effects of refraction must be considered. For the transmission times involved, the law of propagation may be taken as approximately inverse square. However, refraction has a strong effect upon the grazing angles.

To complete the calculation, it is necessary to relate the surface grazing angle to time. For this purpose, the bilinear gradient profile approximation is employed. Figure 38 displays the surface grazing angle as a function of time after the first arrival. Following Marsh for the reduction of the integral, we finally obtain, approximating $\cos \theta$ by 1,

$$10 \log A^2(2k) = N_s - 30 \log k - 40 \log \sin \theta + 3 \quad (27)$$

Values of $A^2(k)$ reduced using this equation are shown in Figure 39. Those values for $k = 0.35$ and 0.60 are obtained from shots 10 - 12, during the time preceding the first bottom arrival. For these values, the bistatic geometry is important, and the integration corresponding to Equation (25) cannot be carried out in closed form. However, the variation of N_S with frequency would be nearly independent of the bistatic geometry. Accordingly, these values have been adjusted to give values of $A^2(k)$ equal to those of the other shots at $k = 5.9$. The other values for these small values of k are not plotted because they are believed to be due primarily to bottom reverberation. However, the corresponding values of scattering strength are included in Table IV.

It may be noted that the rms roughness σ of the surface is given by

$$\sigma^2 = \int_0^\infty A^2(k) dk \quad (28)$$

By numerical integration, $\sigma \cong 3m$, slightly larger than the value derived from forward scatter; but, both are quite compatible with ice thickness measurements of Lyons¹⁰ shown in Table V.

For comparison, the sea-surface spectrum of Burling is also shown in Figure 39. The curves are roughly parallel above $k = 5$, and it appears reasonable that the ice spectrum is asymptotic to k^{-3} . This corresponds to reverberation which is independent of frequency, similar to that in the open sea, but about 40 dB higher. A compilation of various geophysical spectra shown in Figure 40 indicate that the K^{-3} spectrum is typical of naturally occurring rough surfaces.¹¹

There is considerable scatter in the data reported (standard deviation ~ 5 dB), some of which might be eliminated by a detailed computation

of ray paths and losses, taking into account the actual shot and hydrophone depths, in which the refraction could play a part.

An additional feature of the recordings is the peak in levels occurring from 40-50 seconds, particularly evident at the higher frequencies. This peaking is undoubtedly a refraction effect, and has been systematically observed on all shots identified in Table III. The travel time of 50 seconds corresponds to a grazing angle of 16° for the direct ray and an angle of 11° for the singly reflected ray. These angles are on either side of the "critical angle". There is thus additional evidence that reflection is quite poor at grazing angles exceeding some 13° .

More recently, other investigators^{12,13} have made reverberation strength measurements on young sea ice and summer polar ice over a considerably wider range of grazing angles and using improved geometry to eliminate bistatic problems and bottom echoes. While all measurements agree quite well for grazing angles $\sim 10^\circ$ (Figure 41), the angular dependence of the new data is much less than predicted by Equation (27). This may not be surprising since Brown's normal reflectivity is some 15 dB below perfect at 5-10 kHz.

Kuo¹⁴ has considered the Brown experiment by extending Marsh's scattering formula to the imperfect reflector and fitting his modified reflectivity function of grazing angle to the data. The results are shown in Figure 42 and the derived roughness spectrum in Figure 43. For large k , the agreement between the Brown and Mellen-Marsh roughness spectrum levels is fairly good even though Brown's total roughness is apparently much less.

Other discrepancies are evident from the work of Milne¹⁵ on the spring Arctic pack ice shown in Figure 44. Comparing values at 10° grazing angle, his scattering strengths are some 20 dB higher and show even different grazing angle dependence. Milne's normal reflectivity is almost perfect to 1 kHz and only 5 dB down at 5 kHz (Figure 45).

4. AMBIENT NOISE

4.1 Experimental Procedures

Early attempts to measure the ambient noise background with the DT 99 hydrophone were usually frustrated by excessive system noise. For this reason bilaminar-disc hydrophones (USL Type XU 1269 and XU 1333) were used in conjunction with a low noise vacuum tube preamplifier. Since the capacitance of the units was approximately $0.1\mu\text{F}$ and the depth of submergence only 60 meters, the hydrophone was used to drive a suitable length of transmission line directly and the preamplifier was installed above the surface, often in the instrumentation hut.

The noise curves for typical DT 99 and XU systems are shown in Figure 46 which also includes the Knudsen sea state zero curve for a reference. The main disadvantage of the XU system was the low resonant frequency which prevented measurements over as wide a frequency range as the DT 99. However, since the main concern here was for the frequencies less than 1 kHz, this was not considered serious.

Recordings of ambient noise together with approximate calibrations were made at intervals. These recordings were subsequently analyzed by means of a WE 3A4A spectrum analyzer and the corresponding ambient noise spectra calculated.

The measurements with the XU 1269 were made at ARLIS II during the period of September - October 1961. Other measurements were made between May - September 1962 at both T 3 and ARLIS II. The data in no

way represent a complete statistical study of ambient noise even over those restricted periods because of limitations set by the necessity of almost complete shutdown of generators and other camp activity. Usually a small generator, suitably shock mounted, was used to power the equipment. Measurements were concentrated in periods of light winds. High wind speeds tended to increase water currents relative to the ice causing hydrophone flutter which made ambient measurements impossible. Later, cable fairing was employed to solve this problem.

4.2 Experimental Results

Unusually quiet conditions prevail during the summer months when temperatures are stable and winds moderate for a considerable part of the time. This is in part due to the mushy, broken condition of the ice cover which makes it a poor noise generator. In cold weather, however, the ice cracks under thermal and wind stress. During storms ridging and rafting also contribute a variety of noises like hammering, slamming, creaking, etc. Blowing snow adds to the background with a sound like sandblasting. Under these conditions the ambient level may increase as much as 20 dB.

Figure 47 summarizes the results of analysis of more than 100 ambient recordings. A typical "quiet" ambient (curve A) is generally some 5-10 dB below sea state zero. There is evidence of a broad peak centered around 20 Hz. This suggests that propagation from distant noisier areas is involved, since the effects of scattering loss are quite apparent. Curve B is a typical cold weather situation where the air temperature has dropped suddenly. With the rapid decline in temperature, the ice comes under stress, and starts cracking. Under these conditions,

the noise background rises. Curve C is the highest ambient noise level recorded during the observation period.

Ganton and Milne^{16,17} report ambient noise measurements made within the Canadian Archipelago with bottomed hydrophones in various seasons. In the summer, the spectra fell within ± 5 dB of the Knudsen sea state zero curve above 100 Hz and are "flat" from 10-100 Hz. The higher levels were associated with ice motion which caused rafting of the rind that sounded like "escaping steam". In the cold weather with declining air temperature, the cracking sound approached a steady-state hiss and increased the high frequency levels to some 20 dB above sea state zero. A blowing snow contribution to the noise background during windy periods was also identified.

Buck¹⁸ also reported ambient measurements from 20-1000 Hz made in the Beaufort Sea over a two weeks period in April 1963. His average value for the period is about 6 dB above sea state zero with a total variation of roughly ± 10 dB. The higher levels were also associated with thermal cracking.

Figure 48 is a comparison of acoustic and seismic "ambient noise". The seismic measurements were made with a vertical component seismometer mounted on the ice surface¹⁹, with the results presented in terms of a velocity frequency spectrum. The acoustic noise spectrum is derived from the acoustic pressure spectrum by $u^2 = p^2 / \rho_0^2 c_0^2$. This implies that the seismic disturbances in the ice and, probably, in the bottom also, are coupled to the water by direct acoustic radiation.

Occasionally during the summer, noises of obvious biological origin are heard. These include long gliding whistles, short chirps, braying

sounds and grunts. Figure 49 shows several Missilyzer records of these noises, illustrating the differing frequency characteristics. An effort was made to identify these sounds with recordings made by Woods Hole and others. Although there was a similarity to the sounds of certain whales, porpoise, seals, etc., which are known to frequent the Arctic Ocean, no positive identification could be made.

6. ACKNOWLEDGMENT

Before 1960, logistic support for Drift Stations Alpha, Charlie and Fletcher's Ice Island (T3) was directed by the Ice Skate Project Office of the United States Air Force. In 1960, responsibility for T3 was transferred to the Arctic Research Laboratory, Barrow, Alaska, under contract with the Geography Branch of the Office of Naval Research. In 1961, the second "permanent" drift station ARLIS II was established. At present, a diversified program of geophysical research continues at T3. ARLIS II, however, was abandoned in 1965 when it drifted out of the Arctic Ocean, east of Greenland.

The participation of the U. S. Navy Underwater Sound Laboratory was supported by the U. S. Navy Bureau of Ships. Credit is especially due to Dr. G. S. Harris, formerly Associate Director of the U. S. Navy Underwater Sound Laboratory, for his initiation and continued support of the Arctic Program. Mention should also be made of those staff members who participated in the field activities:

1958	A. Kelley, R. Hecht
1959	R. Mellen, A. Kelley, E. Demock, A. Reynolds, F. Williams
1960	R. Mellen, C. Milner, A. Kelley, E. Demock
1961	R. Mellen, C. Milner
1962	R. Mellen, C. Milner, A. Reynolds, G. Adkins, E. Demock, D. Abraham, R. Soccoli, T. Wamback, A. Silverio, R. McCarthy

BIBLIOGRAPHY

1. Hecht, R. J. ,
"Sound Propagation Experiments Conducted under the Polar Ice
Pack During the Summer of 1958"
USN/USL Report #465 (9 February 1960) CONFIDENTIAL
2. Hecht, R. J. ,
"Arctic Ocean Propagation Measurements"
USN/USL Tech. Memo 911-010-61 (25 July 1961) CONFIDENTIAL
3. Marsh, H. W. and Mellen, R. H. ,
"Underwater Sound Propagation in the Arctic Ocean"
J. Acoustical Society of Am. 35, 552 (1963)
4. Mellen, R. H. and Marsh, H. W. ,
"Underwater Sound Reverberation in the Arctic Ocean"
J. Acoustical Society of Am. 35, 1645 (1963)
5. Weston, D. E. ,
"Underwater Explosives as Acoustic Sources"
Proc. Phy. Soc. (London) 76, 233 (1960)
6. Buck, B. M. and Greene, C. R. ,
"Arctic Deep Water Propagation Measurements"
J. Acoustical Society of Am. 36, 1526 (1964)
7. Milne, A. R. ,
"A 90 Km Sound Transmission Test in the Arctic"
J. Acoustical Society of Am. 35, 1439 (1963)
8. Marsh, H. W. ,
"Doctoral Dissertation"
Brown University (1950)
9. Marsh, H. W. ,
"Sound Reflection and Scattering from the Sea Surface"
J. Acoustical Society of Am. 35, 240 (1963)

BIBLIOGRAPHY

(cont'd)

10. Lyons, W. K. ,
"Private Communication"
11. Marsh, H. W. and Mellen, R. H. ,
"Boundary Scattering Effects In Underwater Sound Propagation"
Radio Science, National Bureau of Standards (1965)
12. Chapman, R. P. and Scott, H. D. ,
"Backscatter Strength of Young Sea Ice"
J. Acoustical Society of Am. 36, 2417 (1964)
13. Brown, J. R. ,
"Reverberation Under Arctic Ice"
J. Acoustical Society of Am. 36, 601 (1964)
14. Kuo, E. Y. T. ,
"Wave Scattering and Transmission at Irregular Surfaces"
J. Acoustical Society of Am. 36, 2135 (1964)
15. Milne, A. R. ,
"Underwater Backscattering Strength of Arctic Pack Ice"
J. Acoustical Society of Am. 36, 1551 (1964)
16. Milne, A. R. and Ganton, J. H. ,
"Ambient Noise Under Arctic Sea Ice"
J. Acoustical Society of Am. 36, 855 (1964)
17. Ganton, J. H. and Milne, A. R. ,
"Temperature and Wind Dependent Ambient Noise Under
Midwinter Pack Ice"
J. Acoustical Society of Am. 38, 406-411 (1965)

BIBLIOGRAPHY
(cont'd)

18. Greene, C. R. and Buck, B. M. ,
"Arctic Ambient Noise"
J. Acoustical Society of Am. 36, 1218 (L) (1964)
19. Prentice, D. , Davis, E. and Kutschale, H. ,
"Natural and Man-Made Ice Vibrations in the Central Arctic
Ocean in the frequency range 0.1 to 100 cps. ",
Tech. Report #4, Lamont Geological Observatory, Palisades,
New York (1965)

A

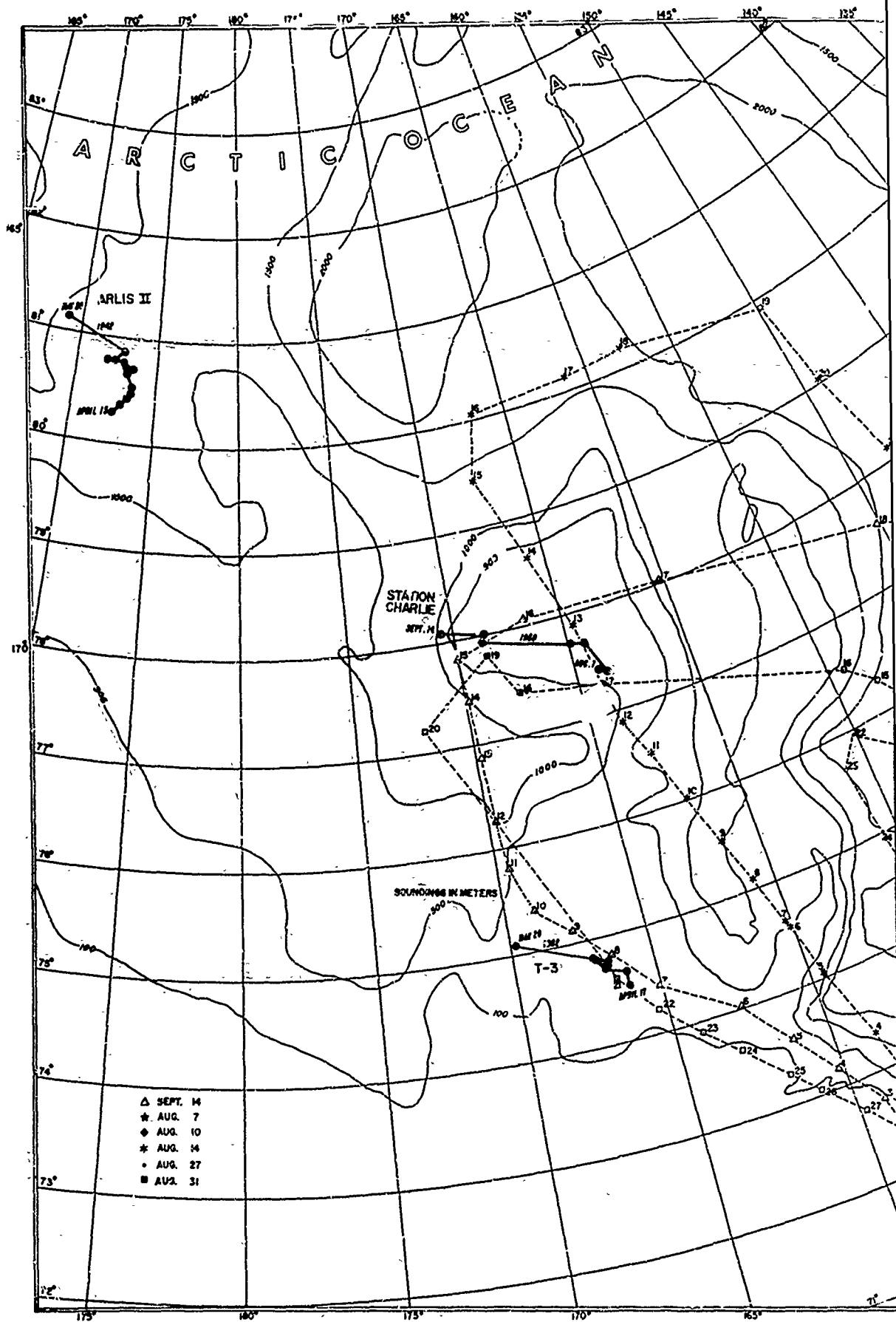
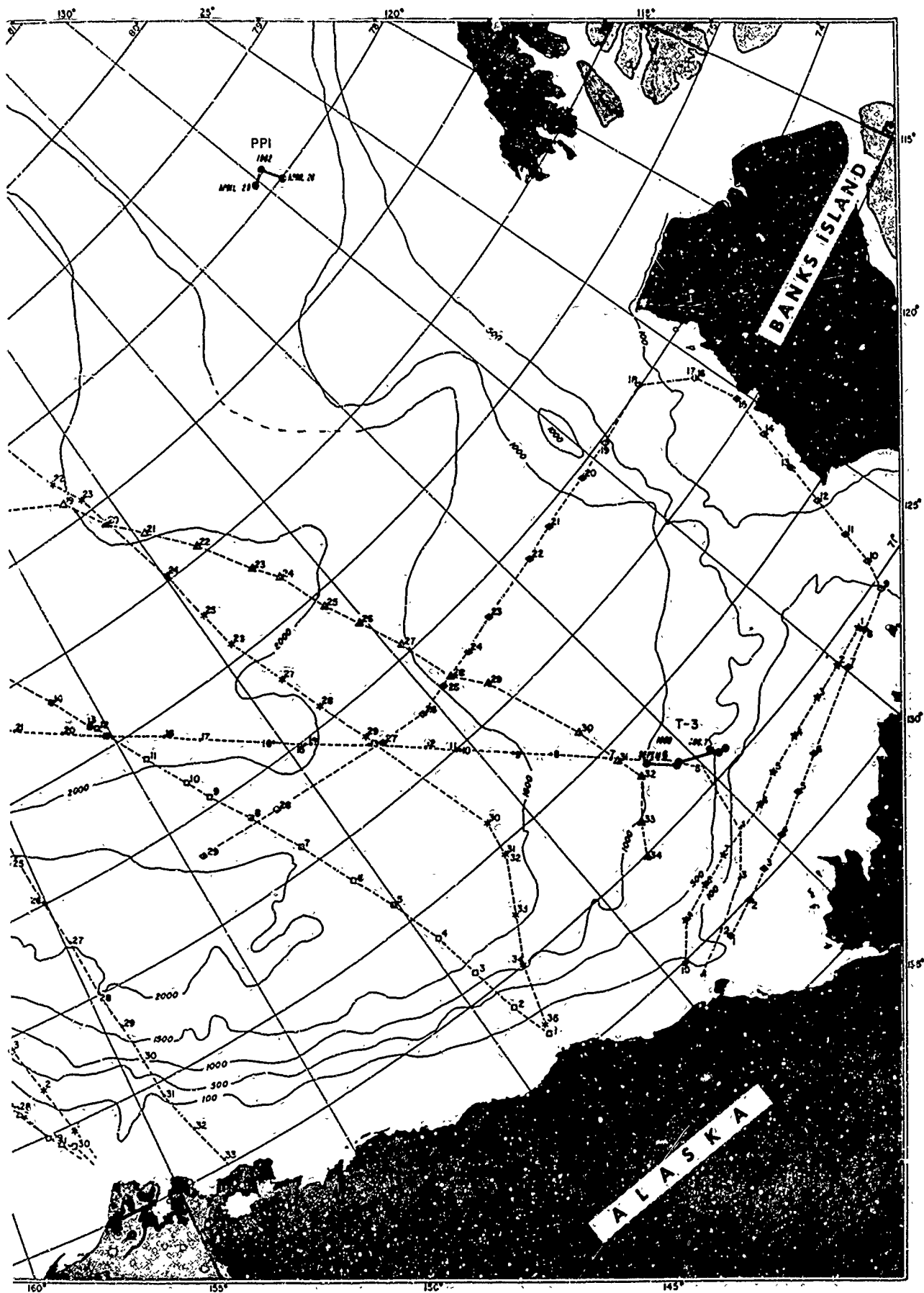


FIGURE I. DRAFT STATION LOC



ATIONS AND AIRCRAFT TRACKS

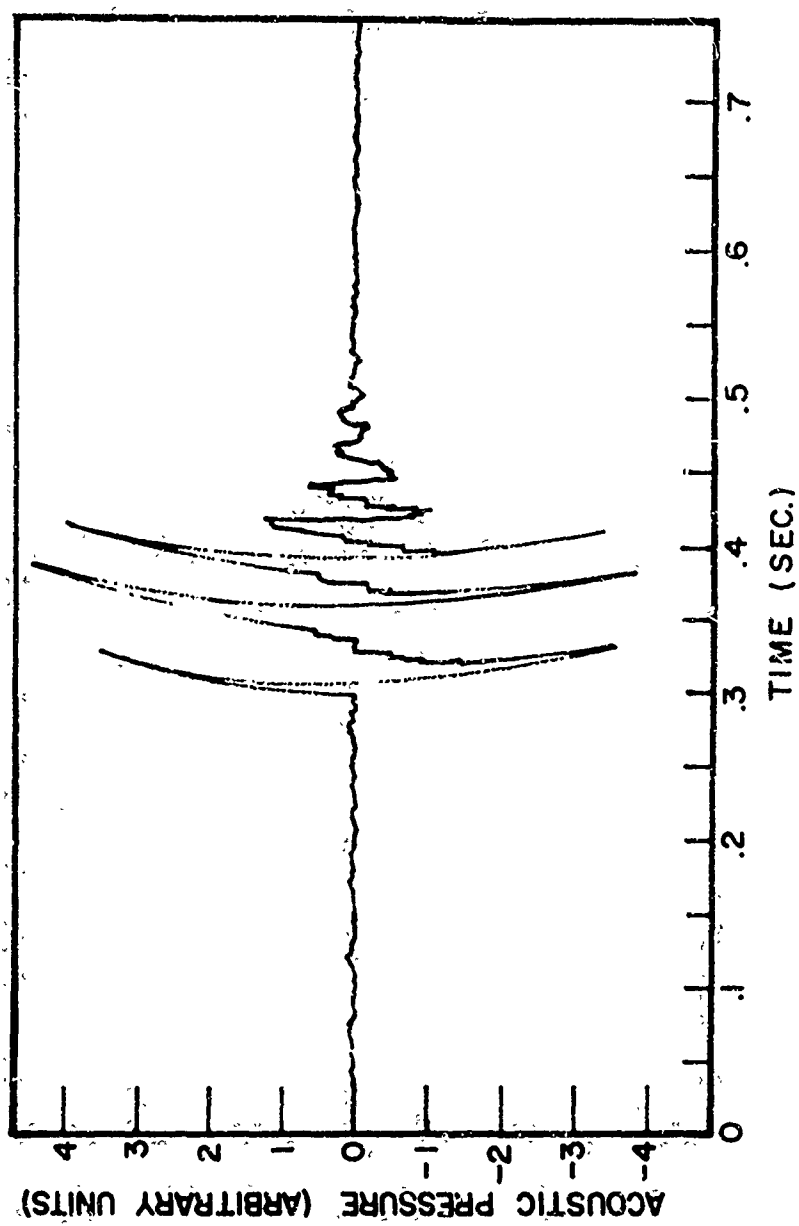


FIGURE 2 LOCAL SHOT PRESSURE SIGNATURE

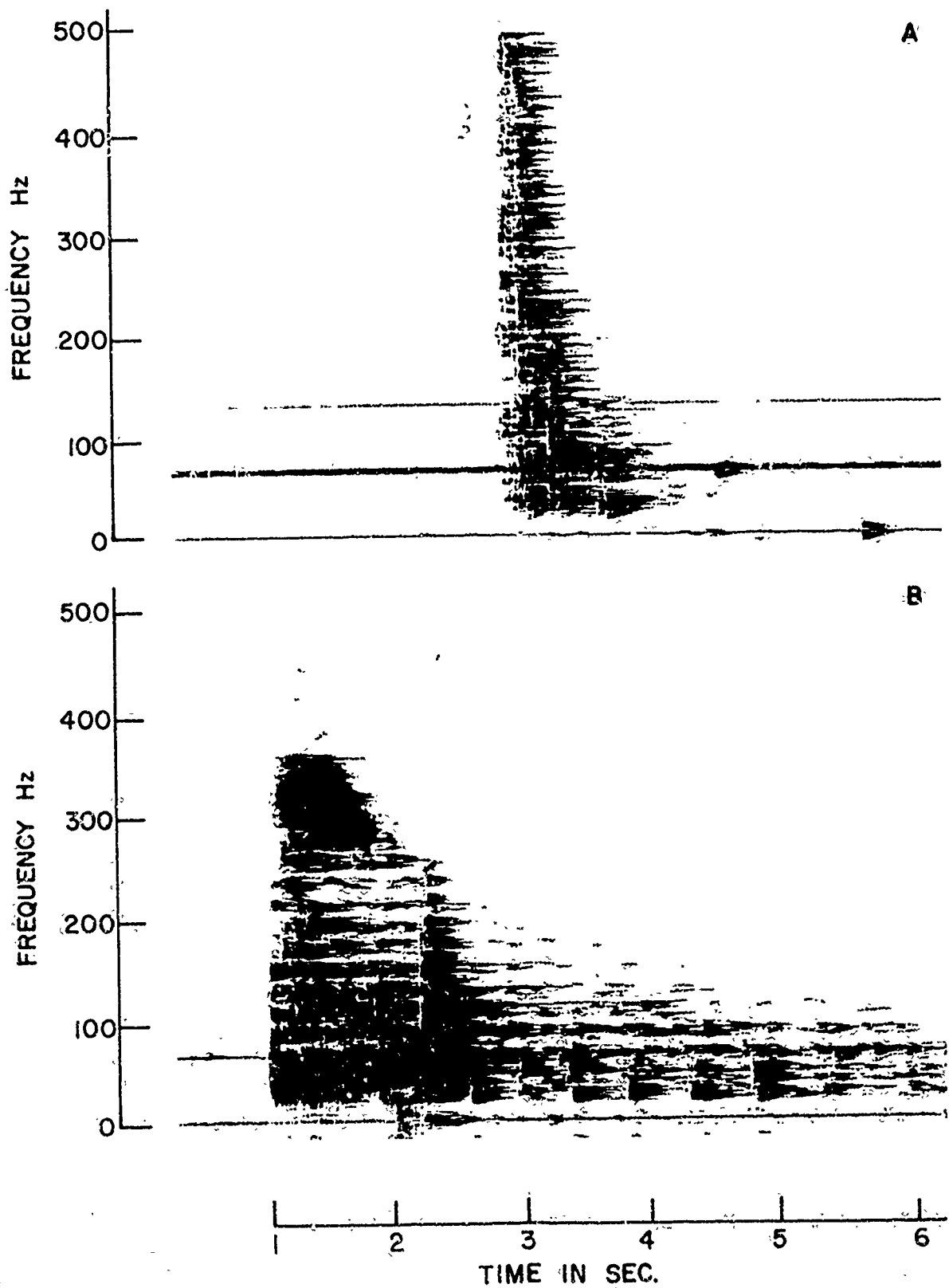


FIGURE 3

LOCAL SHOT MISSILYZER SPECTRA

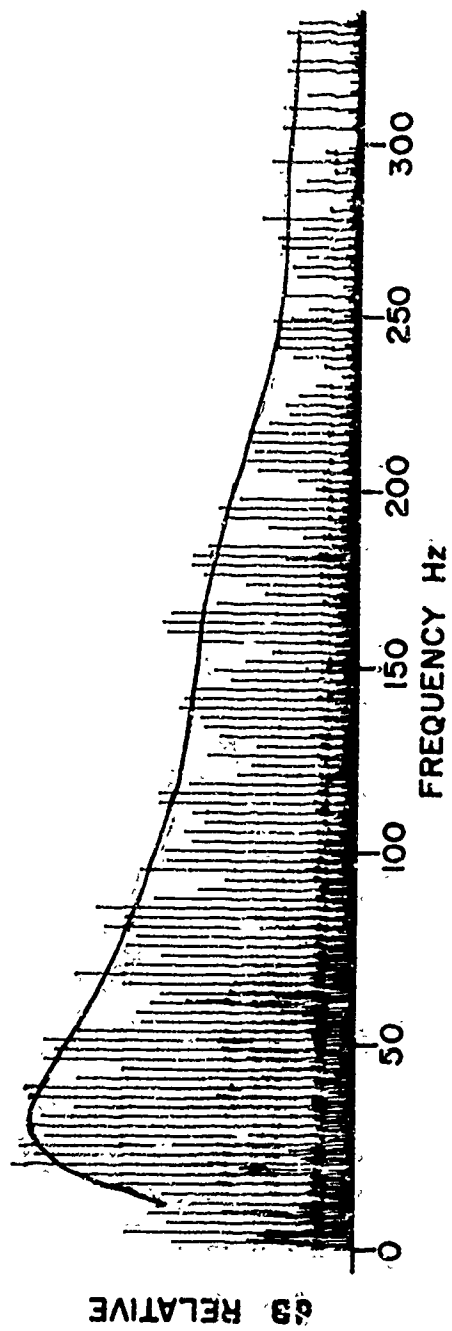


FIGURE 4 NARROW BAND ANALYSIS SPECTRUM

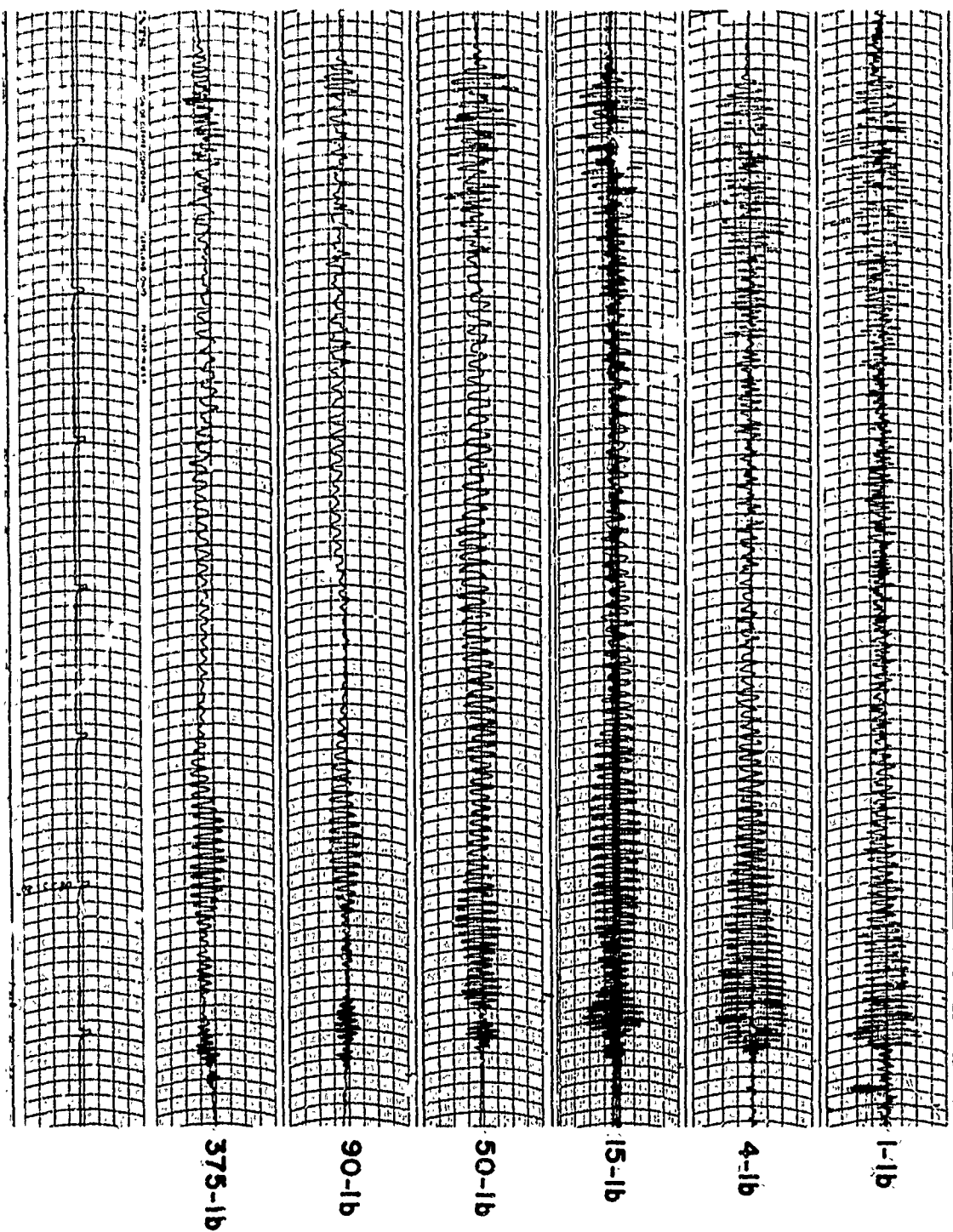


FIGURE 5
LONG RANGE GRAPHIC RECORDINGS

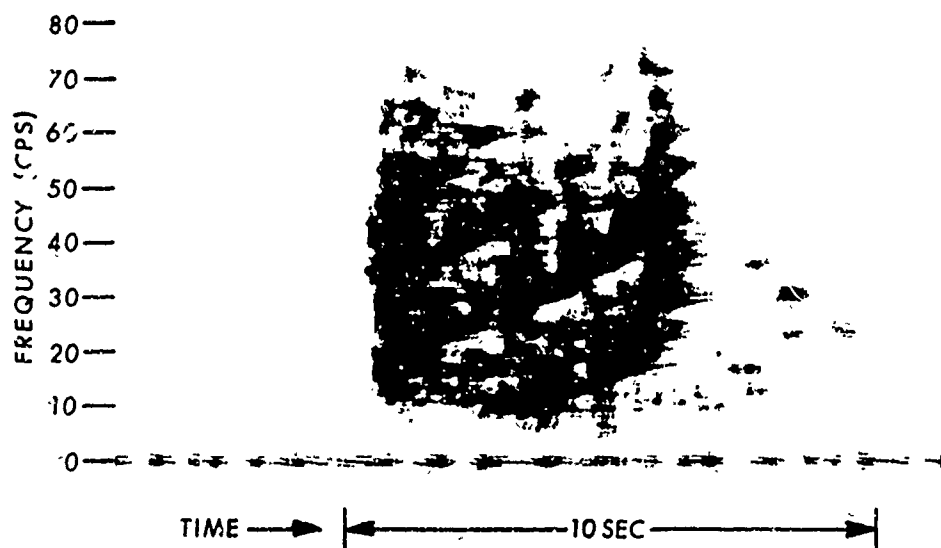
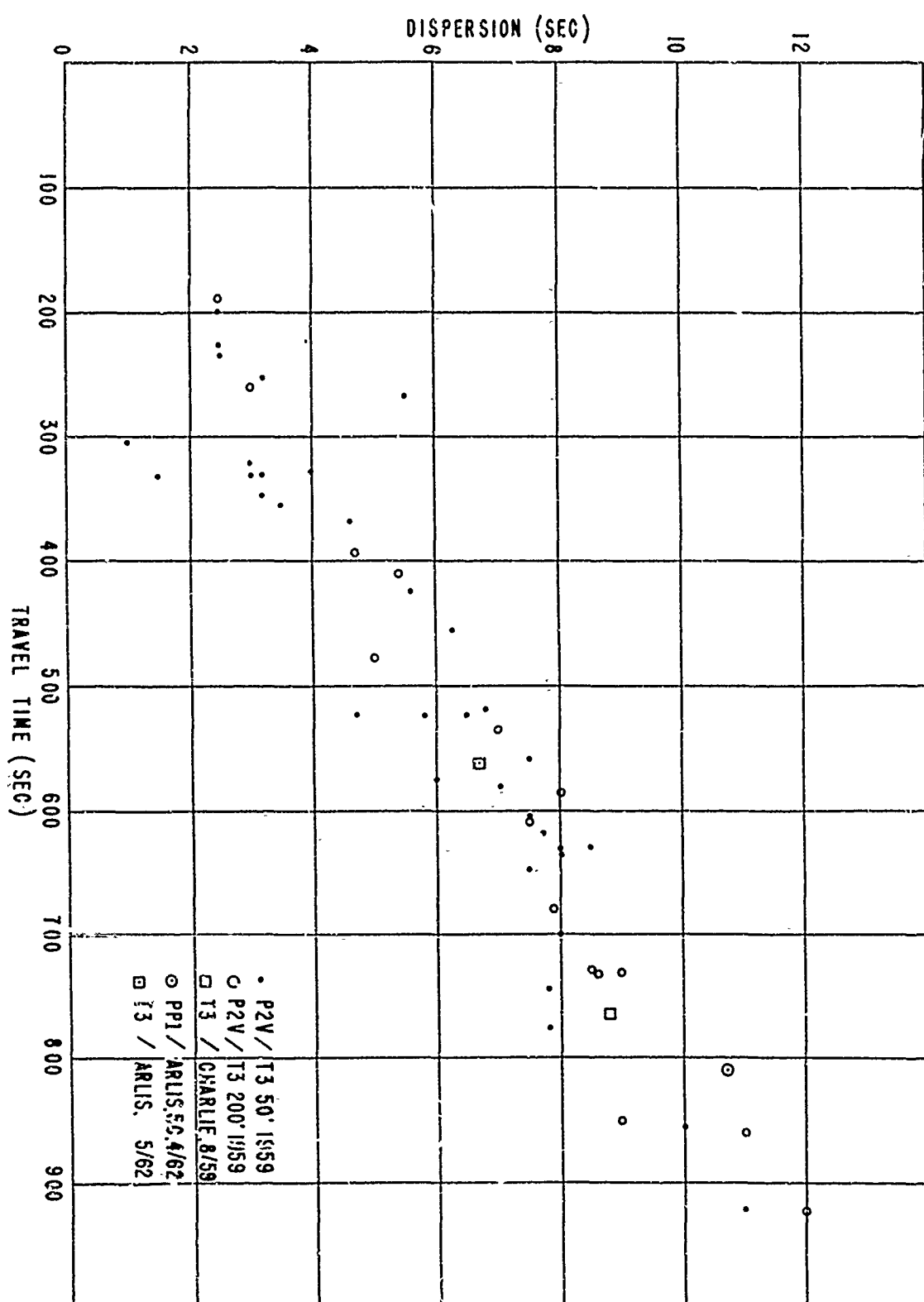


FIGURE 6 LONG RANGE MISSILE SPECTRA

FIGURE 7

DISPERSION TIME VS TRAVEL TIME



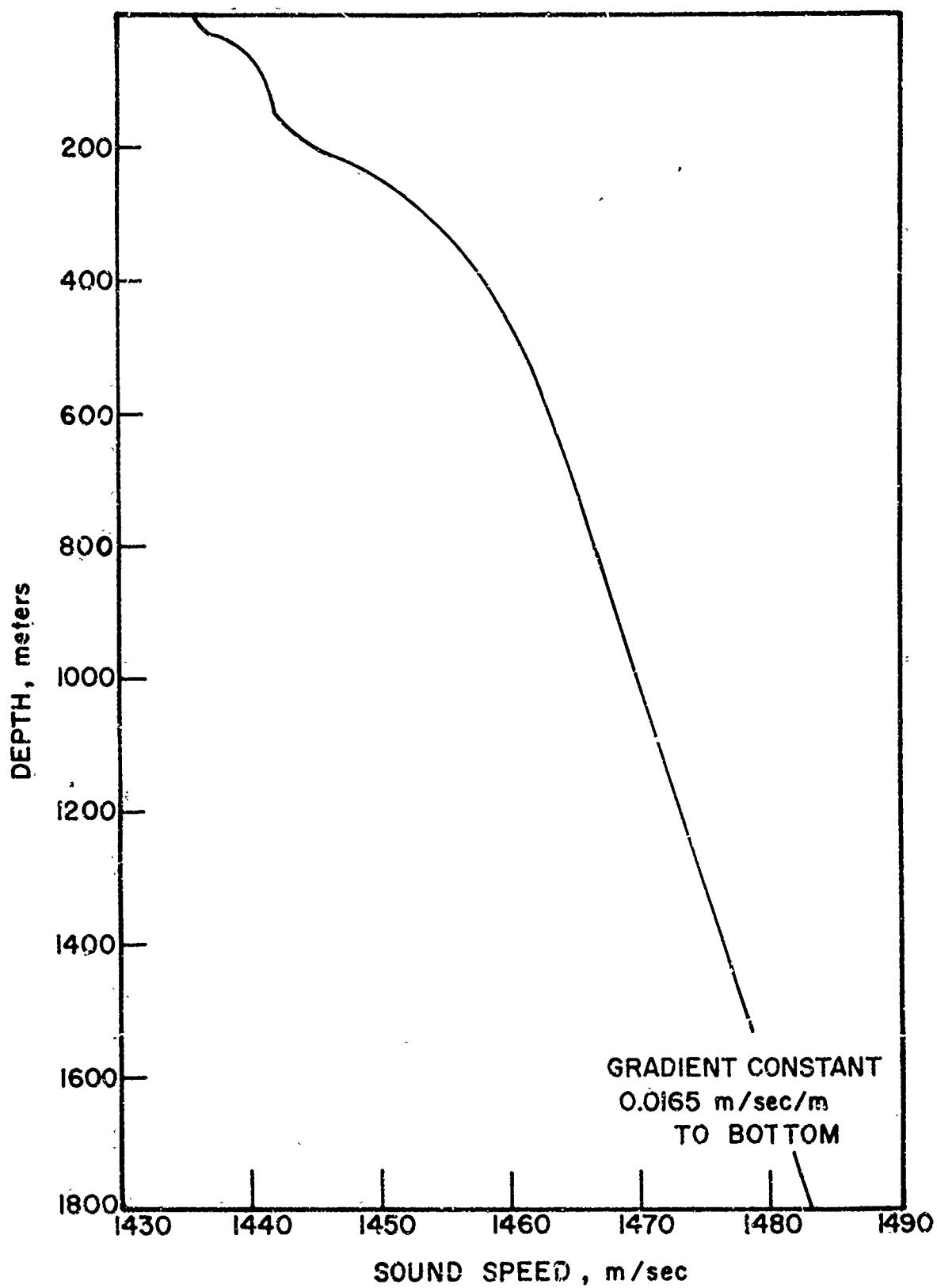


FIGURE 8

SOUND VELOCITY PROFILE

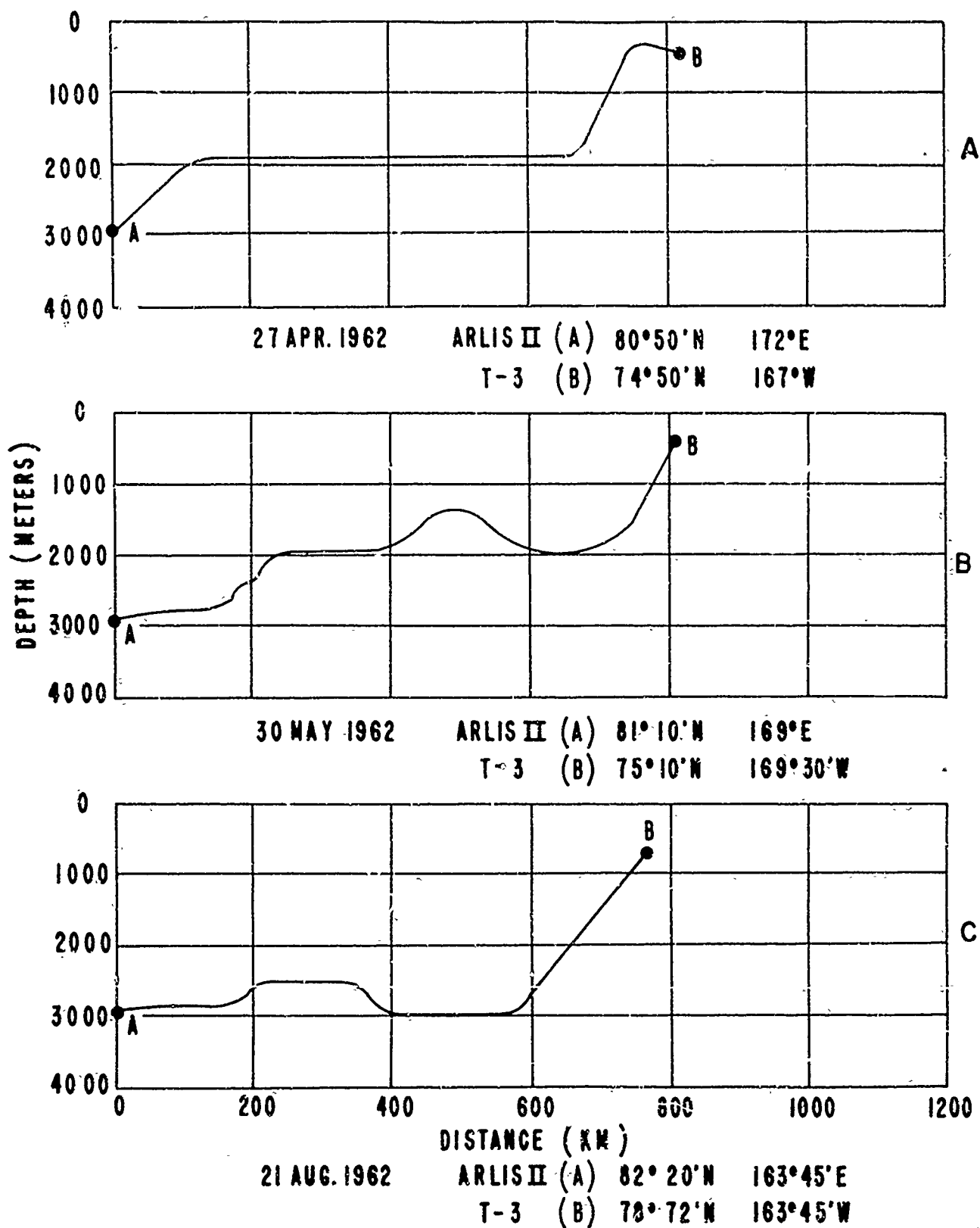
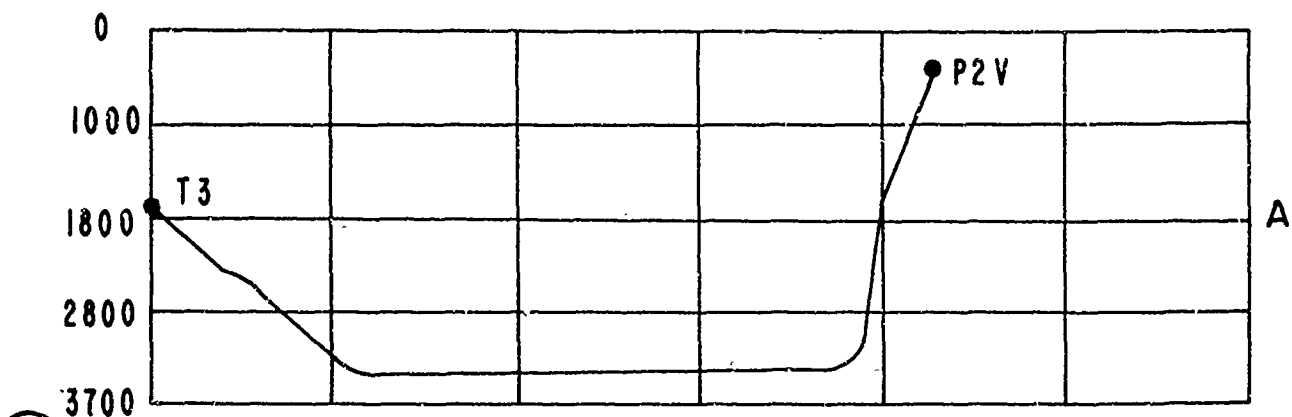


FIGURE 9 BOTTOM PROFILES

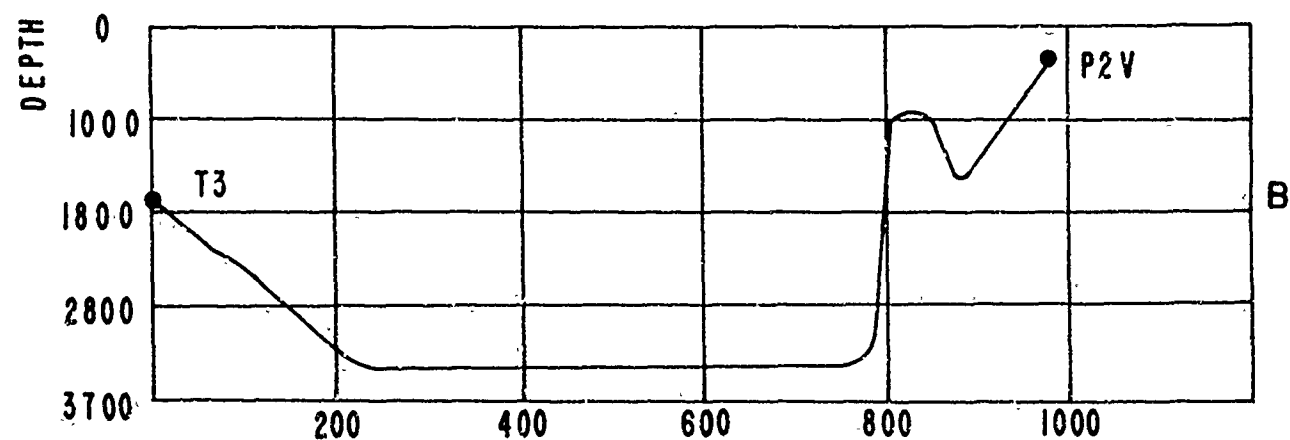


9/14/59

T3/P2V

P2V 73° 36' N 161° 20' W

T3 71° 38' N 138 10' W



9/14/59

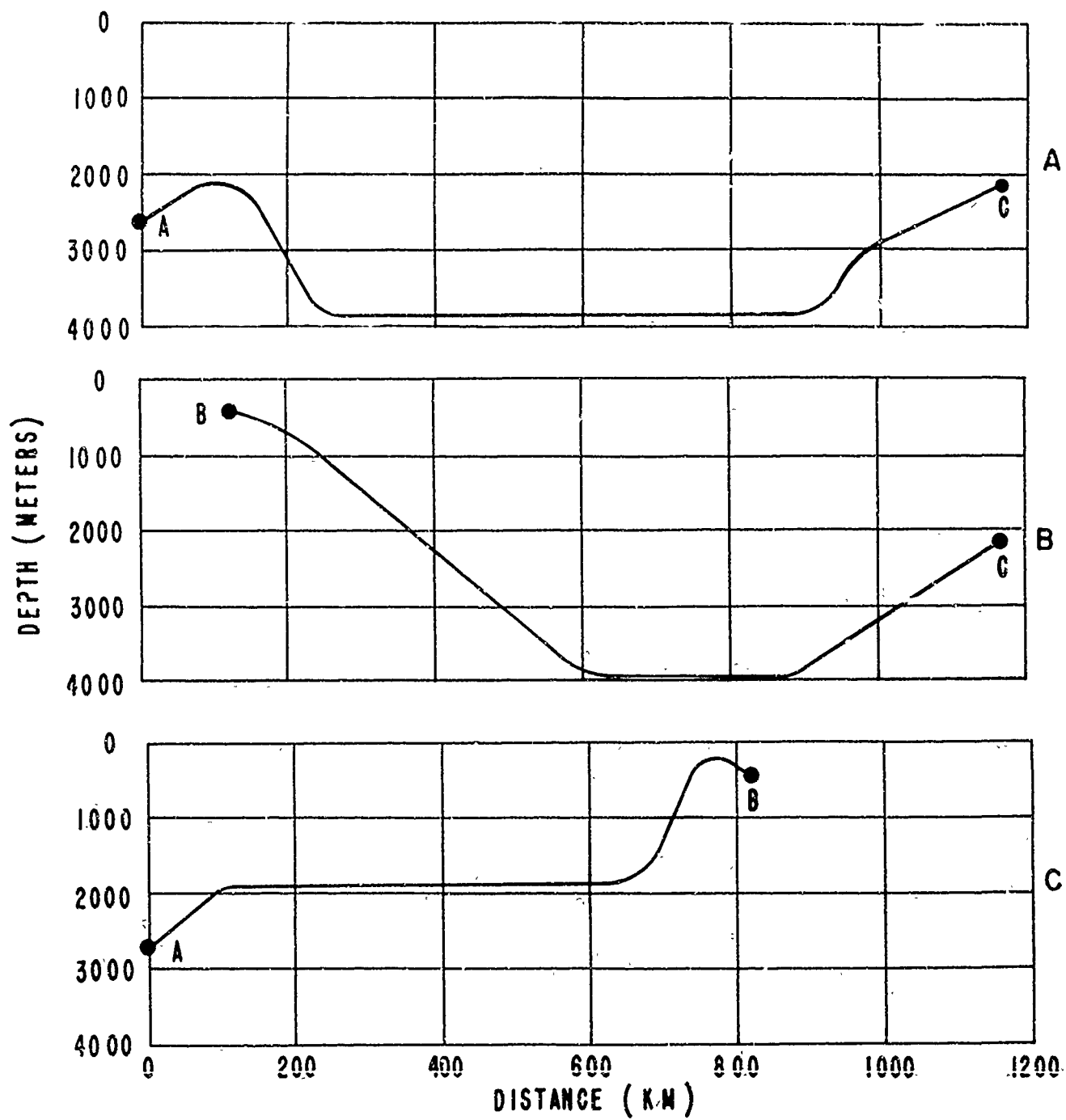
T3/P2V

P2V 74° 26' N 165° 02' W

T3 71° 38' N 136 10' W

FIGURE 10

BOTTOM PROFILES



27 APR. 1962

A - ARLIS II	80° 50' N	172° E
B - T3	74° 50' N	167° W
C - PPI	78° 10' N	130° W

FIGURE 11 BOTTOM PROFILES

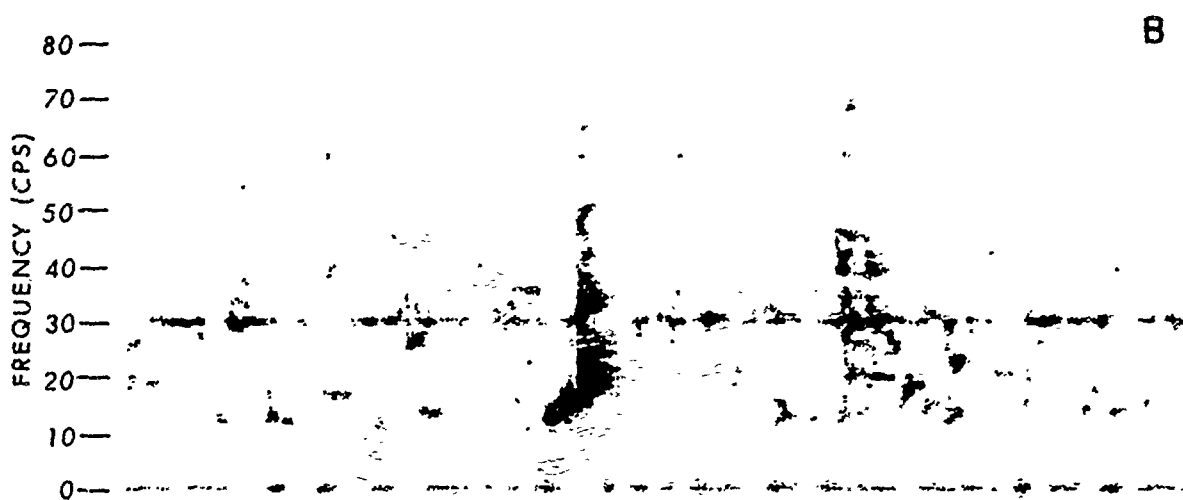
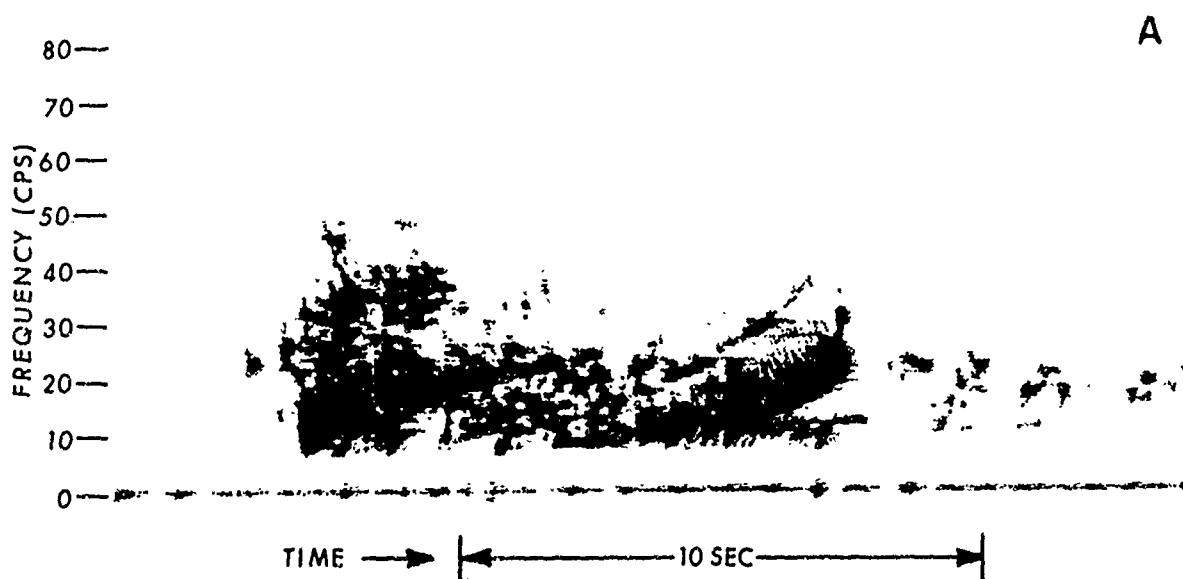
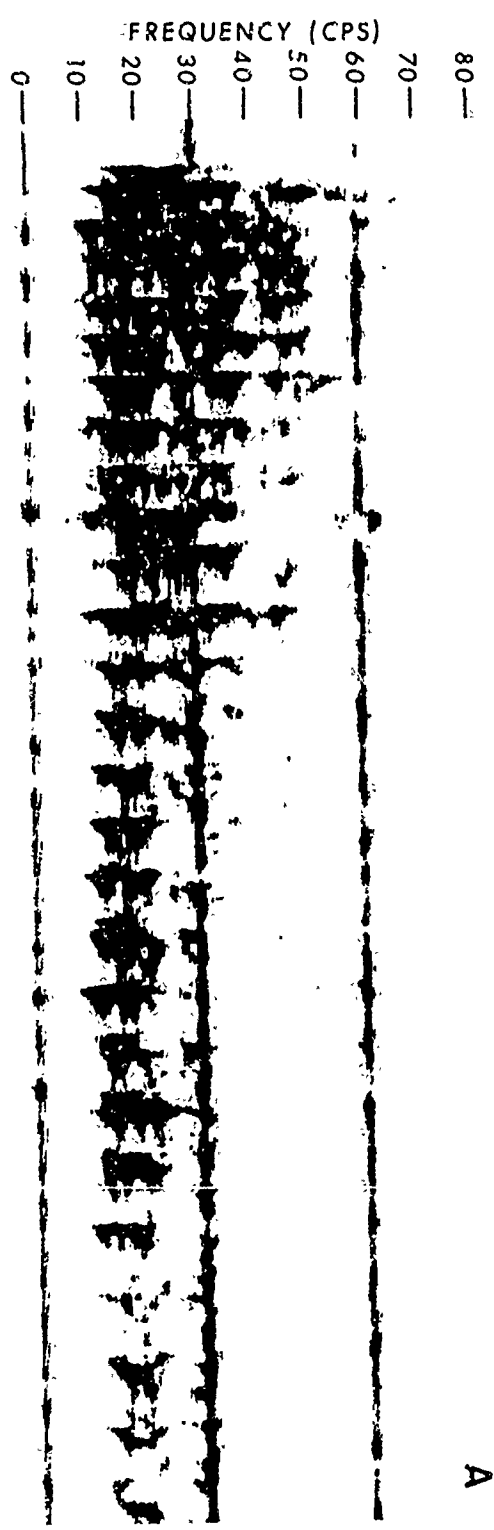
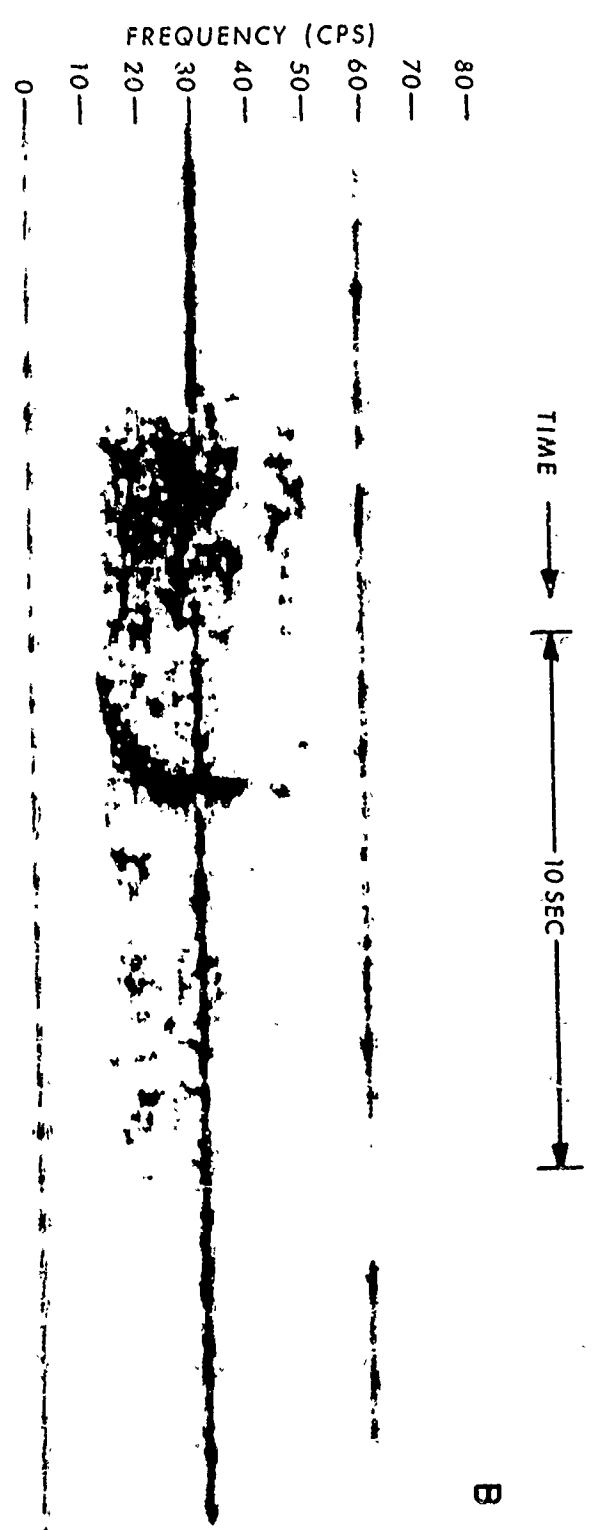


FIGURE 12

MISSILYZER SPECTRA



A



B

FIGURE 13 MISSILYZER SPECTRA (A SHOWS BOTTOM ARRIVALS)

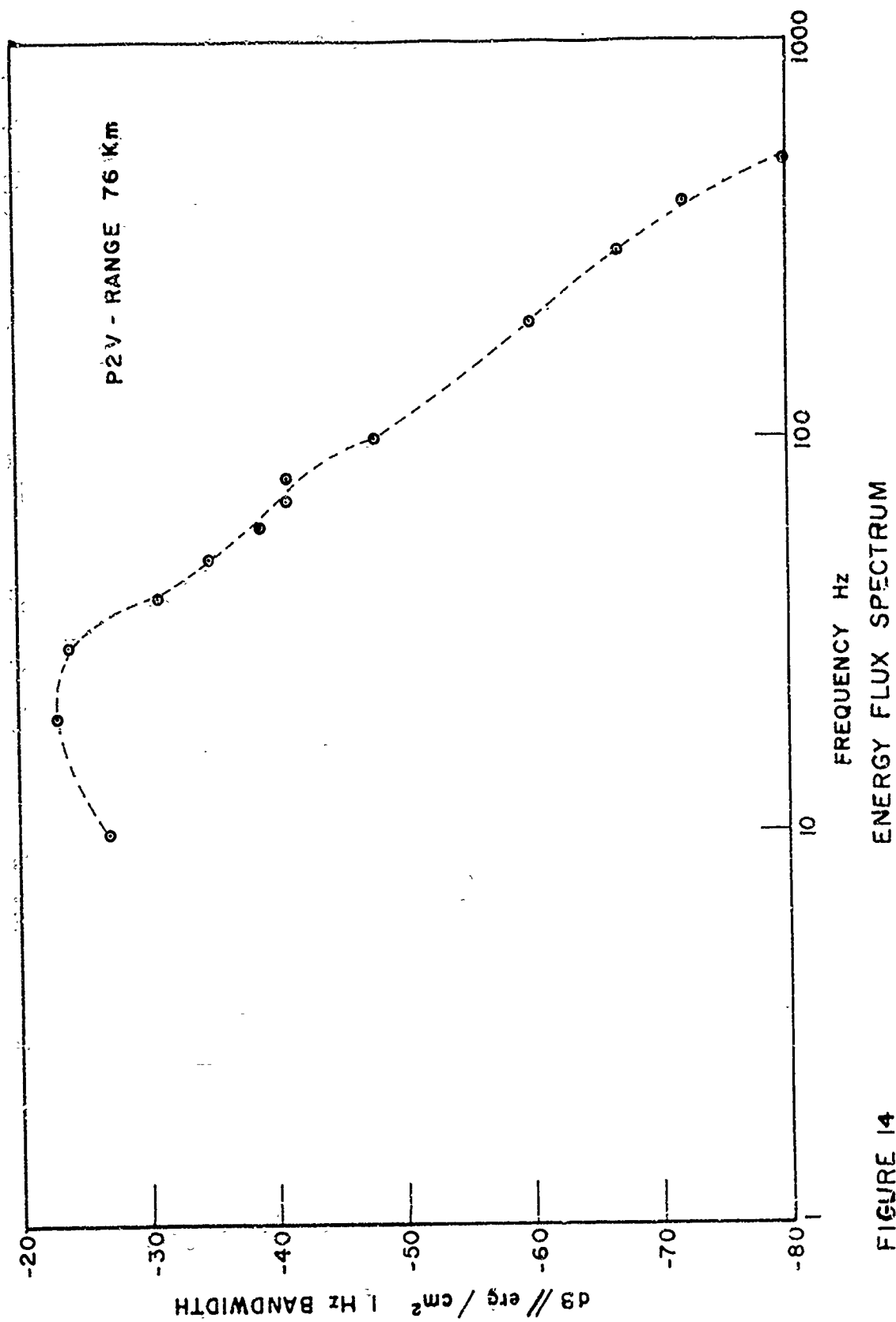
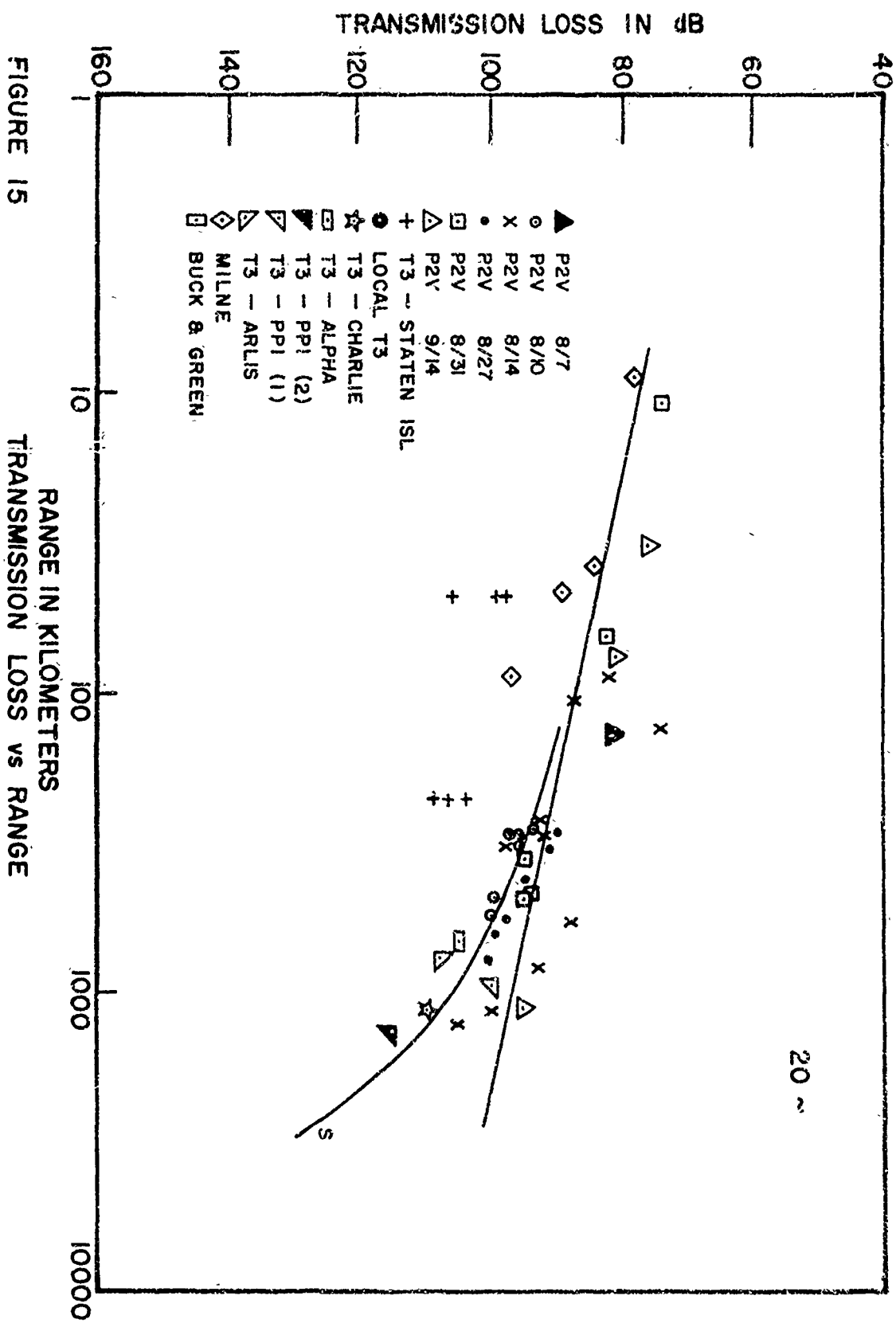
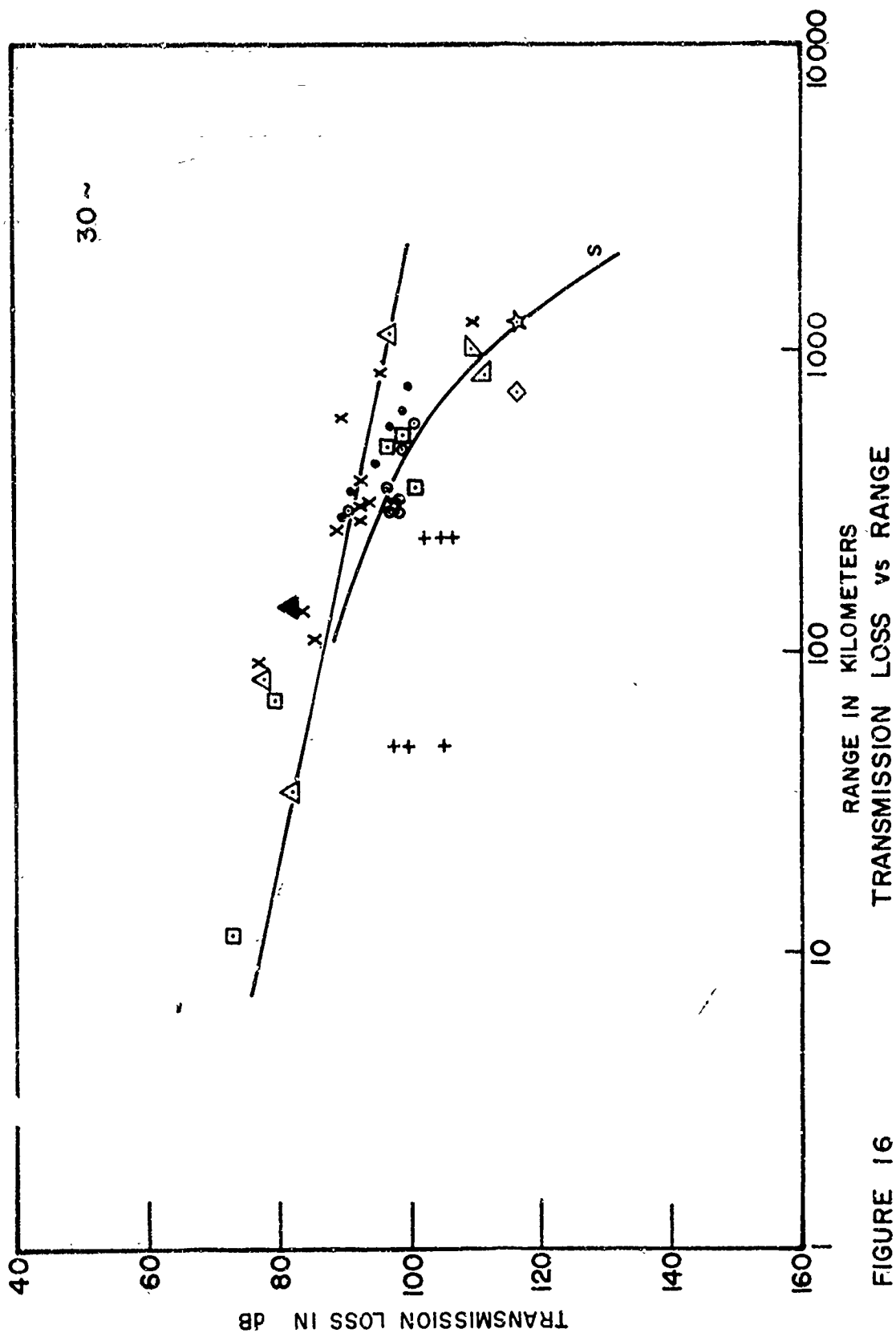
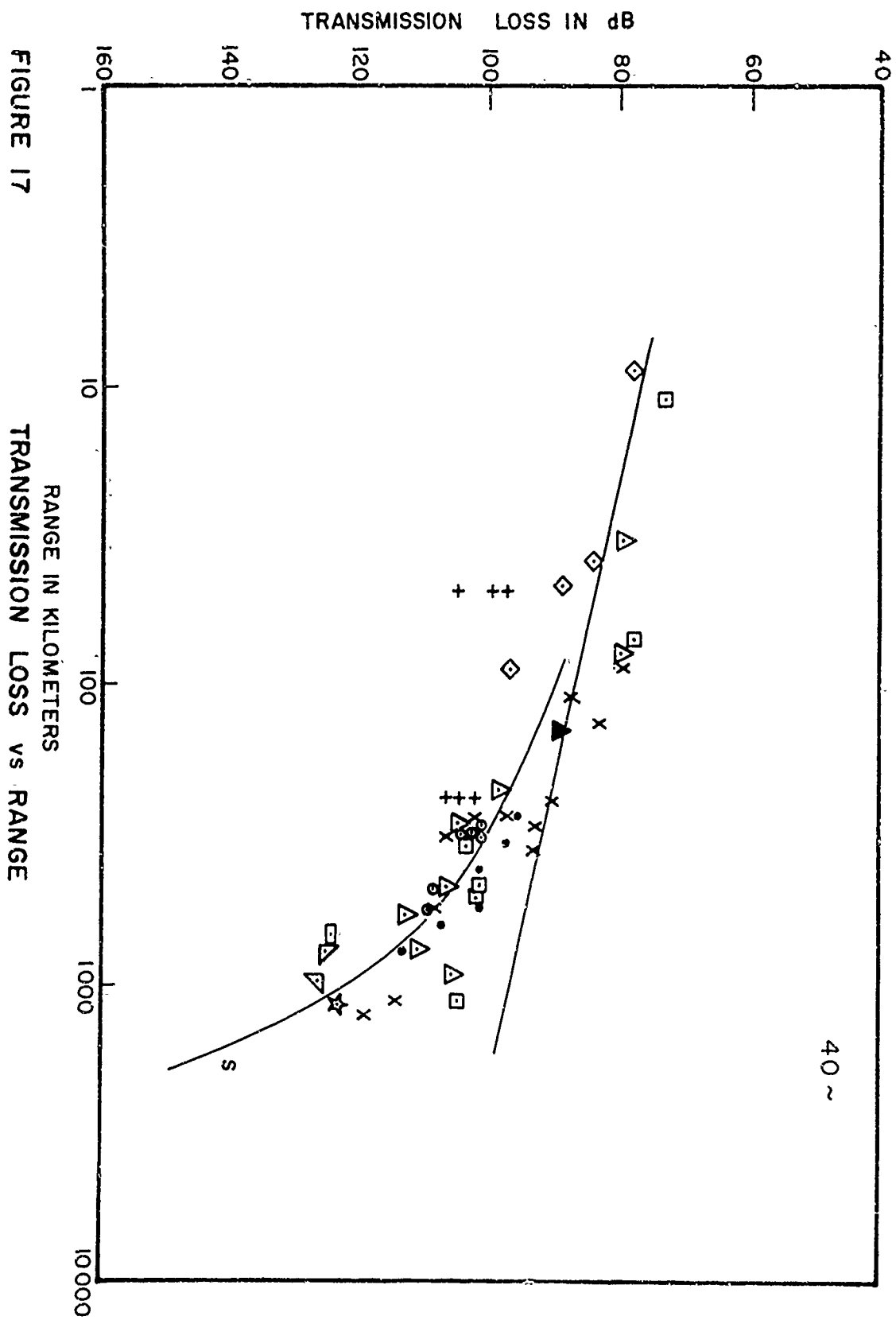


FIGURE 14







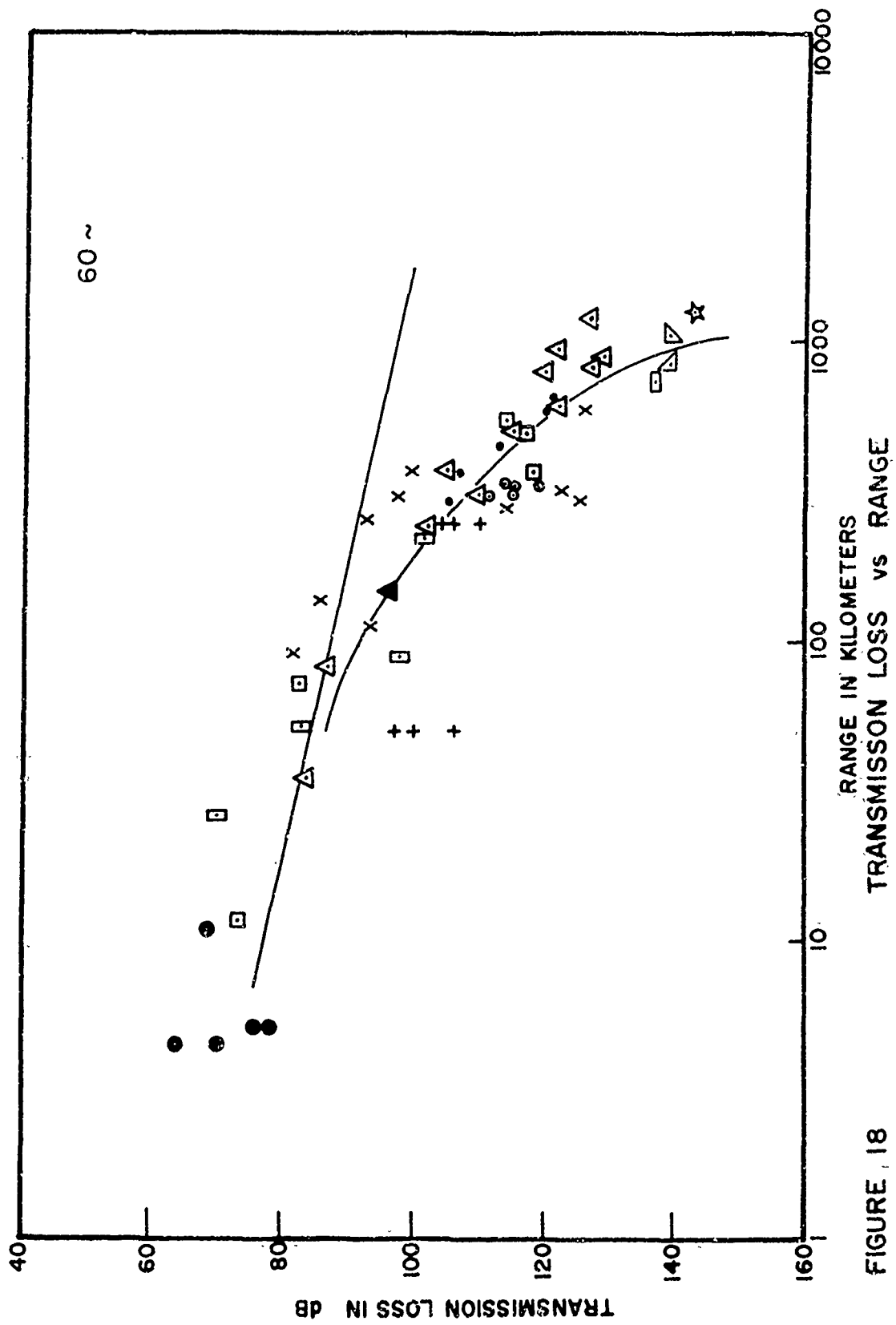


FIGURE 18

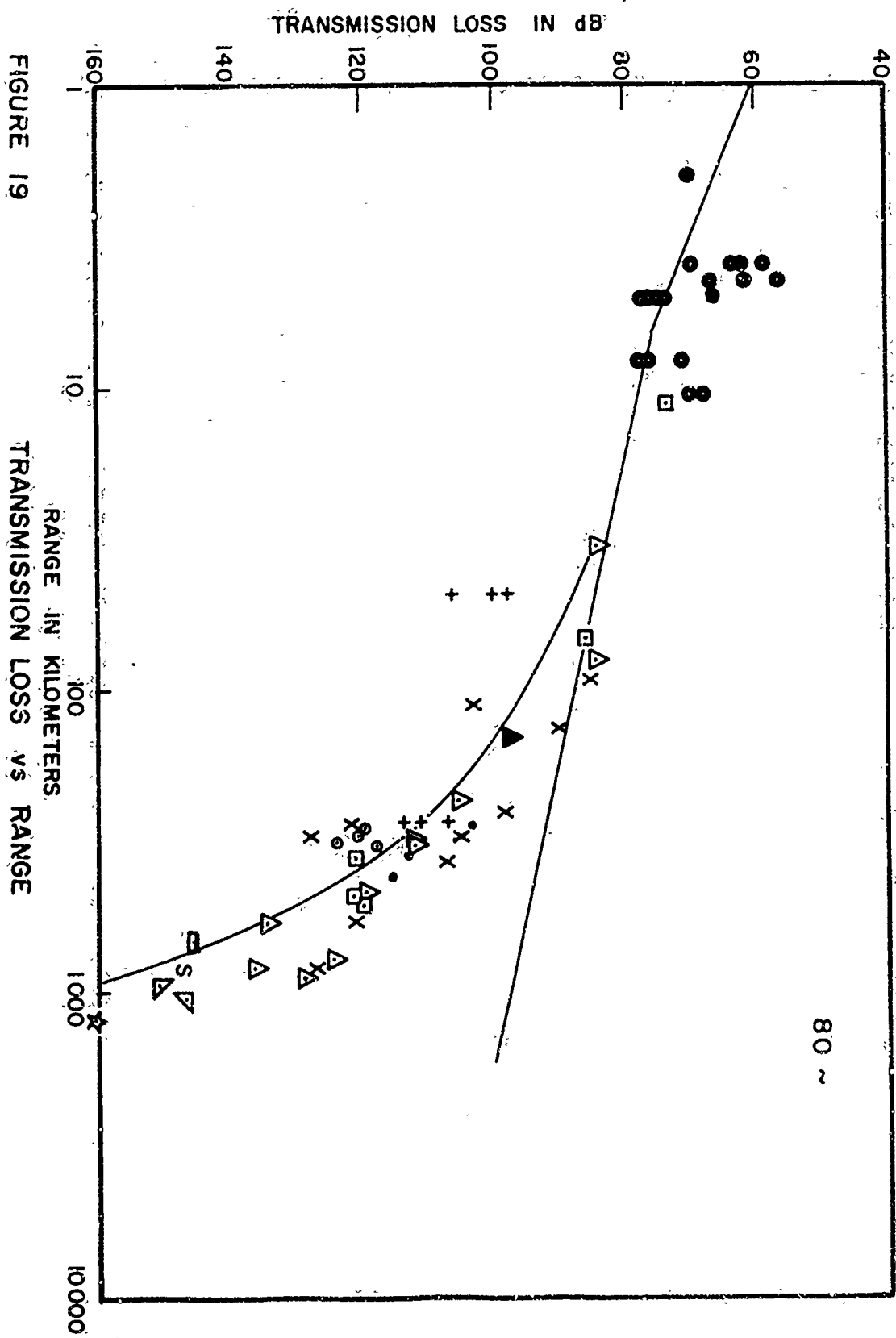


FIGURE 19

RANGE IN KILOMETERS
TRANSMISSION LOSS vs RANGE

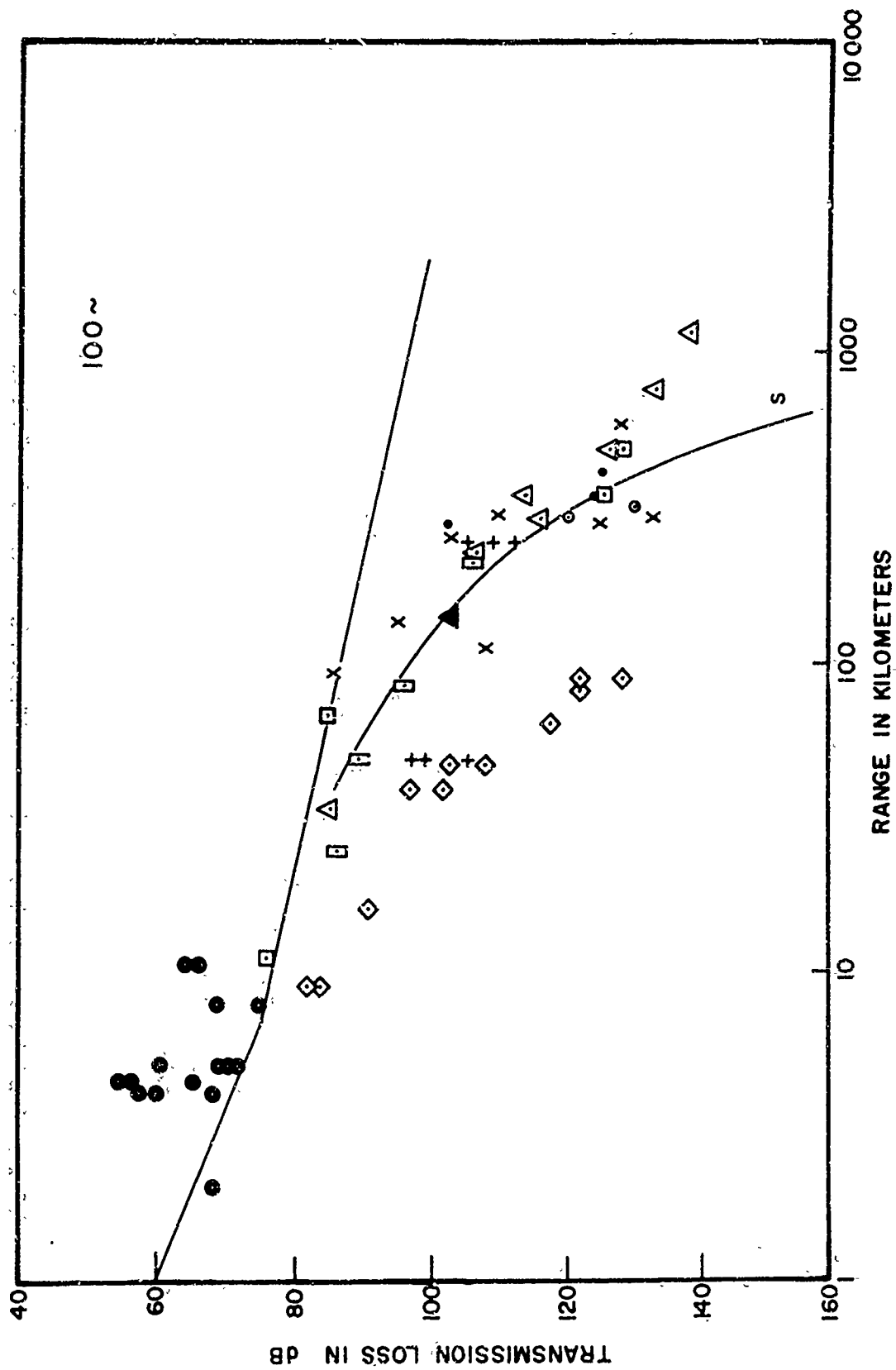


FIGURE 20 RANGE IN KILOMETERS , TRANSMISSION LOSS vs RANGE

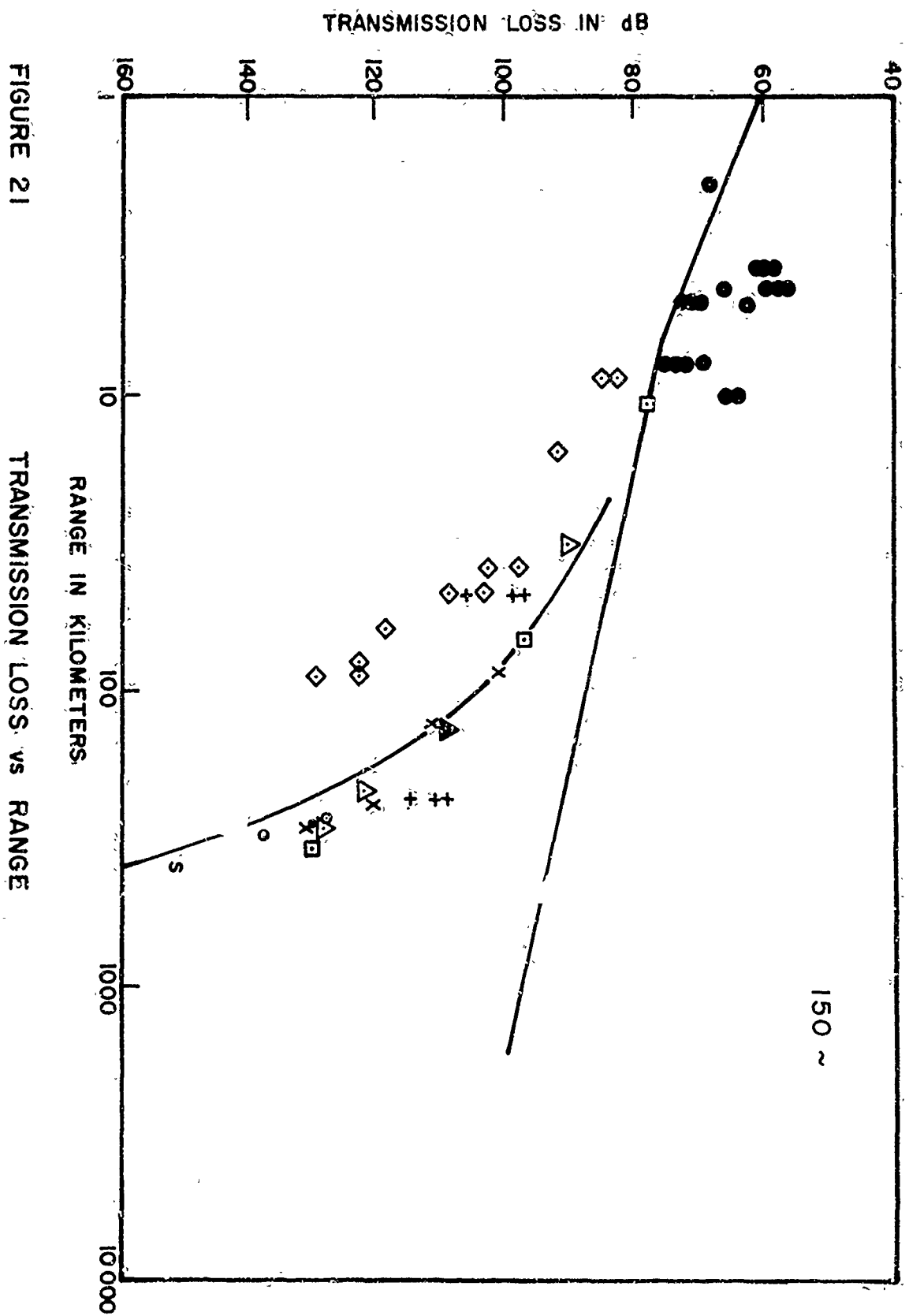
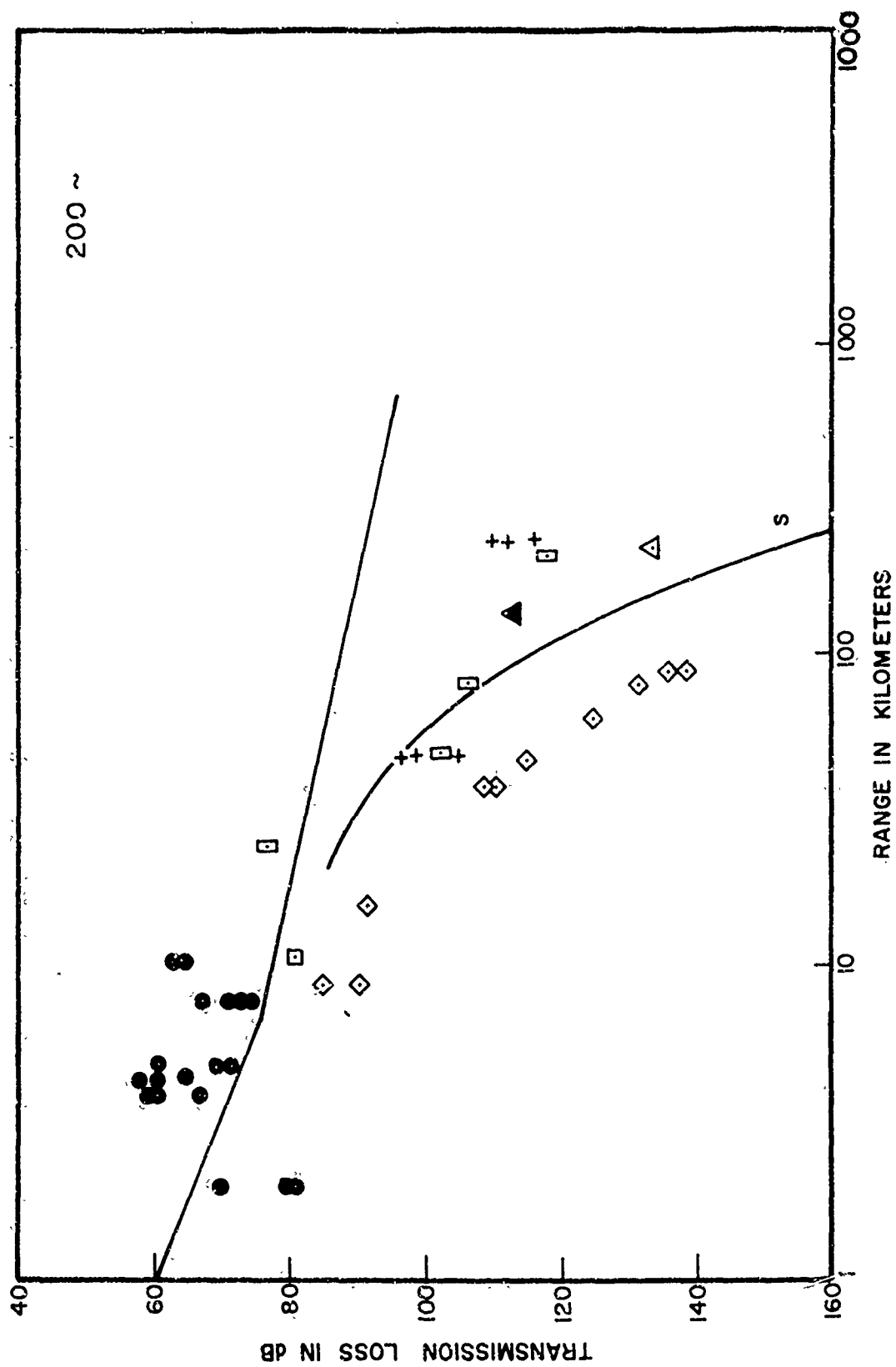


FIGURE 21

TRANSMISSION LOSS vs RANGE



TRANSMISSION LOSS vs RANGE

FIGURE 22

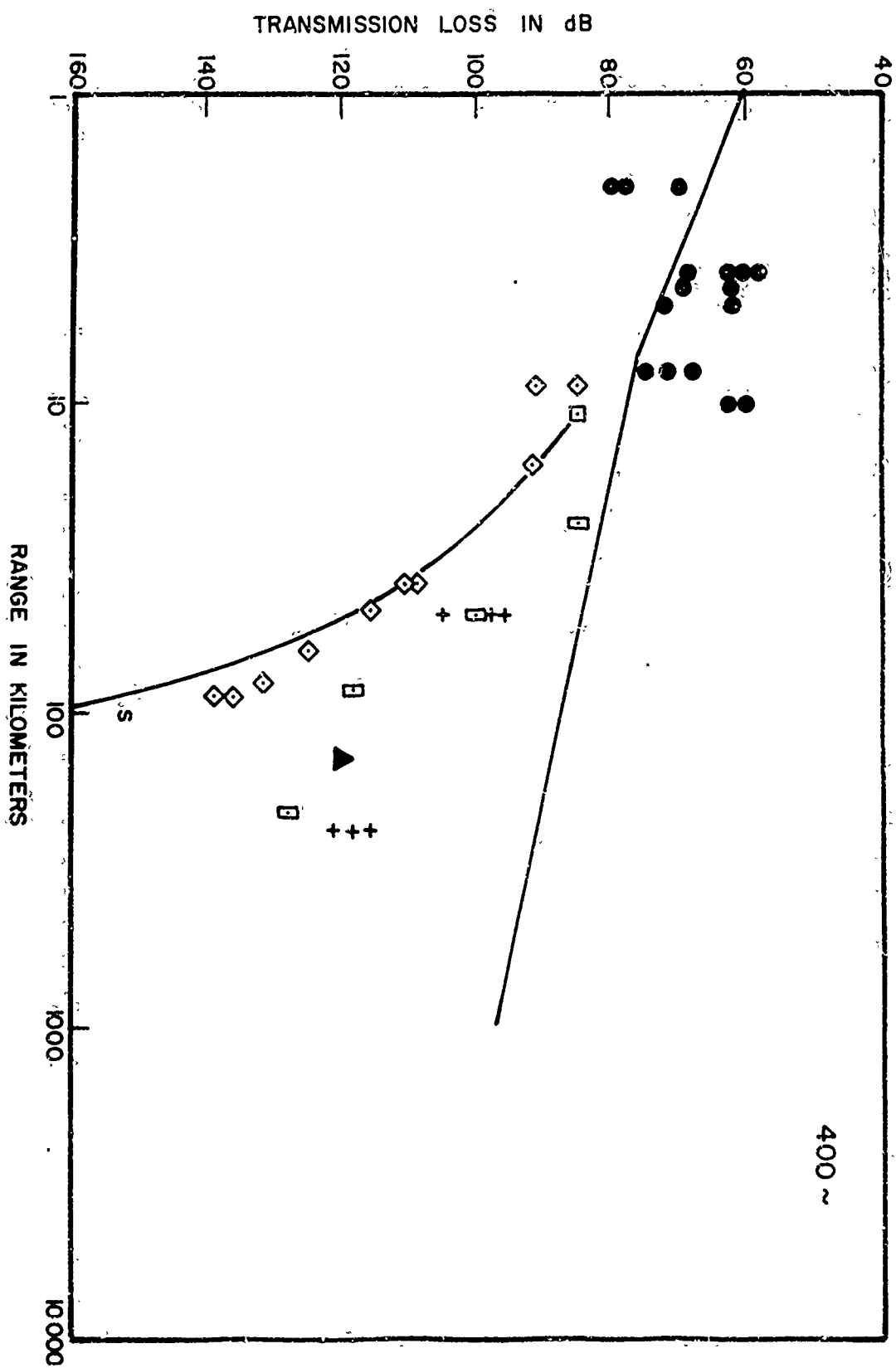
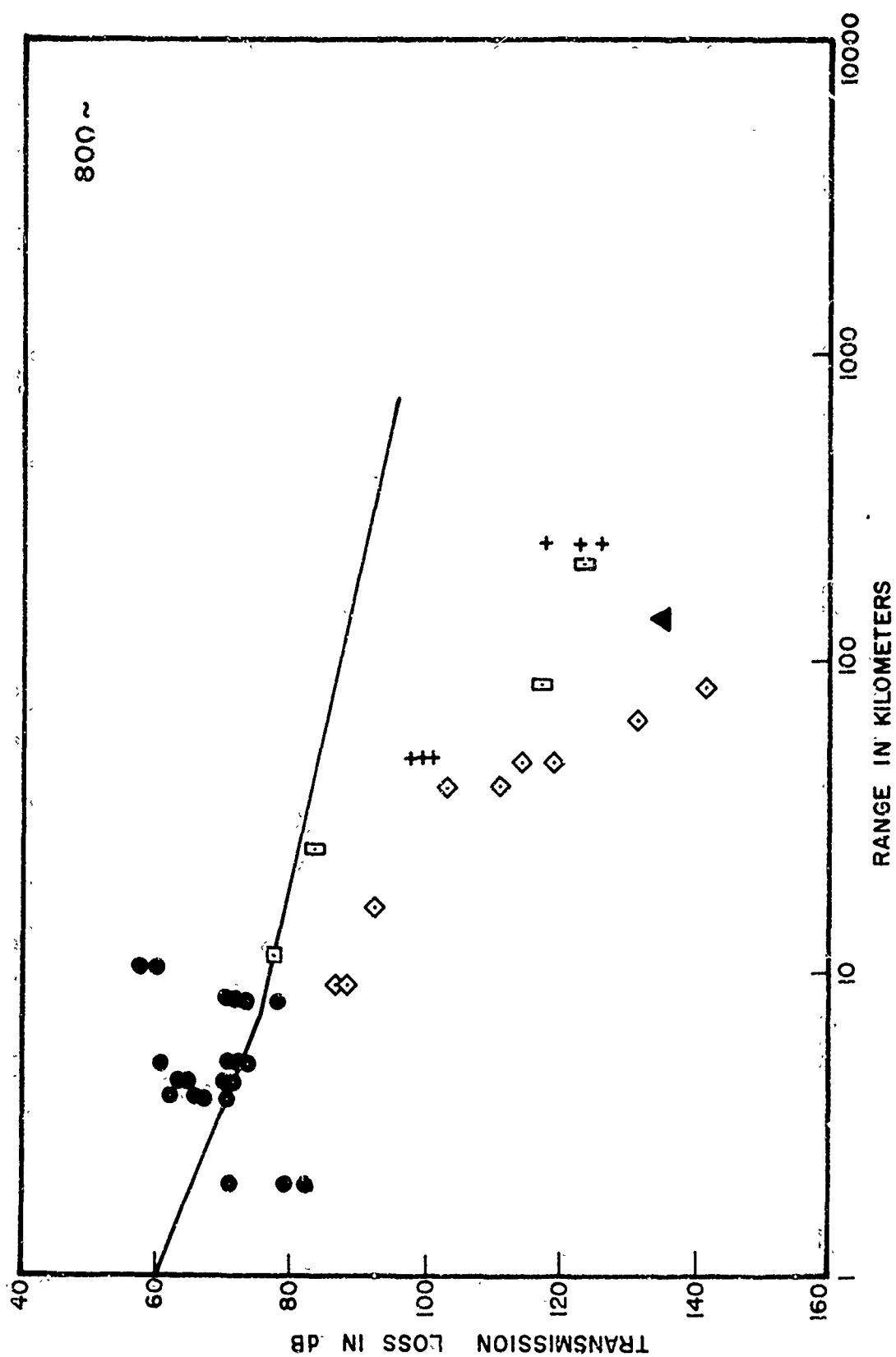


FIGURE 23

TRANSMISSION LOSS VS RANGE

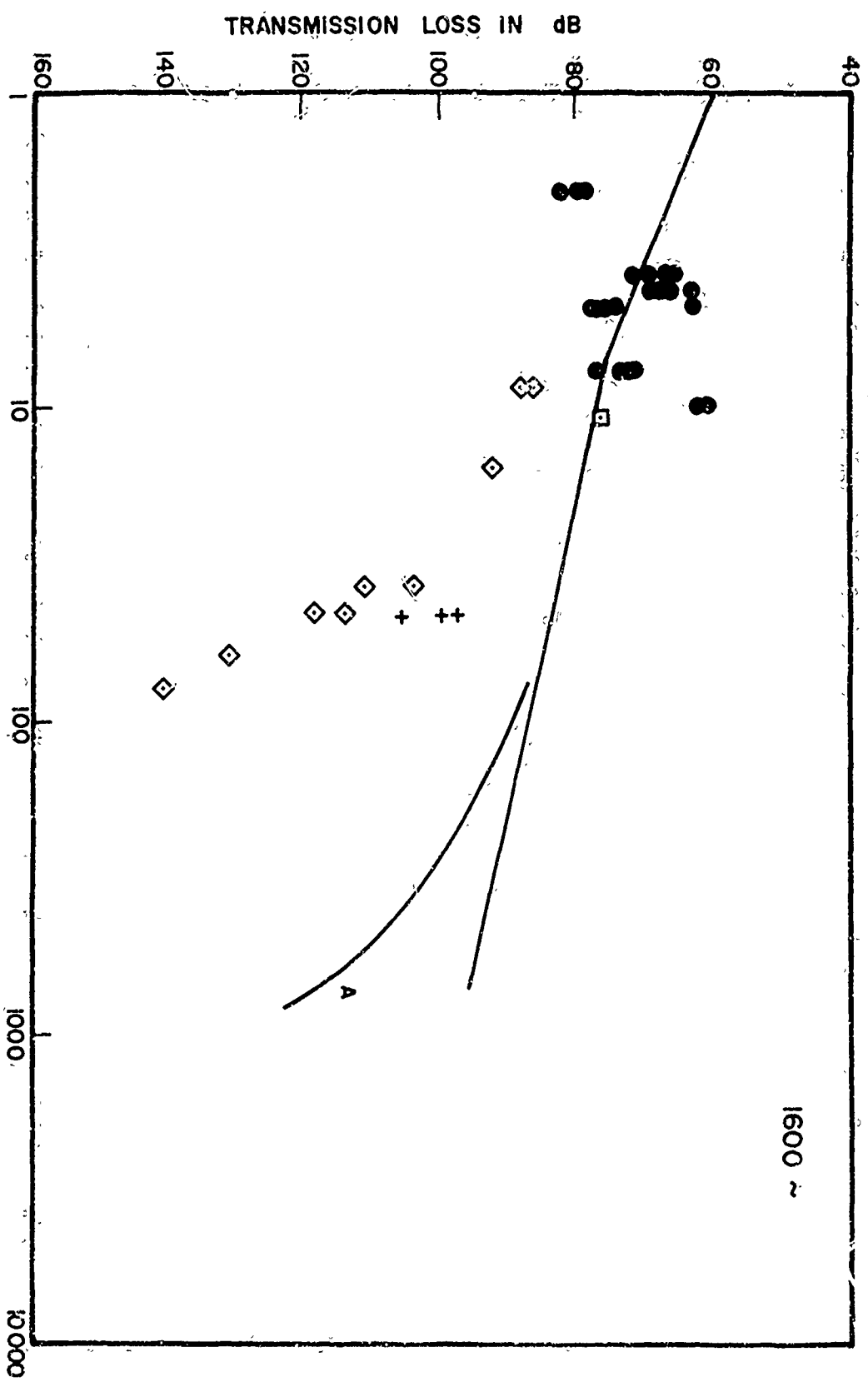


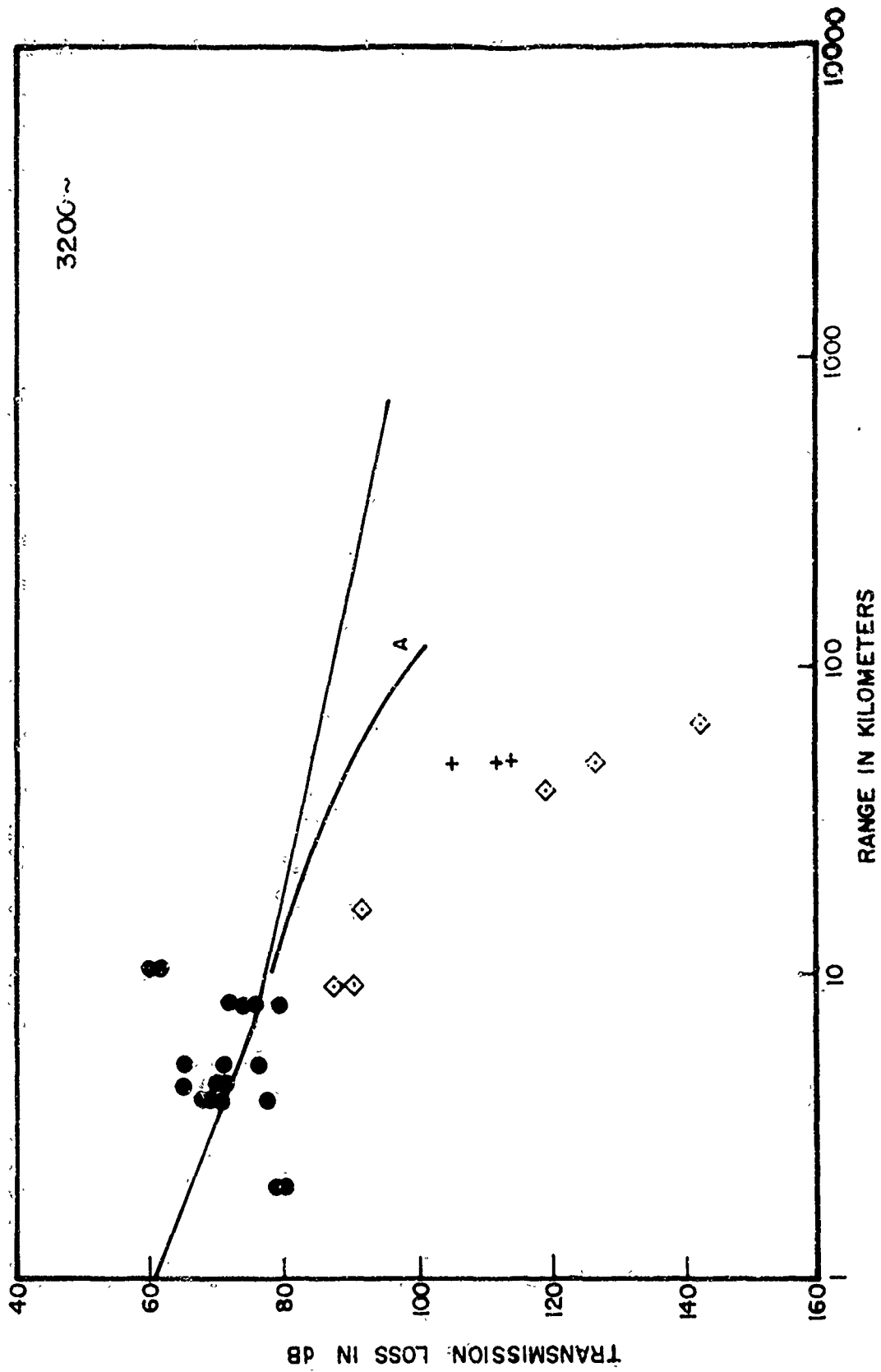
TRANSMISSION LOSS vs RANGE

FIGURE 24

FIGURE 25

RANGE IN KILOMETERS
TRANSMISSION LOSS VS RANGE



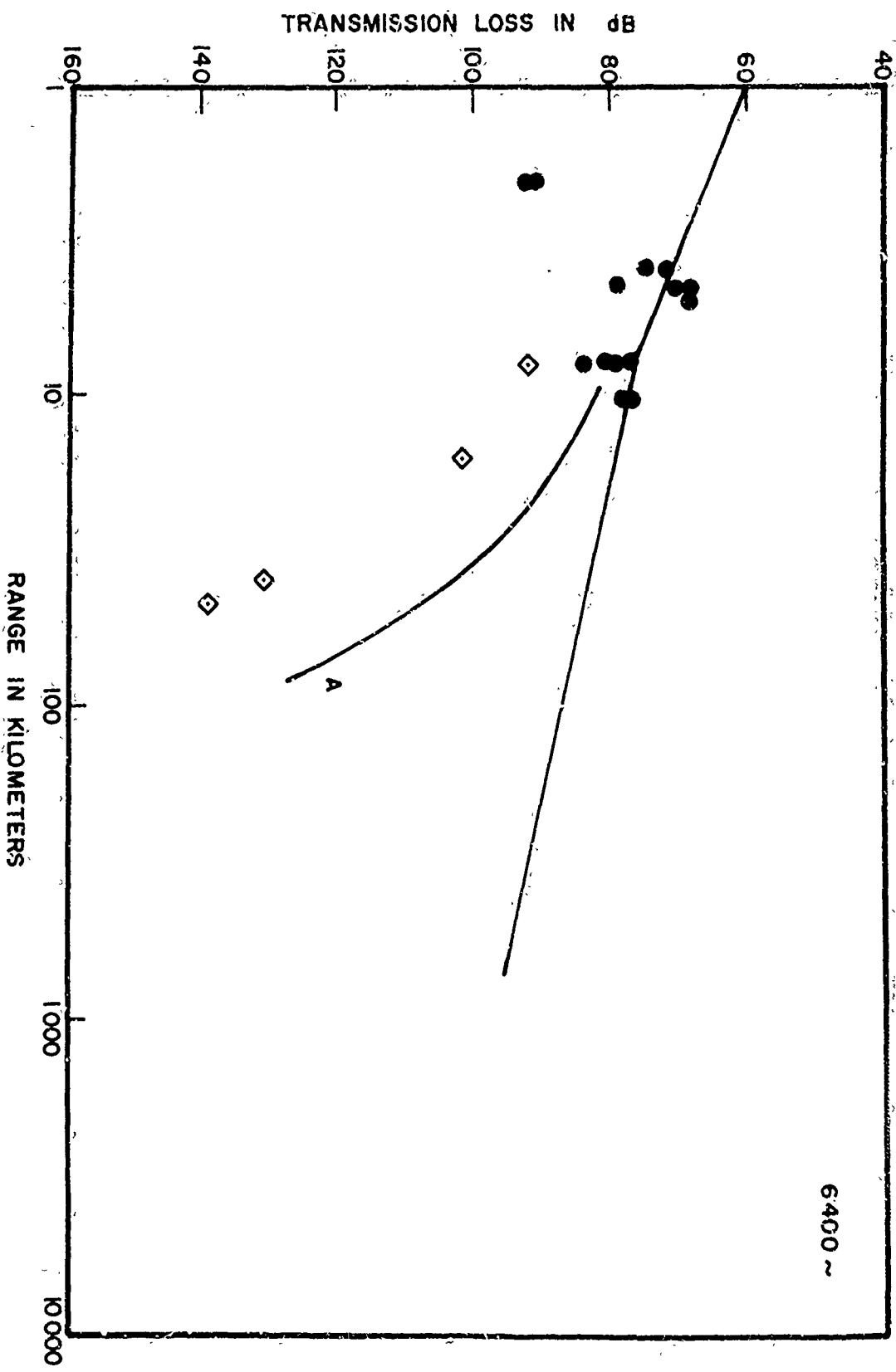


TRANSMISSION LOSS vs RANGE

FIGURE 26

FIGURE 27

TRANSMISSION LOSS VS RANGE



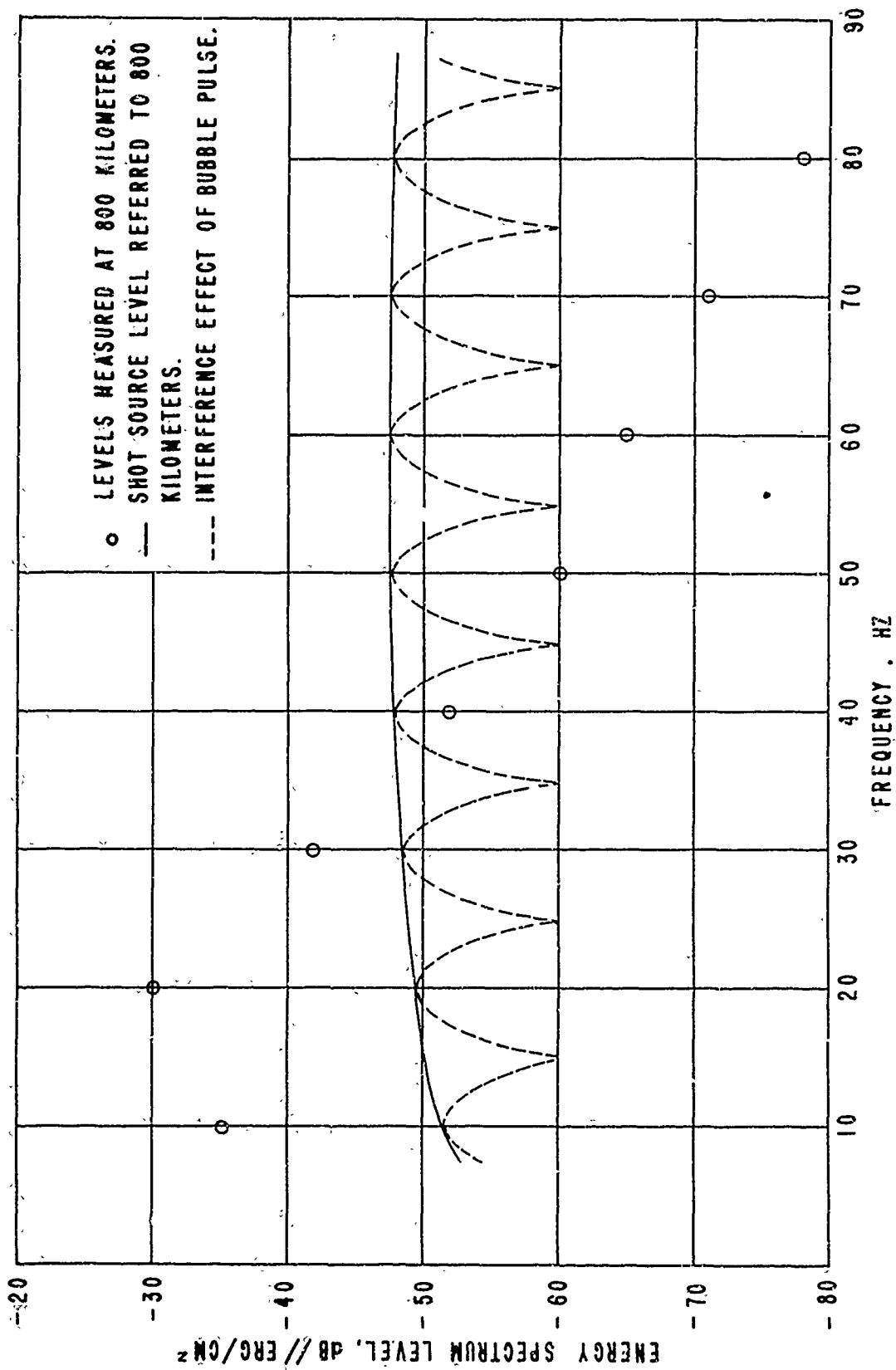


FIGURE 28 WESTON'S SOURCE LEVEL SPECTRUM

A



B

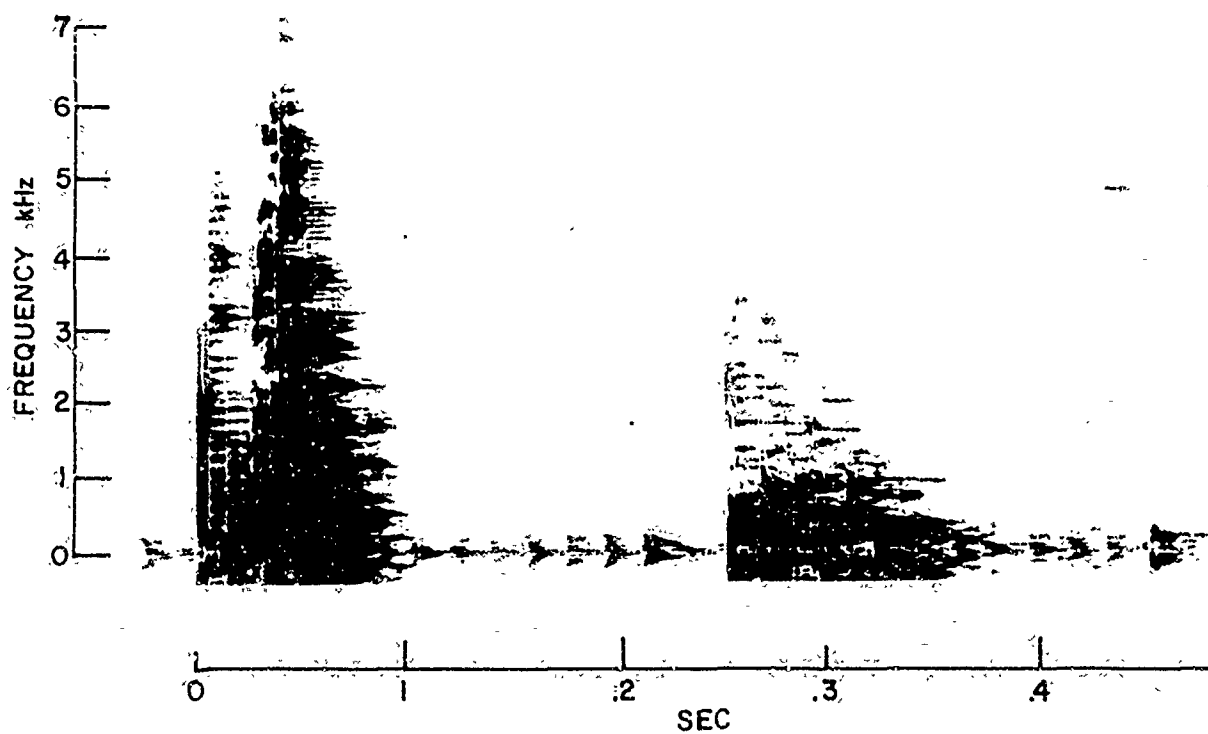


FIGURE 29 SHORT RANGE SHOT SIGNATURES (B CONVERGENCE)

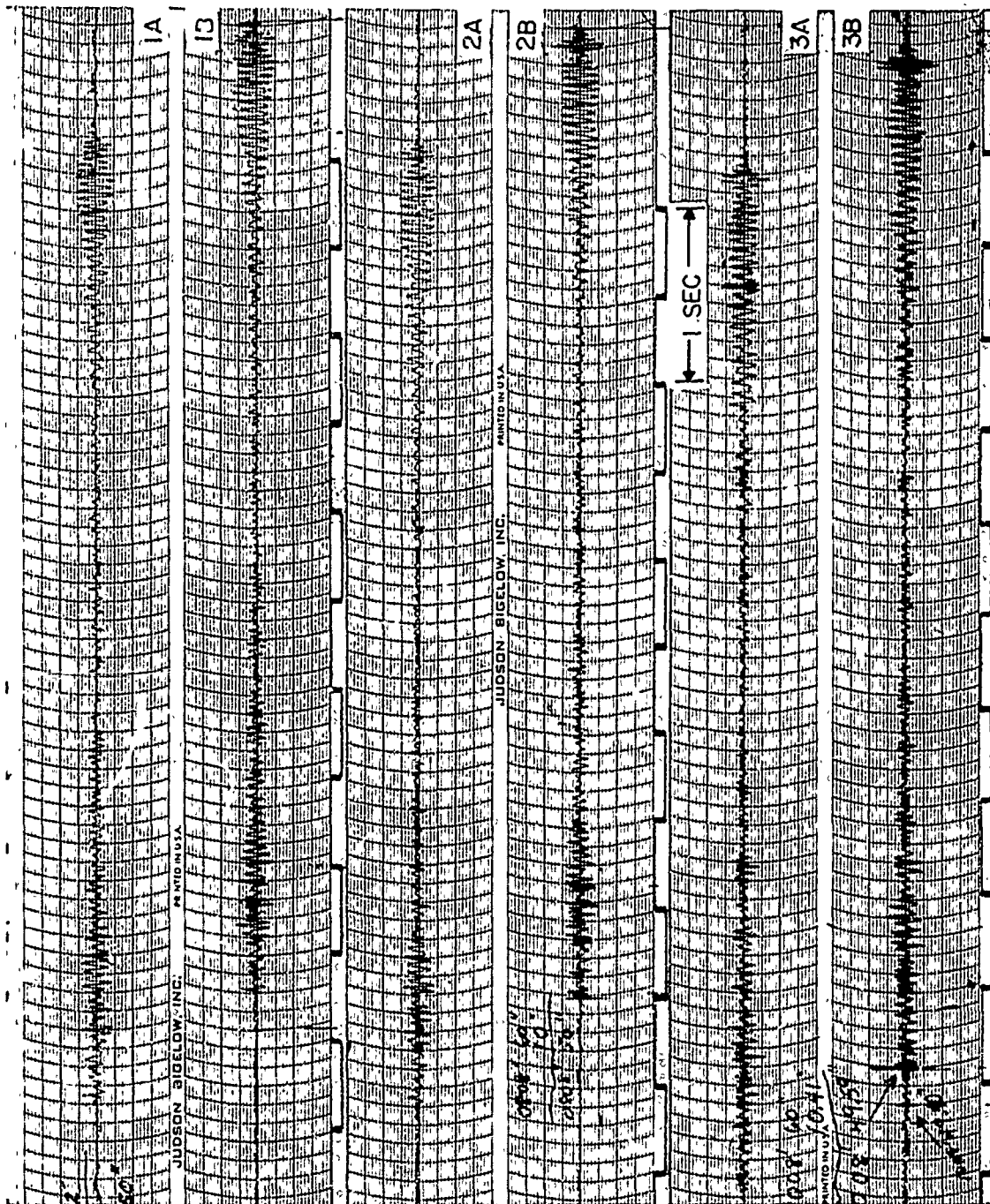


FIGURE 30 LONG RANGE ONE POUND SHOT SIGNATURES

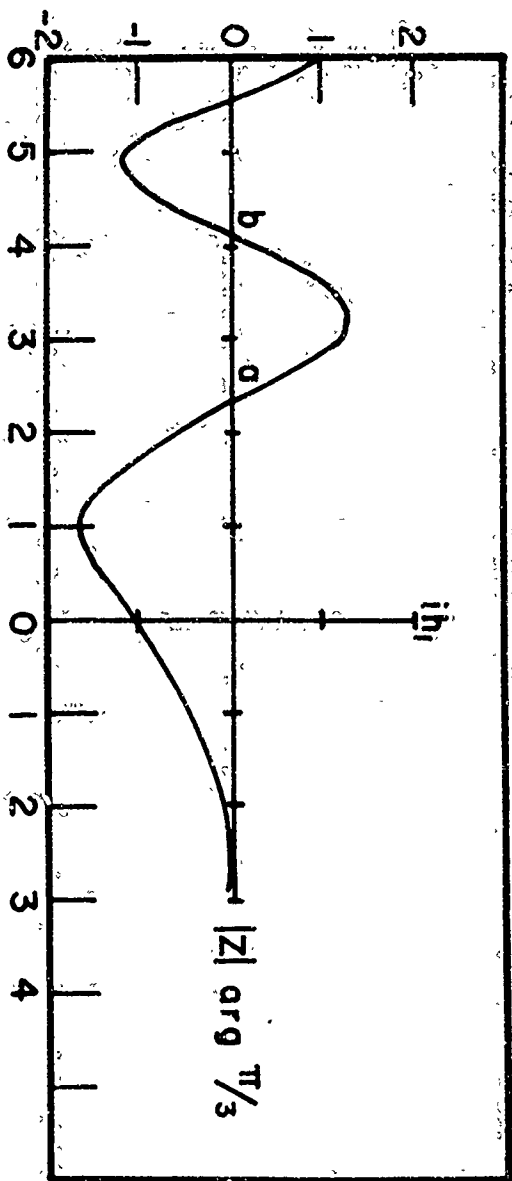


FIGURE 31 HANKEL FUNCTION

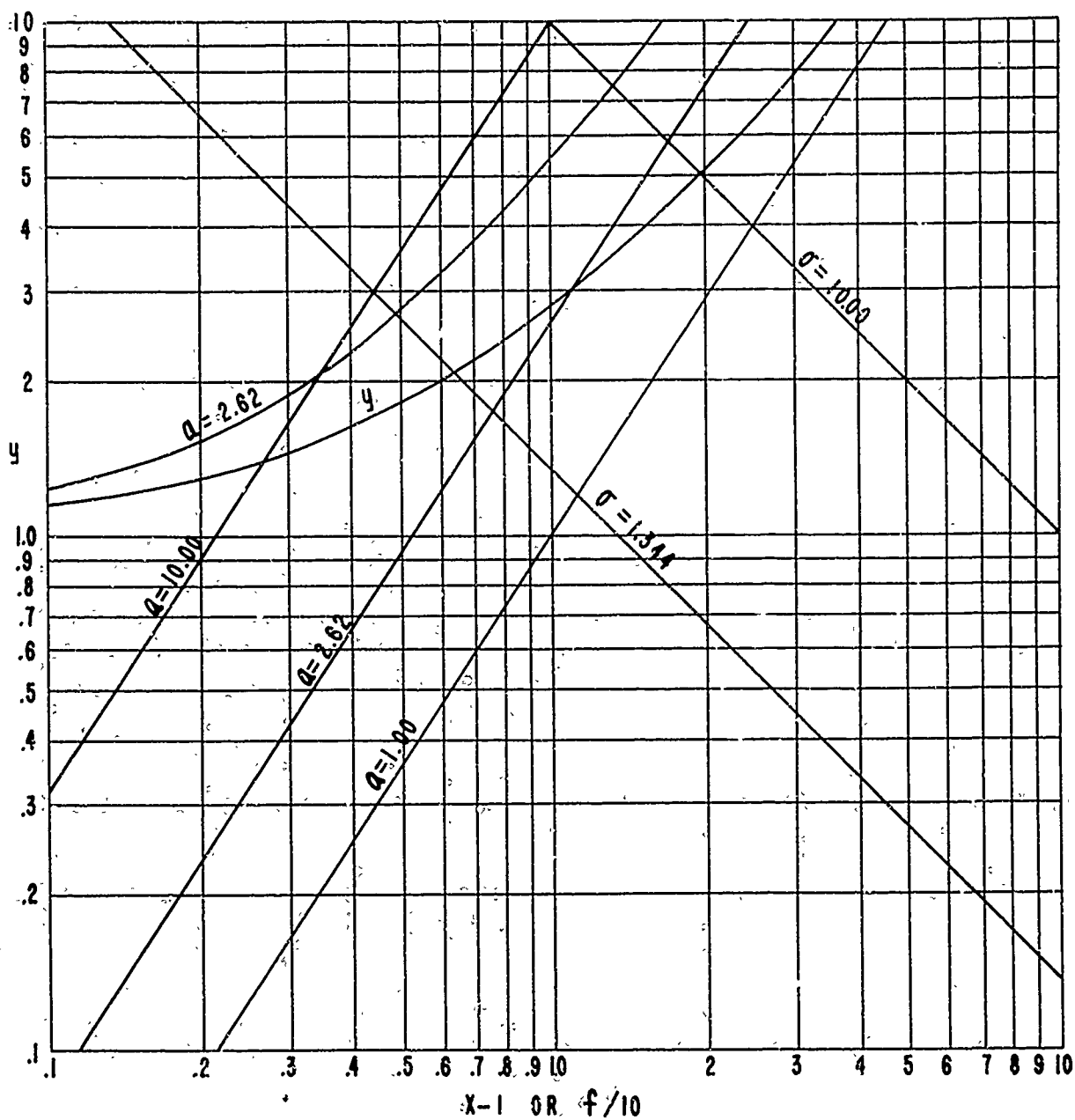


FIGURE 32 EIGEN VALUE NOMOGRAPH FOR BILINEAR GRADIENT

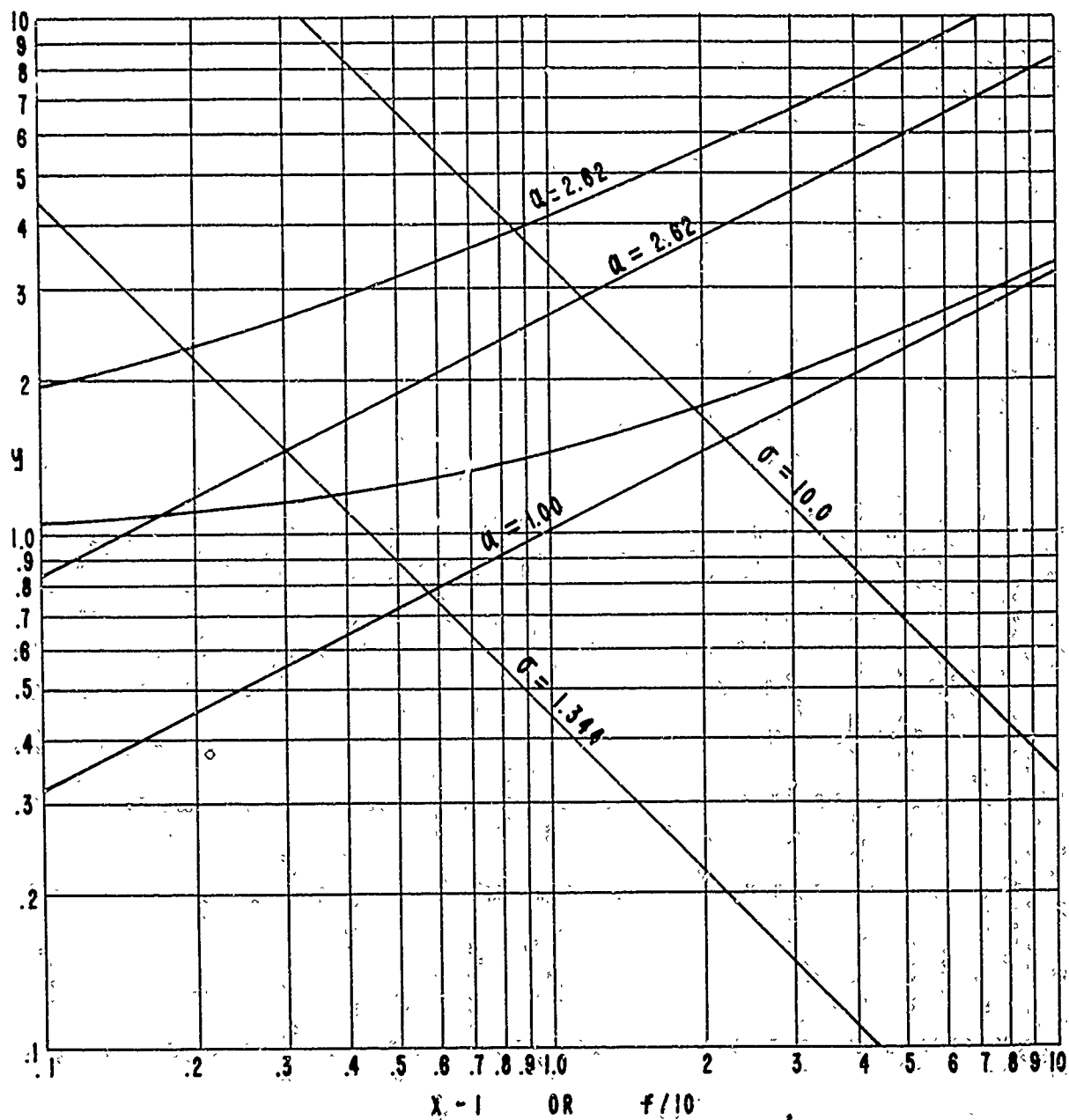


FIGURE 33 GROUP VELOCITY NOMOGRAPH FOR BILINEAR GRADIENT

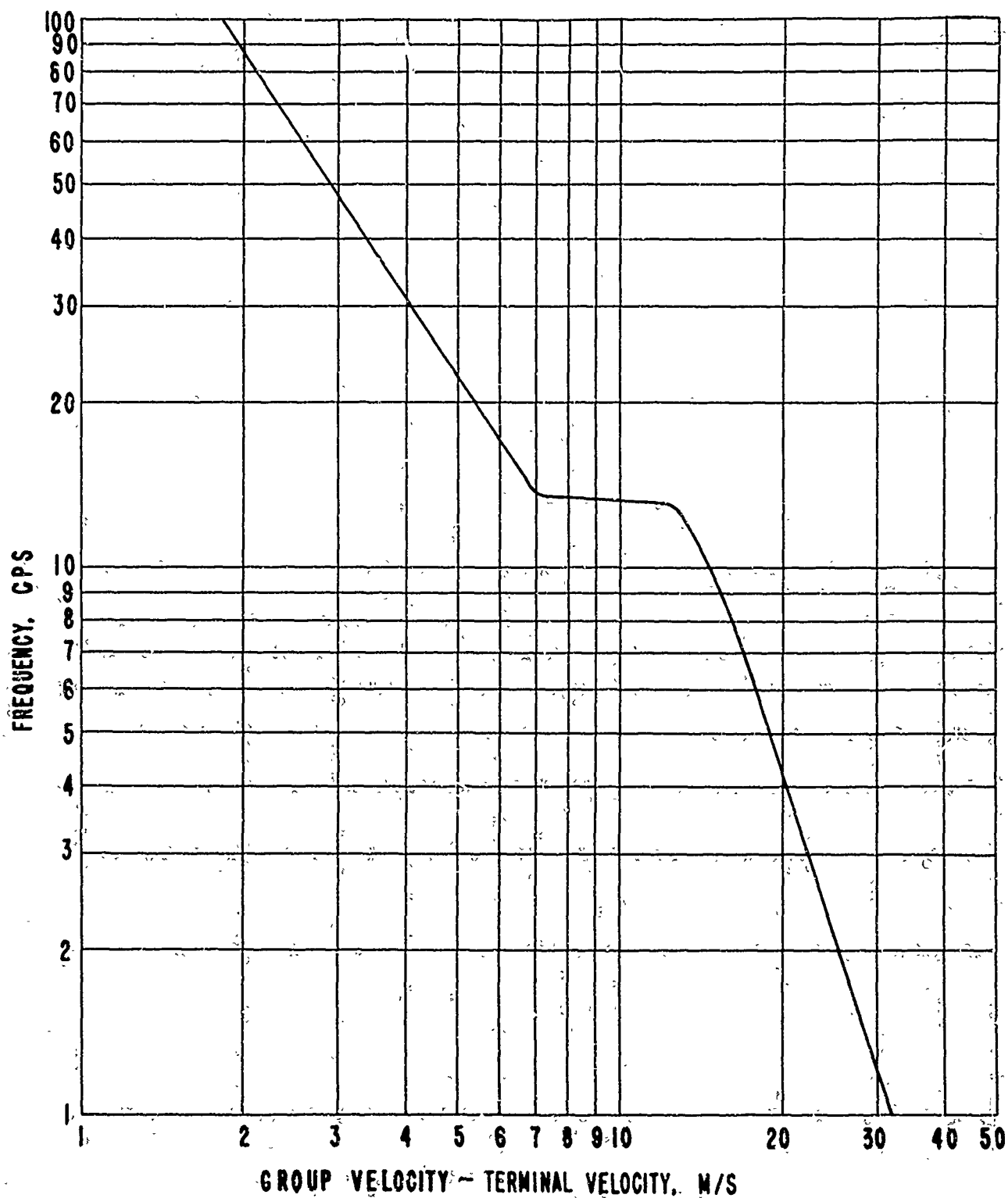


FIGURE 34 FREQUENCY DISPERSION vs GROUP VELOCITY
FOR BILINEAR GRADIENT

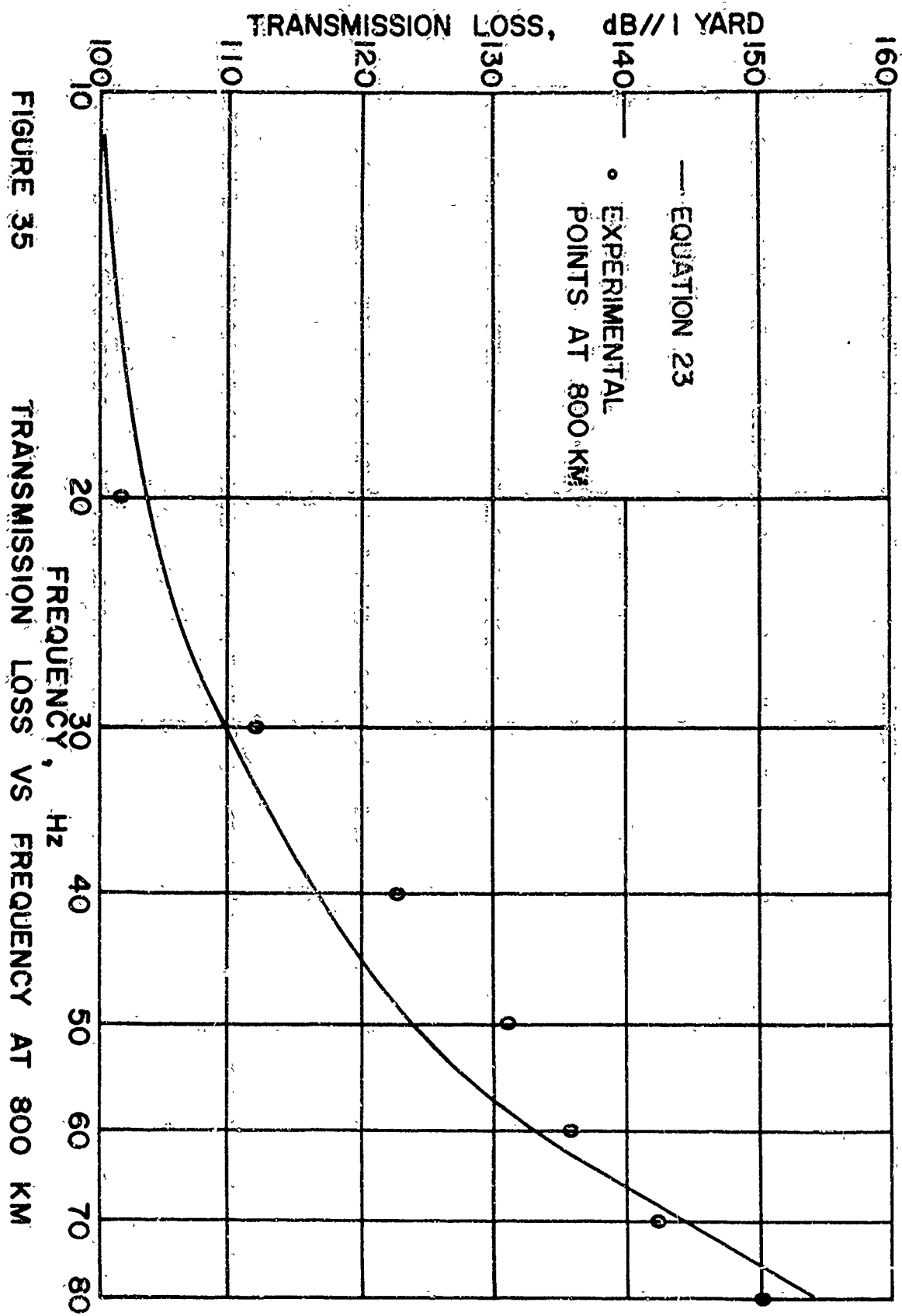


FIGURE 35

TRANSMISSION LOSS VS FREQUENCY AT 800 KM

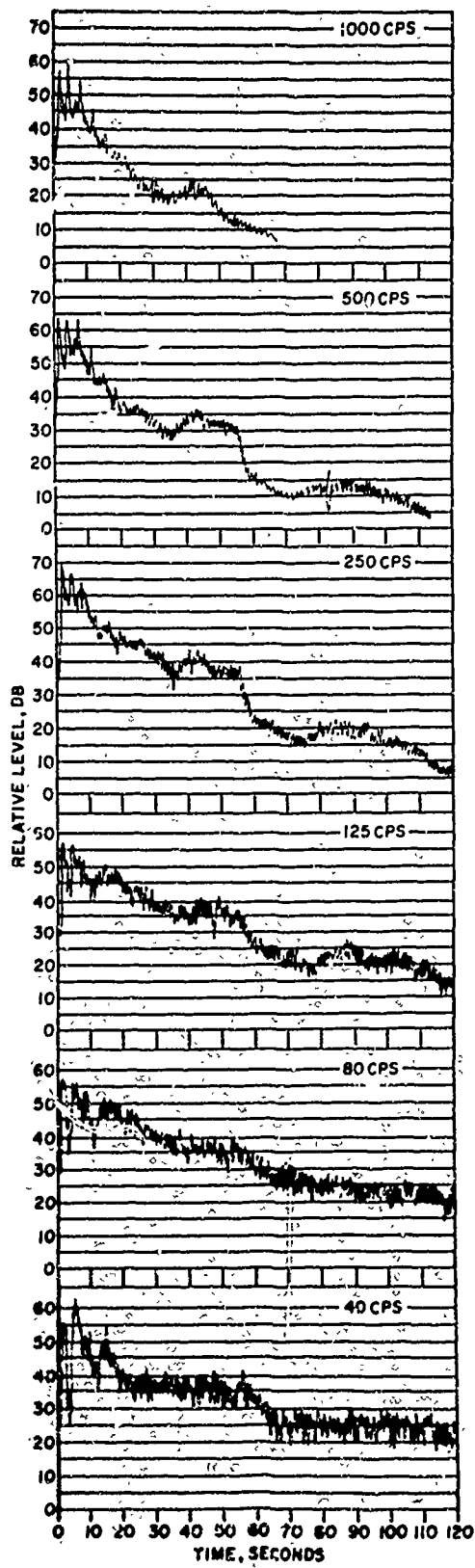


FIGURE 36 REVERBERATION LEVEL vs TIME FOR 100 LB CHARGE

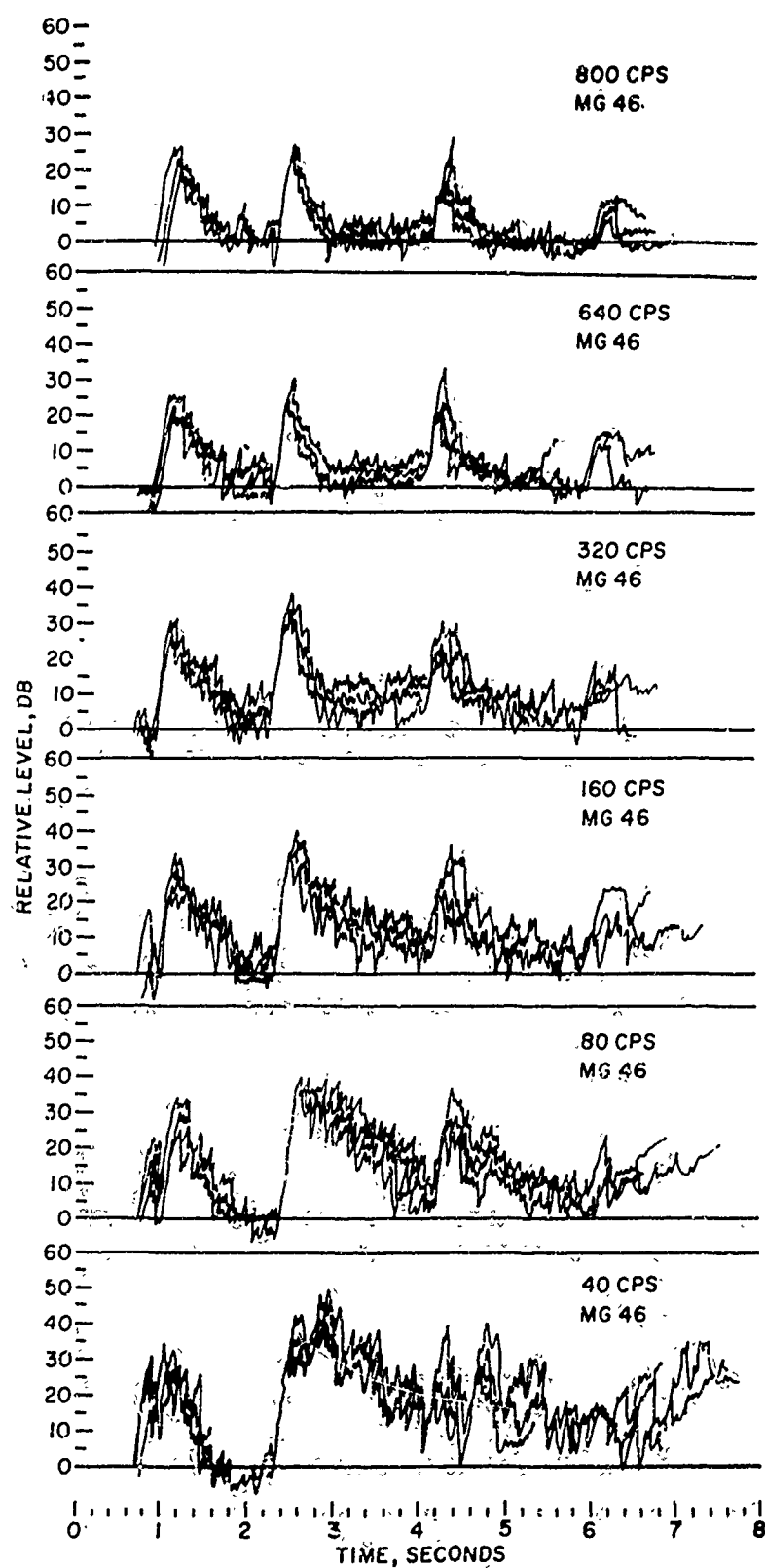


FIGURE 37 REVEBRERATION LEVEL vs TIME FOR 1.8 LB CHARGE

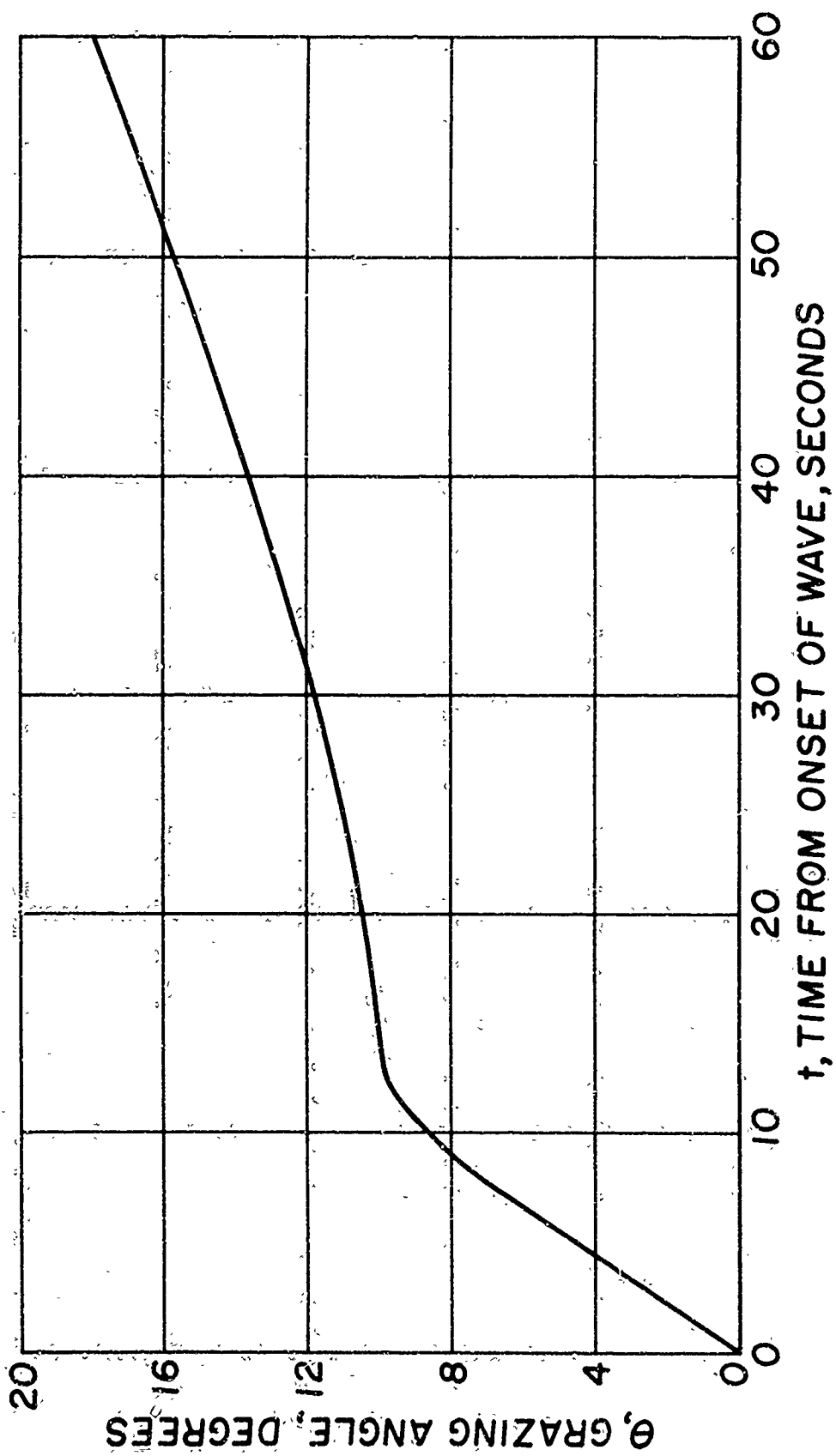


FIGURE 38

REVERBERATION GRAZING ANGLE vs TIME

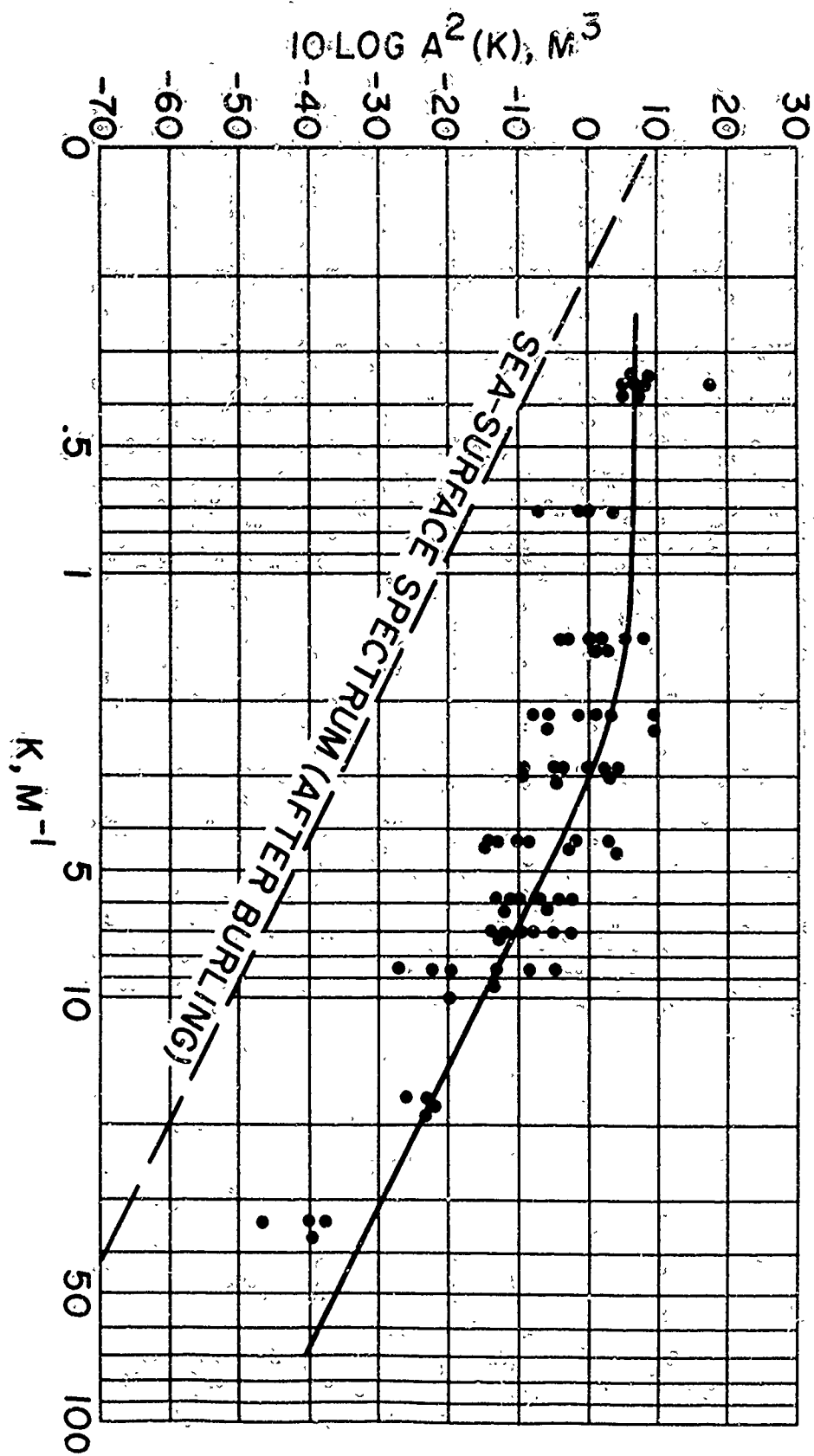


FIGURE 39

ROUGHNESS SPECTRUM

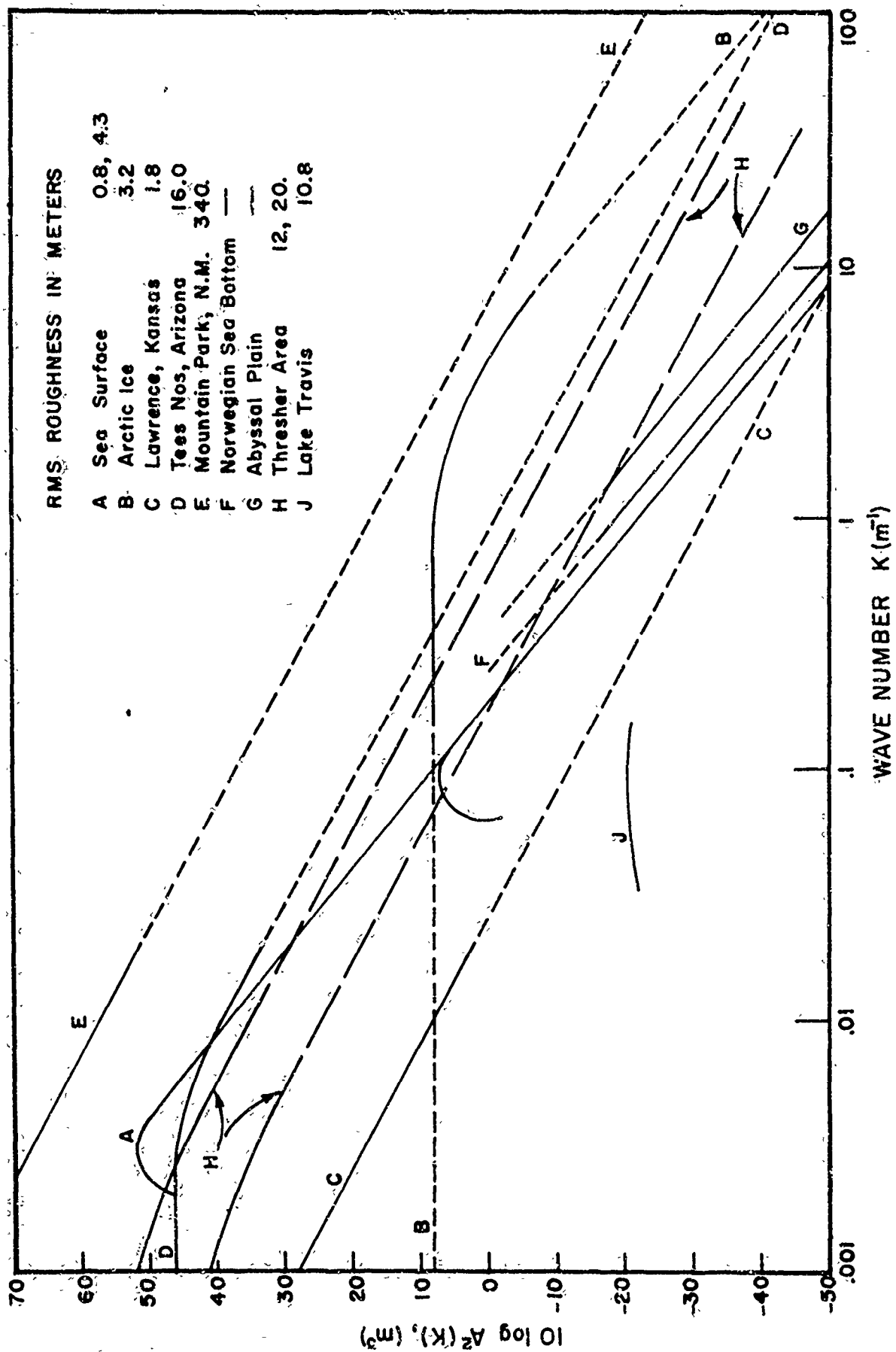
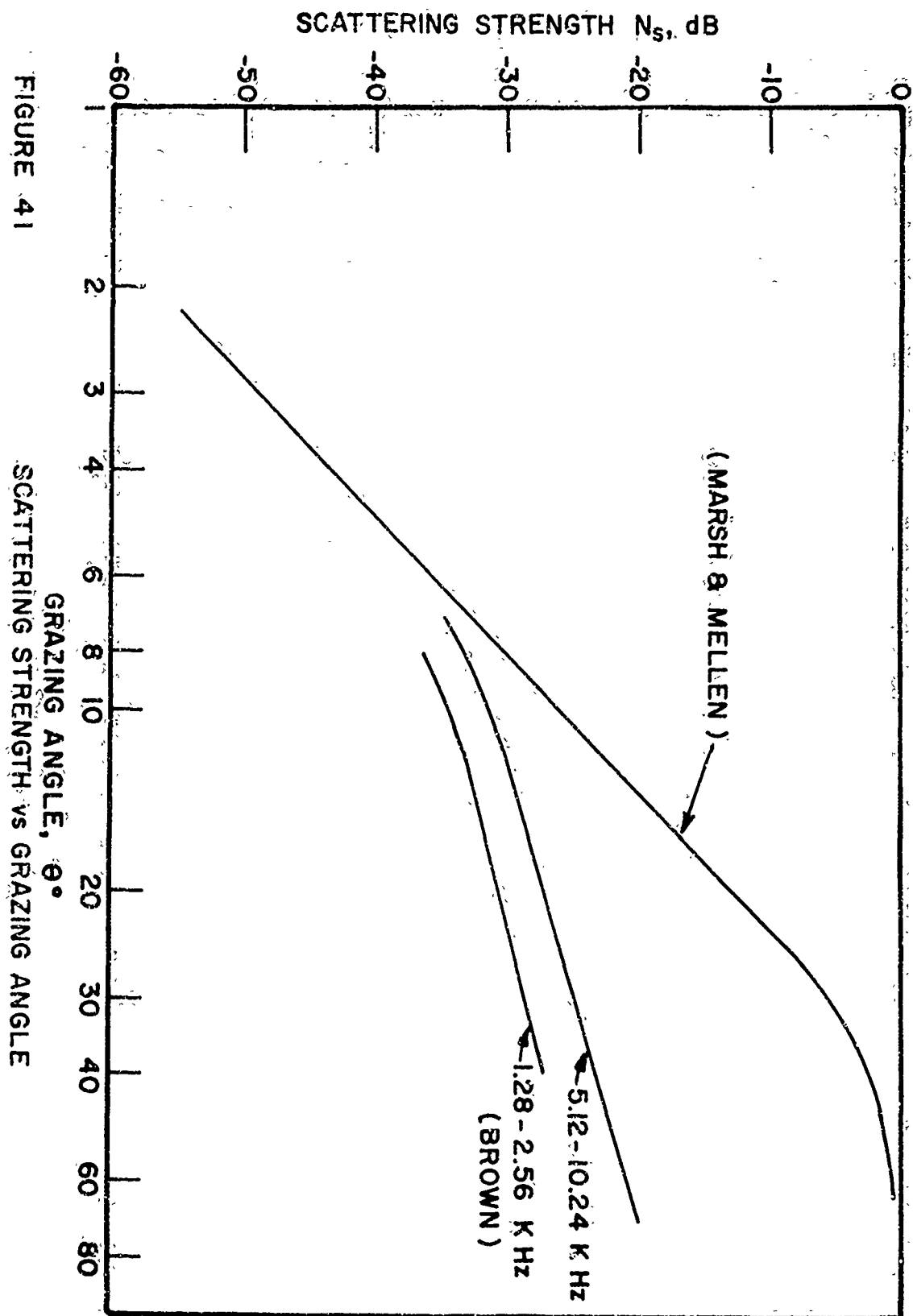


FIGURE 40 GEOPHYSICAL ELEVATION SPECTRA



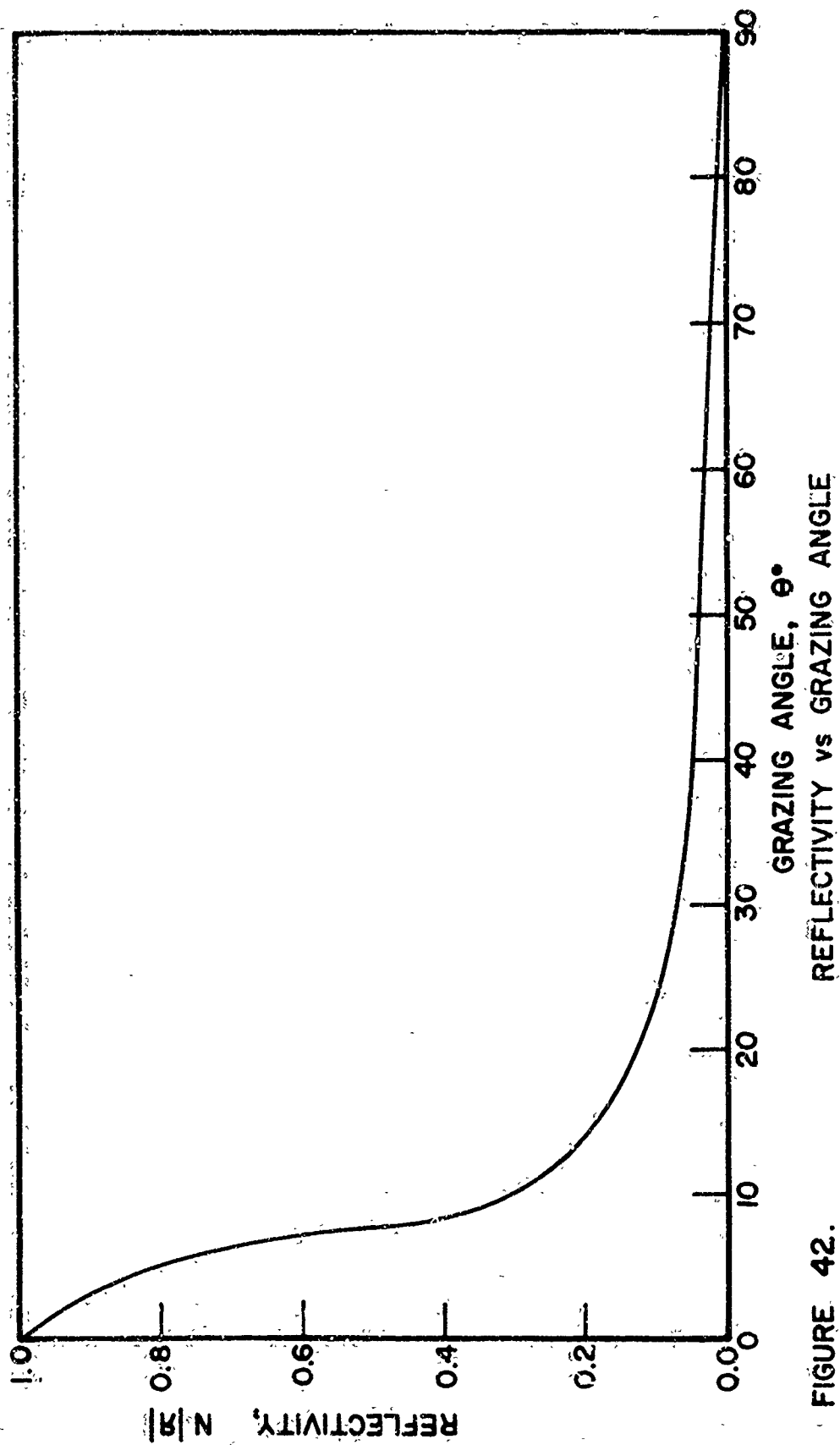


FIGURE 42.

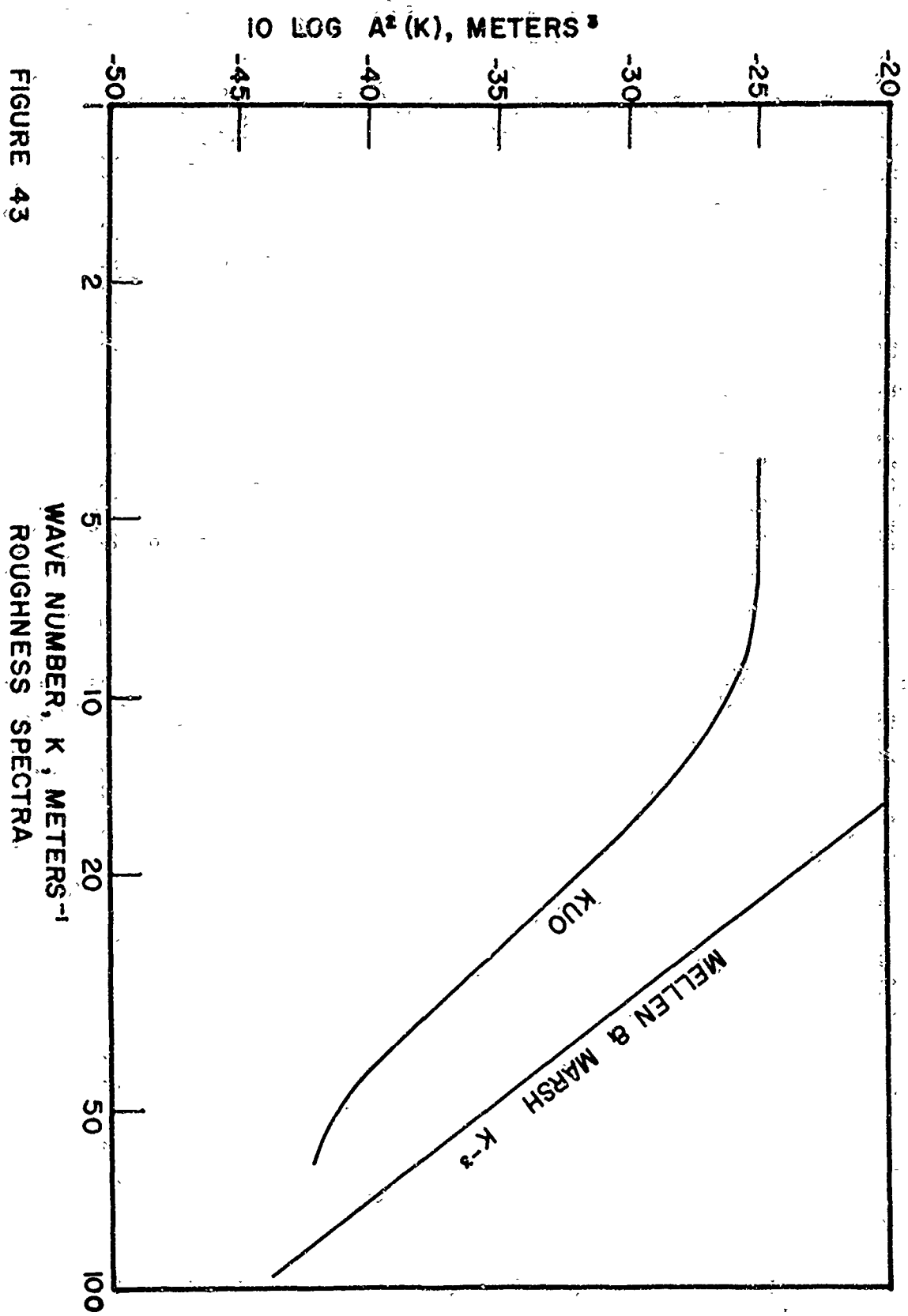


FIGURE 43

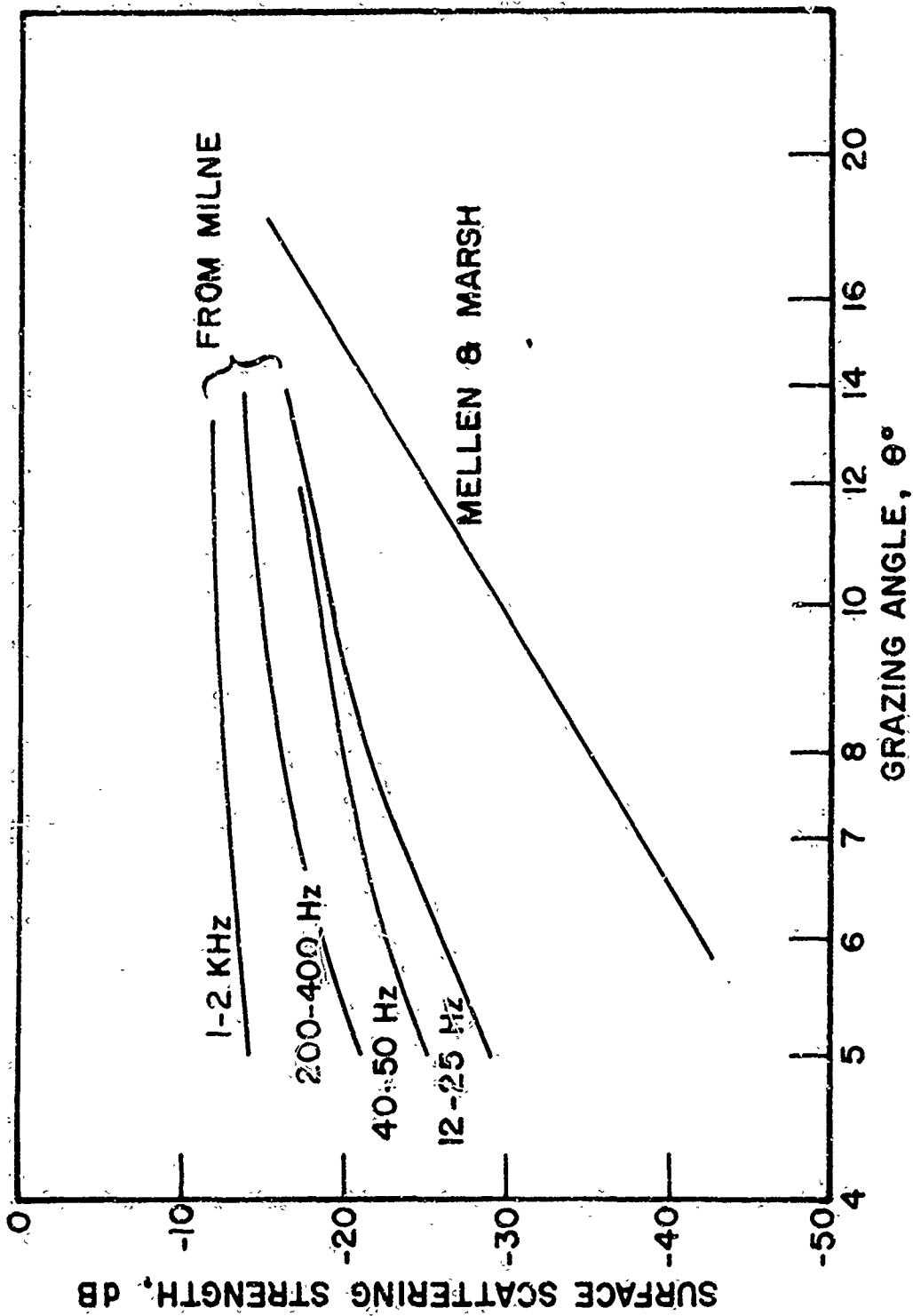


FIGURE 44 SCATTERING STRENGTH vs GRAZING ANGLE

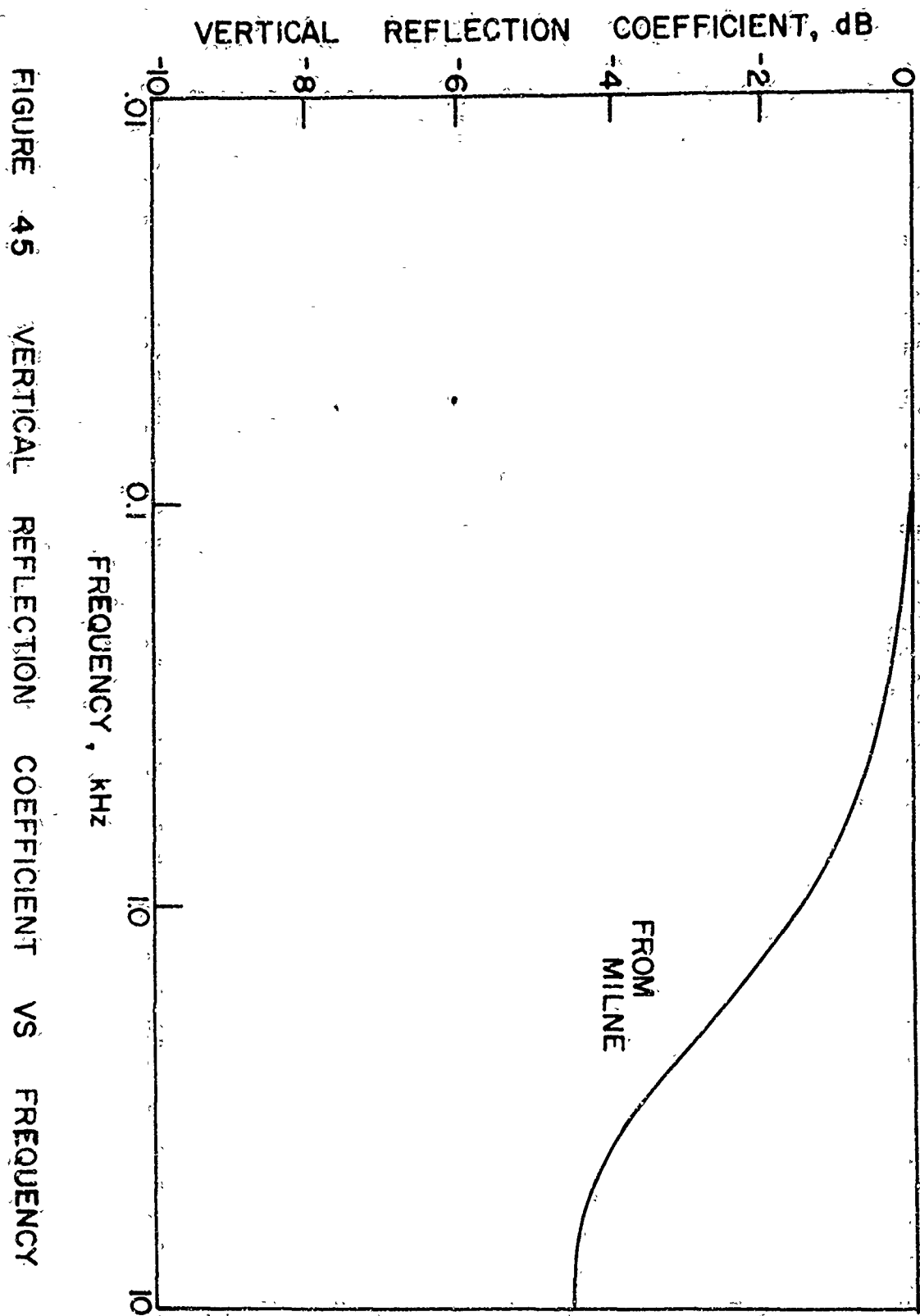


FIGURE 45 VERTICAL REFLECTION COEFFICIENT VS FREQUENCY

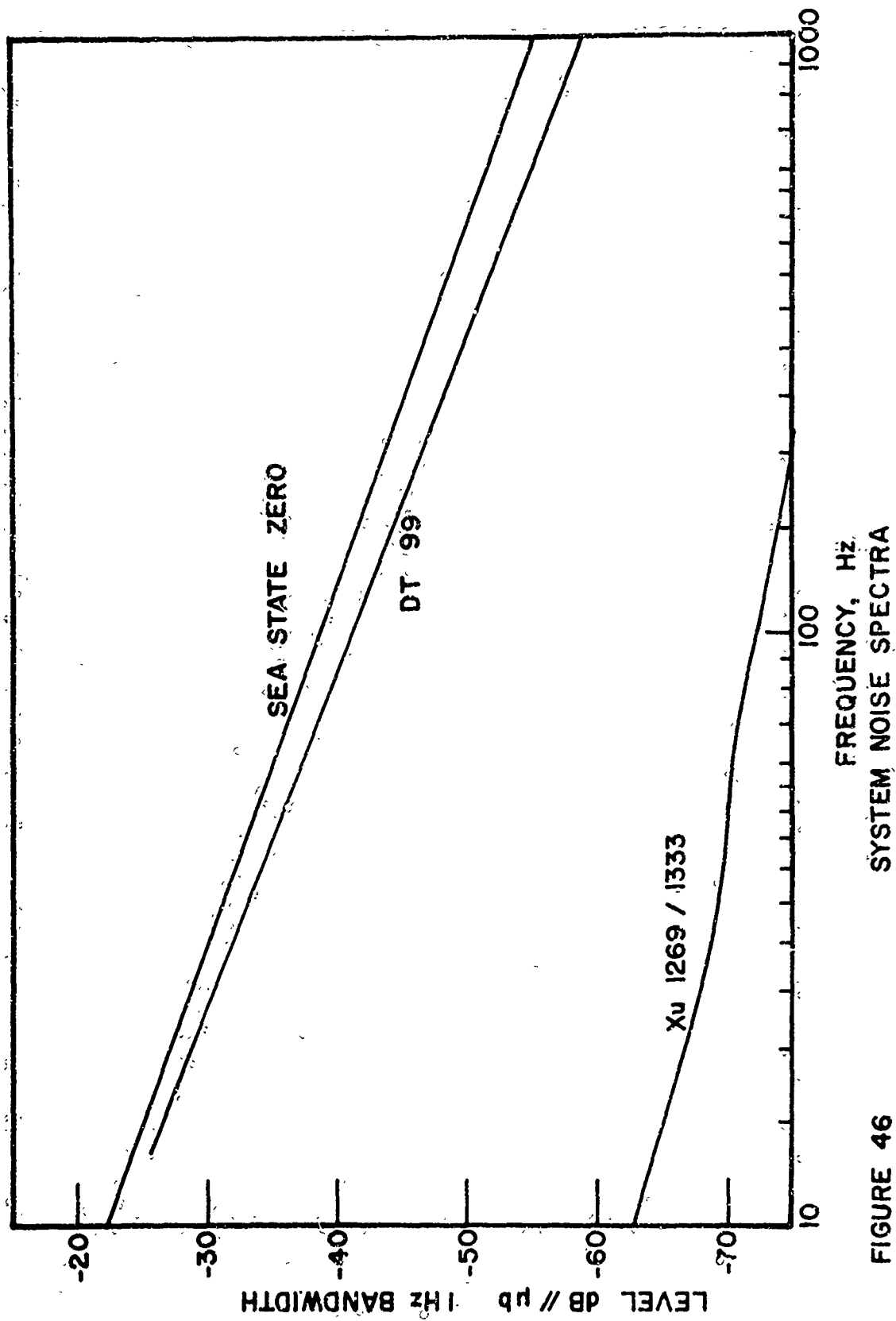


FIGURE 46

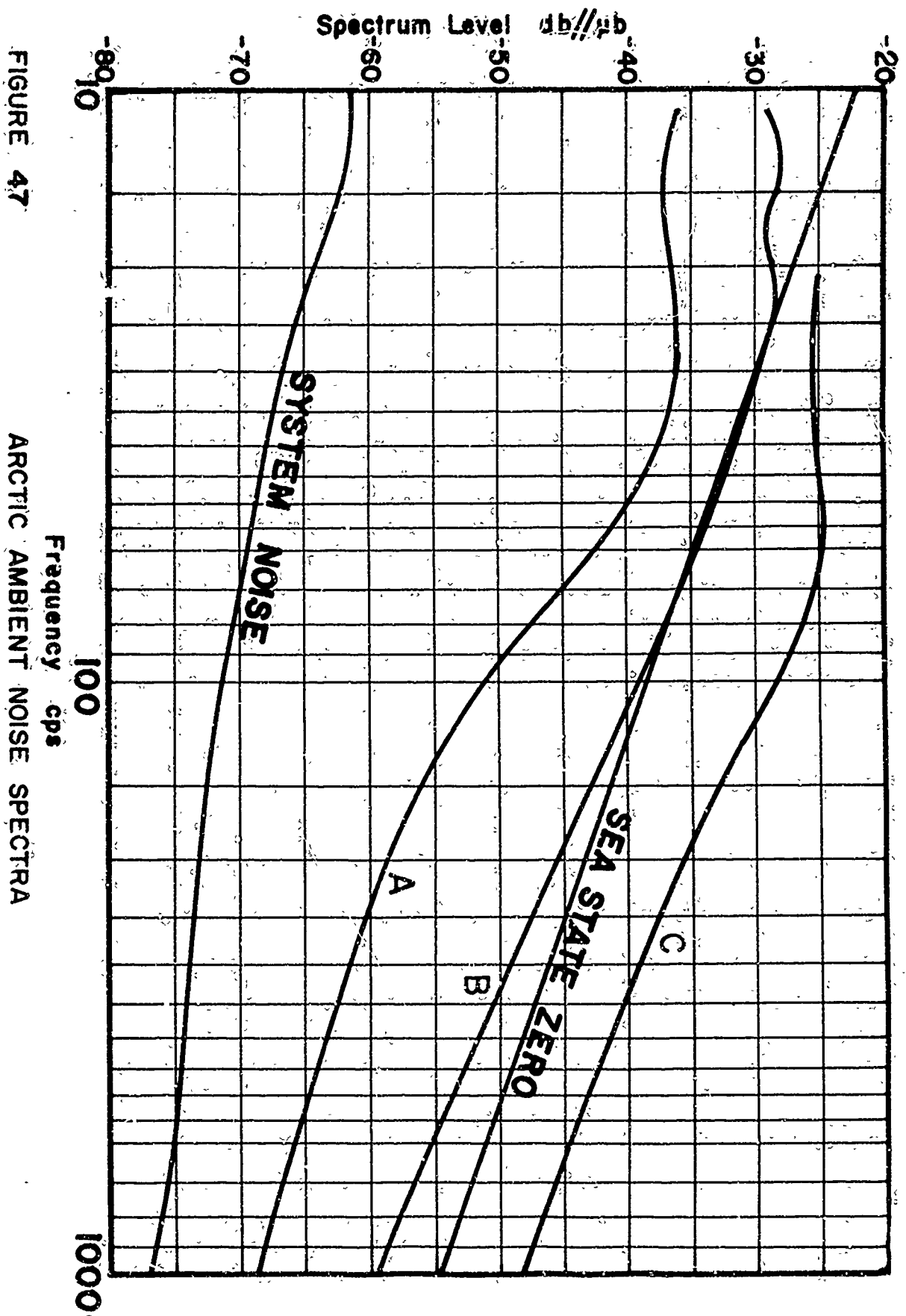


FIGURE 47

ARCTIC AMBIENT NOISE SPECTRA

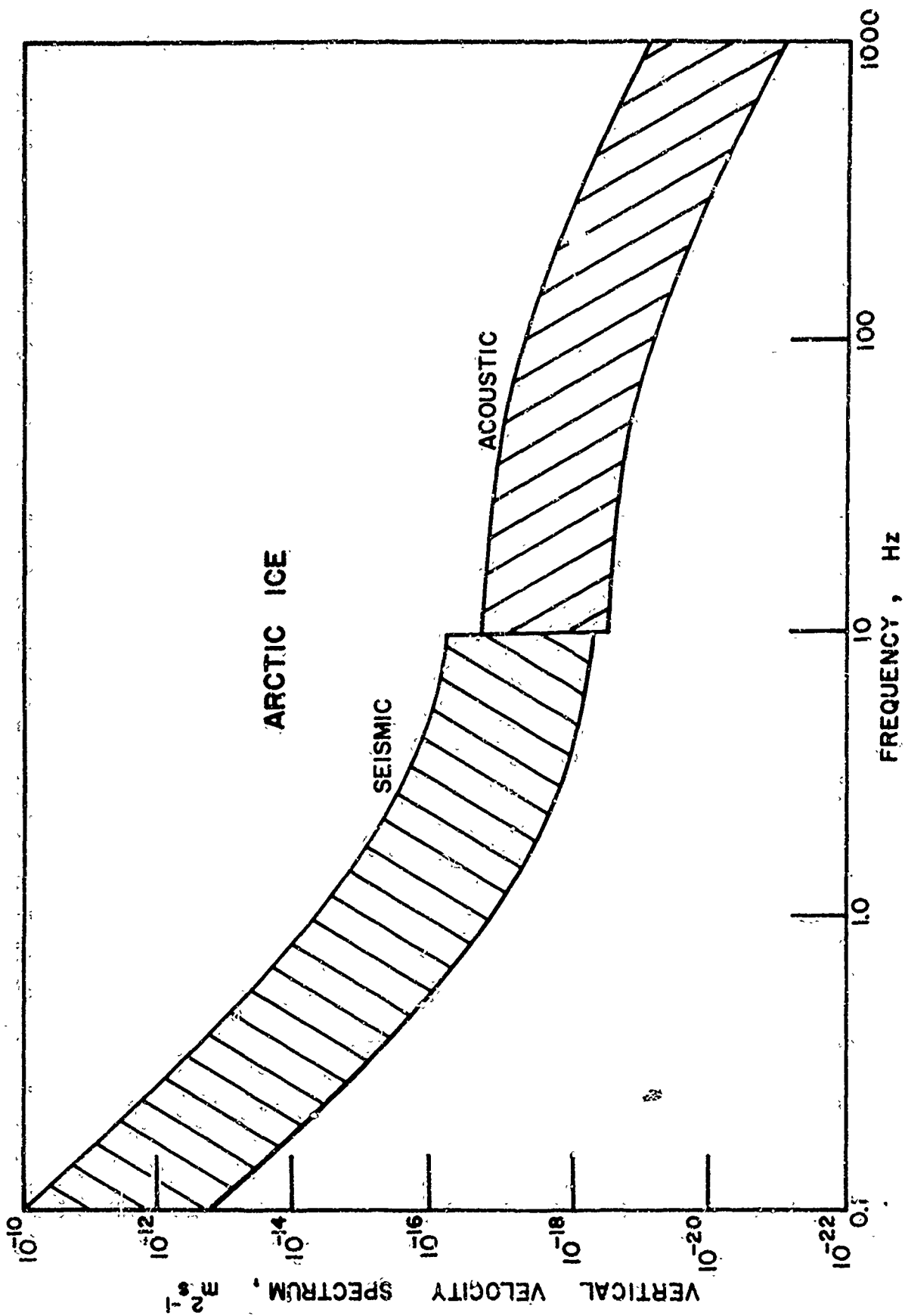


FIGURE 48 SEISMIC/ACOUSTIC ICE SURFACE VELOCITY SPECTRUM

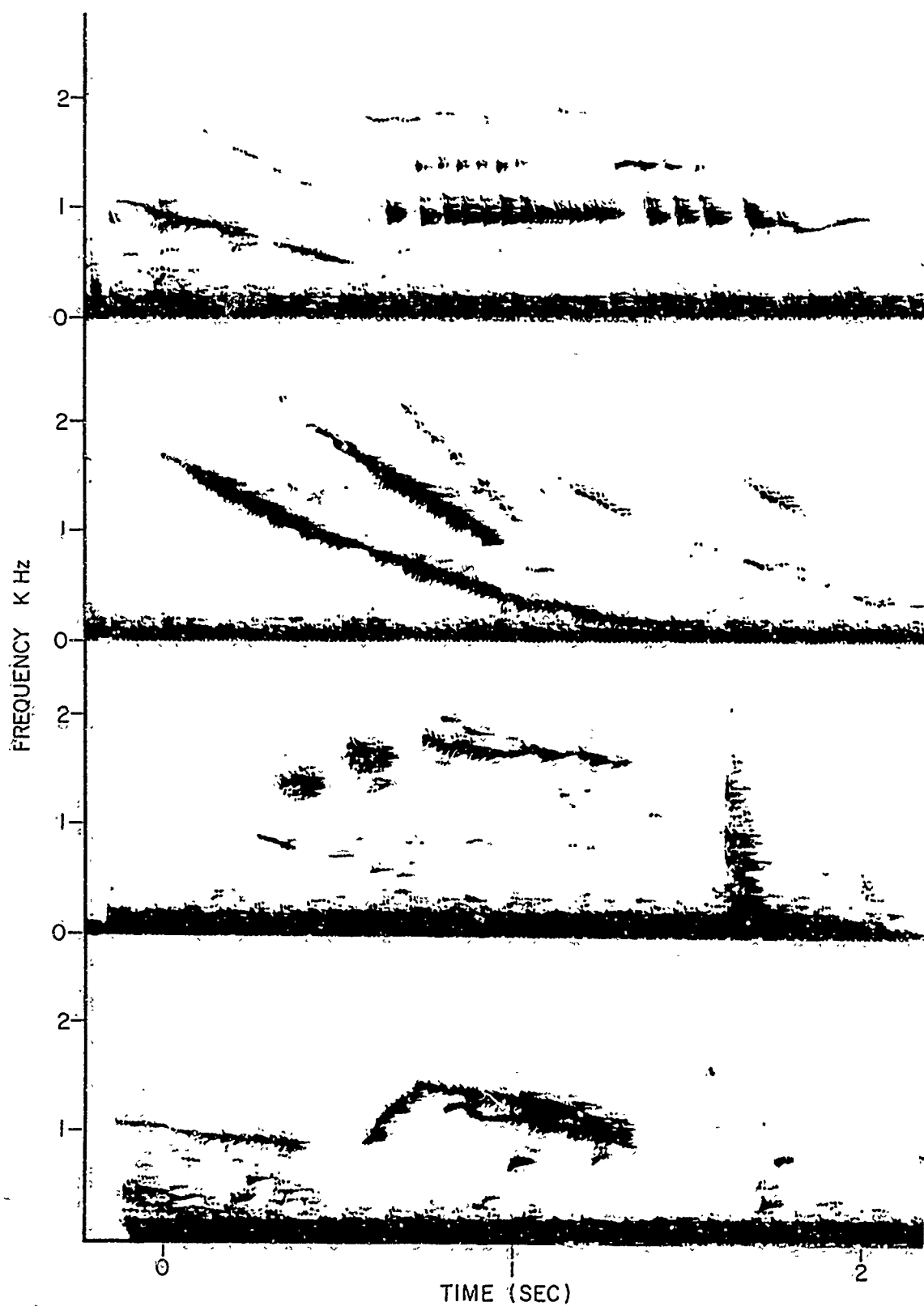


FIGURE 49 BIOLOGICAL NOISE MISSILYZER SPECTRA

TABLE I PROPAGATION STUDY SHOT DATA

DATA USED BY MARSH AND MELLEEN FOR INITIAL PROPAGATION STUDY

SHOT NO.	DATE	FIRE FROM	RECEIVED AT	DEPTH(m)	WEIGHT*	RANGE(km)
B29	5-30-62	T3	ARLIS II	120	15.0*	810
B30	5-30-62	T3	ARLIS II	120	3.5*	810
B31	5-30-62	T3	ARLIS II	120	45.0*	810
B32	5-30-62	T3	ARLIS II	120	95.0*	810
B33	5-30-62	T3	ARLIS II	120	.7	810
B34	6-02-62	T3	ARLIS II	220	375.0*	810
12C	4-27-62	PP1	ARLIS II	150	17.0	1160
B9	4-28-62	T3	ARLIS II	60	50.0*	820
5	9-14-59	A/C	T3	60	4.0	820
7	9-14-59	A/C	T3	60	4.0	915
395	8-04-59	T3	CHARLIE	150	9.0	1140
0703	8-22-62	T3	ARLIS II	60	50.0	735
0645	8-22-62	T3	ARLIS II	120	50.0	735

*Asterisk indicates yield. All others are weight

OTHER DATA ANALYZED.

SHOT NO.	DATE	FIRE	FROM	RECEIVED AT	DEPTH(m)	WEIGHT	RANGE(km)
2-3	6-07-59	T3		T3	3.5	CAP	2.0
2-4	6-07-59	T3		T3	3.5	CAP	2.0
2-6	6-07-59	T3		T3	3.5	.5	2.0
2-7	6-07-59	T3		T3	3.5	.5	2.0
3-5	6-09-59	T3		T3	38.0	.5	5.0
3-6	6-09-59	T3		T3	38.0	.5	5.0
3-7	6-09-59	T3		T3	38.0	.0033*	5.0
3-9	6-09-59	T3		T3	38.0	.0065	5.0
3-12	6-09-59	T3		T3	38.0	.0026	7.9
3-13	6-09-59	T3		T3	38.0	CAP	7.9
3-14	6-09-59	T3		T3	38.0	.5	7.9
3-15	6-09-59	T3		T3	38.0	.5	7.9
4-2	6-12-59	T3		T3	38.0	.0027	3.8
4-3	6-12-59	T3		T3	38.0	CAP	3.8
4-5	6-12-59	T3		T3	38.0	CAP	3.8

SHOT NO.	DATE	FIRE FROM	RECEIVED AT	DEPTH(m)	WEIGHT*	RANGE(km)
4-11	6-12-59	T3	T3	38	.0026	4.4
4-12	6-12-59	T3	T3	38	CAP	4.4
4-14	6-12-59	T3	T3	38	CAP	4.4
4-17	6-12-59	T3	T3	38	0.5	4.4
20-7	7-12-59	T3	T3	60	0.5	10.3
20-8	7-12-59	T3	T3	60	0.5	10.3
343	7-28-59	CHARLIE	T3	90	55.0*	1200.0
344	7-28-59	CHARLIE	T3	60	6.0	1200.0
27-0047	8-07-59	A/C#8	T3	15	4.0	139.0
28-2107	8-10-59	A/C#14	T3	15	4.0	342.0
28-2117	8-10-59	A/C#15	T3	15	4.0	384.0
29-2209	8-10-59	A/C#20	T3	15	4.0	326.0
29-2221	8-10-59	A/C#21	T3	15	4.0	302.0
30-2245	8-10-59	A/C#23	T3	15	4.0	288.0
30-2253	8-10-59	A/C#24	T3	15	4.0	293.0
30-2302	8-10-59	A/C#25	T3	15	4.0	308.0

SHOT NO.	DATE	FIRE	FROM	RECEIVED AT	DEPTH(m)	WEIGHT*	RANGE(km)
31-2347	8-10-59	A/C#28		T3	60	4.0	482
31-0004	8-10-59	A/C#29		T3	15	4.0	567
34-2305	8-14-59	A/C#16		T3	60	4.0	1295
35-2334	8-14-59	A/C#18		T3	60	4.0	1170
35-0035	8-14-59	A/C#21		T3	15	4.0	865
35-0126	8-14-59	A/C#25		T3	15	4.0	584
36-0230	8-14-59	A/C#30		T3	60	4.0	274
36-0254	8-14-59	A/C#33		T3	15	4.0	291
36-0303	8-14-59	A/C#34		T3	15	4.0	322
40-2033	8-27-59	A/C#12		T3	15	4.0	278
40-2046	8-27-59	A/C#13		T3	15	4.0	338
40-2100	8-27-59	A/C#15		T3	60	4.0	426
40-2128	8-27-59	A/C#18		T3	15	4.0	560
41-2143	8-27-59	A/C#19		T3	60	4.0	626
41-2210	8-27-59	A/C#22		T3	15	4.0	785
43-1914	8-31-59	A/C#3		T3	15	4.0	311

SHOT NO.	DATE	FIRE FROM	RECEIVED AT	DEPTH(m)	WEIGHT*	RANGE(km)
43-1924	8-31-59	A/C#4	T3	60	4.0	346.0
44-2010	8-31-59	A/C#8	T3	15	4.0	469.0
44-2020	8-31-59	A/C#9	T3	60	4.0	510.0
52-2009	9-14-59	A/C#4	T3	15	4.0	820.0
52-2019	9-14-59	A/C#5	T3	60	4.0	858.0
52-2029	9-14-59	A/C#6	T3	15	4.0	900.0
53-2205	9-14-59	A/C#15	T3	60	4.0	1175.0
53-2334	9-14-59	A/C#18	T3	15	4.0	770.0
53-0008	9-14-59	A/C#21	T3	60	4.0	595.0
53-0030	9-14-59	A/C#23	T3	60	4.0	472.0
53-0036	9-14-59	A/C#24	T3	15	4.0	430.0
54-0054	9-14-59	A/C#26	T3	15	4.0	344.0
53-0013	9-14-59	A/C#27	T3	60	4.0	293.0
54-0112	9-14-59	A/C#28	T3	15	4.0	232.0
48-2300	9/59	STATEN ISLAND	T3	15	0.5*	47.5
48-2400	9/59	STATEN ISLAND	T3	15	.5	47.5

SHOT NO.	DATE	FIRED FROM	RECEIVED AT	DEPTH(m)	WEIGHT*	RANGE(km)
48-0100	9/59	STATEN ISLAND	T3	6.1	0.5	47.5
49-2000	9/59	STATEN ISLAND	T3	15.0	0.5	238.0
49-2100	9/59	STATEN ISLAND	T3	15.0	0.5	238.0
49-2200	9/59	STATEN ISLAND	T3	15.0	0.5	238.0
49-2300	9/59	STATEN ISLAND	T3	15.0	0.5	238.0
49-0000	9/59	STATEN ISLAND	T3	15.0	0.5	238.0
49-0100	9/59	STATEN ISLAND	T3	15.0	0.5	238.0
2040	8-14-59	A/C#7	CHARLIE	15.0	4.0	360.0
2050	8-14-59	A/C#8	CHARLIE	60.0	4.0	300.0
2059	8-14-59	A/C#9	CHARLIE	15.0	4.0	250.0
2119	8-14-59	A/C#11	CHARLIE	15.0	4.0	135.0
2130	8-14-59	A/C#12	CHARLIE	60.0	4.0	90.0
2216	8-14-59	A/C#14	CHARLIE	60.0	4.0	110.0
2142	9-14-59	A/C#14	CHARLIE	15.0	4.0	78.0
2150	9-14-59	A/C#15	CHARLIE	60.0	4.0	33.0
2231	8-31-59	A/C#18	CHARLIE	15.0	4.0	88.0

SHOT NO.	DATE	FIRE FROM	RECEIVED AT	DEPTH(m)	WEIGHT*	RANGE(km)
2242	8-31-59	A/C#19	CHARLIE	60.0	4.0	11.0
C7	4/62	PPI	T3	150.0	10.0	1000.0
C8	4/62	PPI	T3	180.0	10.0	1000.0
C11	4/62	PPI	T3	150.0	17.0	1000.0
C17	4/62	PPII	T3	150.0	17.0	1400.0
A13	4/62	ARLIS	T3	90.0	10.0	820.0
iv	8/58	ALPHA	T3	60.0	55.0	700.0

TABLE II RAY CALCULATIONS

θ_c	z_0	r_0	t_0	u_0	f_0	δ_0
4.5	65	4041	3.09	1438.2	—	—
5.0	100	5723	3.98	1438.8	—	—
5.5	161	7480	5.20	1439.3	—	—
6.0	182	6878	4.78	1438.9	—	—
6.5	202	6506	4.52	1438.6	—	—
7.0	217	6123	4.26	1438.1	—	—
7.5	234	6027	4.19	1438.0	—	—
7.7	241	6021	4.18	1438.0	—	—
8.0	251	6277	4.36	1438.5	28.0	.034
8.5	282	7106	4.94	1440.0	24.4	.134
9.0	315	7629	5.30	1440.7	20.0	.20
9.5	349	8099	5.61	1441.6	18.0	.25
10.0	404	9870	6.83	1444.3	16.0	.44
10.5	473	12715	8.78	1447.7	13.0	.68
11.0	594	16376	11.28	1450.8	10.4	.89
11.5	721	18925	13.02	1452.6	8.6	1.0
12.0	854	21124	14.52	1454.0	7.2	1.1
12.5	993	23126	15.90	1455.4	5.8	1.2
13.0	1138	25028	17.18	1456.6	5.0	1.3
13.5	1290	26837	18.40	1457.9	4.2	1.4
14.0	1448	28585	19.60	1459.1	3.5	1.5

 θ_0 grazing angle (degrees) u_0 sound velocity (meters/sec) z_0 vertex depth (meters) f_0 ray frequency (sec^{-1}) r_0 skip distance (meters) δ_0 time dispersion (%) t_0 time (sec)

TABLE III REVERBERATION STUDY SHOT DATA

Shot no.	Date	Firing station	Corrected yield	Detonation depth	Water depth	Horizontal range	Hydrophone	
							type	depth
1	8/58	Alpha	50.0 lb	60 m	2150 m	250 m	DT-99	60 m
2	7/59	T-3	3.5	30	930	100	DT-99	60
3	7/59	T-3	4.0	120	930	100	DT-99	60
4	7/59	T-3	4.5	150	930	100	DT-99	60
5	4/62	Arlis II	8.5	270	2700	1000	XU-1320	60
6	4/62	Arlis II	1.7	240	2700	1000	XU-1320	60
7	4/62	Arlis II	3.7	180	2700	1000	XU-1320	60
8	7/62	Arlis II	100.0	210	3000	1000	XU-1320	60
9	7/62	Arlis II	2.0	180	3000	1000	XU-1320	60
10	7/62	Arlis II	1.8	60	3000	1000	XU-1320	60
11	7/62	Arlis II	1.8	60	3000	1000	XU-1320	60
12	7/62	Arlis II	1.8	60	3000	1000	XU-1320	60

TABLE IV EXPERIMENTAL VALUES OF SCATTERING STRENGTH (DB)

Time (sec)	Shot no.								
	1	2	3	4	5	6	7	8	9
Center frequency 40 cps									
10	-15	-29	-25	-24	-34	-36	-29	-40	-33
15	-19	-23	-13	-17	-25	-28	-21	-33	-27
20	-17	-23	-17	-15	-29	-30	-25	-34	-33
25	-18	-21	-14	-15	-27	-29	-21	-32	-31
30	-14	-21	-13	-16	-20	-27	-20	-33	-31
Center frequency 80 cps									
10	-30	-31	-19	-20	-37	-38	-33	-40	-36
15	-22	-19	-16	-16	-28	-27	-23	-28	-28
20	-18	-19	-15	-13	-28	-28	-24	-29	-29
25	-17	-19	-15	-11	-27	-28	-23	-29	-29
30	-13	-19	-15	-13	-24	-24	-21	-28	-33
Center frequency 125 cps									
10	-14	-27	-17	-18	-34	-36	-29	-34	-34
15	-18	-24	-13	-16	-26	-28	-21	-27	-31
20	-15	-22	-12	-14	-23	-27	-20	-27	-29
25	-16	-21	-13	-14	-25	-27	-21	-26	-30
30	-12	-17	-9	-12	-21	-25	-17	-22	-25
Center frequency 250 cps									
10	-24	-30	-21	-21	-34	-38	-31	-38	-36
15	-28	-25	-20	-17	-31	-35	-26	-34	-33
20	-30	-26	-17	-19	-28	-33	-27	-34	-38
25	-28	-26	-18	-19	-28	-33	-27	-31	-37
30	-22	-24	-16	-16	-26	-29	-24	-28	-34
Center frequency 500 cps									
10	-24	-25	-21	-19	-31	-37	-28	-33	-35
15	-20	-22	-17	-16	-31	-35	-27	-33	-36
20	-25	-23	-19	-16	-32	-33	-32	-33	-38
25	-25	-25	-18	-19	-31	-35	-29	-32	-38
30	-24	-25	-21	-20	-32	-38	-32	-33	-41
Center frequency 1000 cps									
10	-23	-25	-20	-15	-28	-38	-29	-30	-30
15	-23	-22	-18	-13	-29	-35	-28	-30	-36
20	-25	-23	-18	-14	-30		-34	-31	-40
25	-28	-25	-21	-17	-32		-32	-35	-40
30	-24	-26	-23	-19	-33		-33	-35	-40
Center frequency 2000 cps									
10	-22	-23	-20	-20					
15	-22	-22	-17	-17					
20	-26	-24	-19	-19					
25	-29	-26	-22	-22					
30	-26	-29	-26	-26					
Center frequency 4000 cps									
10	-12	-17	-15	-14					
15	-14	-18	-14	-14					
20	-13	-20	-16	-17					
25	-15	-25	-19	-22					
30	-17	-30	-24	-25					

TABLE V ICE THICKNESS DISTRIBUTION

Thickness in meters	Percentage	
	Winter	Summer
0.0 - 0.6	0.9	2
0.6 - 1.2	6	2
1.2 - 1.8	9	7
1.8 - 2.4	16	40
2.4 - 3.0	34	30
3.0 - 3.6	20	12
3.6 - 4.2	14	3
4.2 - 4.8	0.0	1.8
4.8 - 5.4	0.0	0.9
5.4 - 6.0	0.0	1.2
6.0 - 6.6	0.0	0.3

Security Classification

DOCUMENT CONTROL DATA - R&D		
(Security classification of title, body of abstract and indexing annotation must be entered when the overall report is classified)		
1. ORIGINATING ACTIVITY (Corporate author) AVCO Marine Electronics Office 33 Union Street, New London, Connecticut		2a. REPORT SECURITY CLASSIFICATION Unclassified
		2b. GROUP None
3. REPORT TITLE Underwater Sound in the Arctic Ocean		
4. DESCRIPTIVE NOTES (Type of report and inclusive dates) None		
5. AUTHOR(S) (Last name, first name, initial) Mellen, R.H. and Marsh, H.W.		
6. REPORT DATE August 16, 1965	7a. TOTAL NO. OF PAGES 97	7b. NO. OF REFS 19
8a. CONTRACT OR GRANT NO. NONr 3353(00)	8a. ORIGINATOR'S REPORT NUMBER(S) MED-65-1002	
b. PROJECT NO. c. None	8b. OTHER REPORT NO(S) (Any other numbers that may be assigned this report) None	
d.		
10. AVAILABILITY/LIMITATION NOTICES None		
11. SUPPLEMENTARY NOTES None	12. SPONSORING MILITARY ACTIVITY Office of Naval Research Dept. of the Navy Washington 25, D.C.	
13. ABSTRACT A summary of the U.S. Navy Underwater Sound Laboratory experimental program to investigate acoustic phenomena in the Arctic is given. Since the sound velocity is an increasing function of depth, propagation is characterized by upward refraction and surface reflection. A rough-surface model of the ice cover accounts for both forward and back-scatter. The roughness-wavelength spectrum calculated from reverberation measurements is similar to that for the sea surface although the level is higher. Forward scatter loss depends on total roughness and is responsible for severe attenuation of high frequencies. Propagation and reverberation data both imply an R.M.S. roughness of from two to three meters, which is consistent with under-ice profile measurements. Propagation of explosive waves is described by normal mode and ray theories. At short ranges convergence zones are observed. Because the ice cover shows a "critical angle" dependence, the time dispersion of the wave train at long range in deep water is well defined. In shallow water, the bottom may produce reflection modes, or reduced dispersion of the refracted mode. Unusually low ambient noise levels are observed during undisturbed periods. Spectra indicate that the noise background arises mainly via long range propagation at these times. In periods of high wind and rapid temperature change, ice noises are predominantly of local origin. During the summer biological sounds of various marine life are heard.		

DD FORM 1473

1 JAN 64

Security Classification

Security Classification

14. KEY WORDS	LINK A		LINK B		LINK C	
	ROLE	WT	ROLE	WT	ROLE	WT
Underwater Sound Arctic Acoustics Sonar Propagation of Sound						

INSTRUCTIONS

1. **ORIGINATING ACTIVITY:** Enter the name and address of the contractor, subcontractor, grantee, Department of Defense activity or other organization (corporate author) issuing the report.
- 2a. **REPORT SECURITY CLASSIFICATION:** Enter the overall security classification of the report. Indicate whether "Restricted Data" is included. Marking is to be in accordance with appropriate security regulations.
- 2b. **GROUP:** Automatic downgrading is specified in DoD Directive 5200.10 and Armed Forces Industrial Manual. Enter the group number. Also, when applicable, show that optional markings have been used for Group 3 and Group 4 as authorized.
3. **REPORT TITLE:** Enter the complete report title in all capital letters. Titles in all cases should be unclassified. If a meaningful title cannot be selected without classification, show title classification in all capitals in parenthesis immediately following the title.
4. **DESCRIPTIVE NOTES:** If appropriate, enter the type of report, e.g., interim, progress, summary, annual, or final. Give the inclusive dates when a specific reporting period is covered.
5. **AUTHOR(S):** Enter the name(s) of author(s) as shown on or in the report. Enter last name, first name, middle initial. If military, show rank and branch of service. The name of the principal author is an absolute minimum requirement.
6. **REPORT DATE:** Enter the date of the report as day, month, year, or month, year. If more than one date appears on the report, use date of publication.
- 7a. **TOTAL NUMBER OF PAGES:** The total page count should follow normal pagination procedures, i.e., enter the number of pages containing information.
- 7b. **NUMBER OF REFERENCES:** Enter the total number of references cited in the report.
- 8a. **CONTRACT OR GRANT NUMBER:** If appropriate, enter the applicable number of the contract or grant under which the report was written.
- 8b, 8c, & 8d. **PROJECT NUMBER:** Enter the appropriate military department identification, such as project number, subproject number, system numbers, task number, etc.
- 9a. **ORIGINATOR'S REPORT NUMBER(S):** Enter the official report number by which the document will be identified and controlled by the originating activity. This number must be unique to this report.
- 9b. **OTHER REPORT NUMBER(S):** If the report has been assigned any other report numbers (either by the originator or by the sponsor), also enter this number(s).
10. **AVAILABILITY/LIMITATION NOTICES:** Enter any limitations on further dissemination of the report, other than those

imposed by security classification, using standard statements such as:

- (1) "Qualified requesters may obtain copies of this report from DDC."
- (2) "Foreign announcement and dissemination of this report by DDC is not authorized."
- (3) "U. S. Government agencies may obtain copies of this report directly from DDC. Other qualified DDC users shall request through _____."
- (4) "U. S. military agencies may obtain copies of this report directly from DDC. Other qualified users shall request through _____."
- (5) "All distribution of this report is controlled. Qualified DDC users shall request through _____."

If the report has been furnished to the Office of Technical Services, Department of Commerce, for sale to the public, indicate this fact and enter the price, if known.

11. **SUPPLEMENTARY NOTES:** Use for additional explanatory notes.

12. **SPONSORING MILITARY ACTIVITY:** Enter the name of the departmental project office or laboratory sponsoring (paying for) the research and development. Include address.

13. **ABSTRACT:** Enter an abstract giving a brief and factual summary of the document indicative of the report, even though it may also appear elsewhere in the body of the technical report. If additional space is required, a continuation sheet shall be attached.

It is highly desirable that the abstract of classified reports be unclassified. Each paragraph of the abstract shall end with an indication of the military security classification of the information in the paragraph, represented as (TS), (S), (C), or (U).

There is no limitation on the length of the abstract. However, the suggested length is from 150 to 225 words.

14. **KEY WORDS:** Key words are technically meaningful terms or short phrases that characterize a report and may be used as index entries for cataloging the report. Key words must be selected so that no security classification is required. Identifiers, such as equipment model designation, trade name, military project code name, geographic location, may be used as key words but will be followed by an indication of technical context. The assignment of links, rules, and weights is optional.

Security Classification